

University of New Hampshire

University of New Hampshire Scholars' Repository

Doctoral Dissertations

Student Scholarship

Fall 2021

CHARACTERIZING FOREST STANDS USING UNMANNED AERIAL SYSTEMS (UAS) DIGITAL PHOTOGRAMMETRY: ADVANCEMENTS AND CHALLENGES IN MONITORING LOCAL SCALE FOREST COMPOSITION, STRUCTURE, AND HEALTH

Benjamin T. Fraser

University of New Hampshire, Durham

Follow this and additional works at: <https://scholars.unh.edu/dissertation>

Recommended Citation

Fraser, Benjamin T., "CHARACTERIZING FOREST STANDS USING UNMANNED AERIAL SYSTEMS (UAS) DIGITAL PHOTOGRAMMETRY: ADVANCEMENTS AND CHALLENGES IN MONITORING LOCAL SCALE FOREST COMPOSITION, STRUCTURE, AND HEALTH" (2021). *Doctoral Dissertations*. 2618.

<https://scholars.unh.edu/dissertation/2618>

This Dissertation is brought to you for free and open access by the Student Scholarship at University of New Hampshire Scholars' Repository. It has been accepted for inclusion in Doctoral Dissertations by an authorized administrator of University of New Hampshire Scholars' Repository. For more information, please contact Scholarly.Communication@unh.edu.

CHARACTERIZING FOREST STANDS USING UNMANNED AERIAL SYSTEMS (UAS)
DIGITAL PHOTOGRAMMETRY: ADVANCEMENTS AND CHALLENGES IN
MONITORING LOCAL SCALE FOREST COMPOSITION, STRUCTURE, AND HEALTH

BY

BENJAMIN THOMAS FRASER

B.S., University of New Hampshire, 2015

M. S., University of New Hampshire, 2017

DISSERTATION

Submitted to the University of New Hampshire

In Partial Fulfillment of

The Requirements for the Degree of

Doctor of Philosophy

in

Natural Resources and Environmental Studies

September, 2021

This thesis was examined and approved in partial fulfillment of the requirements for the degree of
Doctor of Philosophy in Natural Resources and Environmental Studies by:

Dissertation Director, Dr. Russell G. Congalton, Professor of Remote Sensing and
Geographic Information Systems

Dr. Nathan Torbick, Director, Applied GeoSolutions

Dr. Richard Hallett, Researcher, USDA Forest Service and NRESS Affiliate Faculty

Dr. Mark Ducey, Department Chair, Department of Natural Resources and the Environment

Dr. John Gunn, Research Assistant Professor of Forest Management and UNH Cooperative
Extension

On August 9th, 2021

Approval signatures are on file with the University of New Hampshire Graduate School.

ACKNOWLEDGEMENTS

This research would not have been possible without the help of so many people. I would like to dedicate the successes and lessons of this dissertation first to my wife, Hannah Elizabeth Bowen. Over the last six years, you have bolstered me through the challenges and celebrated my achievements in graduate research. You have continually refined my perspective on this research and my dedication to its outcomes. Without you, I would not be where I am today. To my parents, Manuela and James Fraser, I cannot thank you enough. As part of the acknowledgements, I should have to address that partial funding of my graduate experience has been provided through your generosity. You have looked out for me every step of the way, and both inspired and supported me to explore the passion for this work that I so often found. To my wonderful in-laws, Mark and Elizabeth Bowen, I would like to thank you for exhibiting a lifestyle to strive for. Your love for each other, resilience, and sense of family has given my work purpose more times than I can count. For my grandmother, Martha Fraser, thank you for being one of my biggest supporters. Your routine phone calls have kept me connected to family, especially on those days when I could not escape my own thoughts. To James, Morgan, Jaden, Ryan, and Violet Fraser, I could not ask for a better family. Although we do not get to see each other very often, I know that I can always count on you if needed. Wishing you all the best.

For those that have helped mentor me professionally and sustained my scientific curiosity; I have to begin by thanking my advisor, Dr. Russ Congalton. You have stood as a mentor and role model for me for the last six years. You have served as a teacher and guided me to teach in disciplines that before your coursework, I did not know existed. To my committee members: Dr. Mark Ducey, Dr. John Gunn, Dr. Nathan Torbick, and Dr. Richard Hallett, thank

you for being devoted to my success and for provide unique and invaluable perspectives on this research. I know that I have gained a lot through my interactions with each of you, and only wish that I had had more time to meet with you throughout these projects.

To the members of the Basic and Applied Spatial Analysis Lab (BASAL): Heather Grybas, Jianyu Gu, Molly Yanchuck, Katie Moran, Christine Healy, Peijun Sun, and Kamini Yadav. Thank you for helping me to survive the ups and downs of graduate school. You have each been a critical research, technical, and life support for me over these last six years. I have no doubt that I would still be trying to log into my computer or install ArcMap if not for your help. I would also not be writing this without the help of the several undergraduate research technicians that have supported this project. This includes Jacob Dearborn, Hannah Stewart, Vincent Pagano, and Caleb Russell. Each of you were diligent and patient as we worked through each of these studies. I hope that the lessons that we learned together are as helpful in your careers as they will undoubtedly be for me.

To the conservationists who laid the foundations for much of this research. I would like to thank Philip and George Lovejoy, Ron Klemarczyk, and George Manderscheid. You have provided the resources and knowledge necessary to initiate much of this research. Your devotion to the forests and natural areas is an often-underappreciated service. I hope that these results can be of service to you, and those of similar dedication to you.

Lastly, I have to thank the University of New Hampshire (UNH) for providing the academic environment that has been so accommodating to me for the last 10 years. Although there have been some discrepancies over the years (such as the countless parking tickets), the confluence of culture, people, and opportunities provided by UNH has fostered my growth and given me a community that I will always be grateful for.

Partial funding of this research has been provided through several University of New Hampshire and university associated sources. As a researcher in the Basic and Applied Spatial Analysis Lab (BASAL) within the Department of Natural Resources and the Environment, I received partial funding through the New Hampshire Agriculture Experiment Station. This work was supported by the USDA National Institute of Food and Agriculture McIntire Stennis Project #NH00095-M (Accession #1015520). In February of 2020, I received a Natural Resources and Earth Systems Science (NRESS) PhD Student Support Fund for research related expenses. Additionally, during my graduate research in 2019, I was awarded a Graduate Summer Teaching Assistant Fellowship (STAF) by the University of New Hampshire Graduate School. In 2017, I was awarded travel funds from Department of Natural Resources and the Environment Ruth Farrington Fund, to support expenses related to presenting at the American Society of Photogrammetry and Remote Sensing (ASPRS) Spring conference.

FOREWORD

Unmanned Aerial Systems (UAS) and contemporary tools in geospatial analysis offer exciting opportunities to those prepared to pave their own path and think creatively. The research contained within this document represents a culmination of hardware and software technologies that although presented challenges every step of the way, offered the ability to conduct previously unavailable inquiries into precision forestry. This work is both a continuation and an expansion of my master's research, completed at the University of New Hampshire in 2017. Although in some cases, the accuracy or the depth of the investigation fell short, due to the events of 2020 (Covid pandemic) and the time allotted for completing this degree, the results and insights gathered by both myself and those who collaborated on this research are immeasurable. Additionally, current literature suggests that it is only a matter of time before even more capable and accessible techniques are available. There is a lot to look forward to in the fields of computer science, remote sensing, Geographic Information Systems (GIS), Geographic Information Science, and forestry. Perhaps with the research that these and similar studies inspire, we can be one step closer to monitoring and managing global forests in a sustainable manner.

TABLE OF CONTENTS

ACKNOWLEDGEMENTS	iii
FOREWORD	vi
TABLE OF CONTENTS	vii
LIST OF TABLES	x
LIST OF FIGURES	xii
ABSTRACT	xiv
INTRODUCTION	1
Objectives	8
CHAPTER 1	10
ABSTRACT	10
BACKGROUND AND LITERATURE REVIEW	11
METHODS	16
Study Areas	16
Field Reference Data	18
Remotely Sensed Imagery	20
Classification Scheme	22
Forest Composition from Photo Interpretation	25
Forest Composition from Digital Classification	26
RESULTS	30
Accuracy/Uncertainty in Photo Interpretation	30
Image Segmentation and Tree Detection	38
Automated Classification	39
DISCUSSION	42
Analysis of Photo Interpretation Uncertainty	42
Analysis of Digital Classifications	44
Future Perspectives	47
CONCLUSIONS	48
CHAPTER 2	50
ABSTRACT	50
BACKGROUND AND LITERATURE REVIEW	51
METHODS	56
Study Areas	56
Field Data Collection	58
UAS Data Collection and Processing	61
Individual Tree Detection and Delineation	63

Tree Species Classification	65
UAS Regression Analysis and Biometrics	67
UAS Large Tree Survey.....	68
RESULTS	69
UAS-SfM Modelling	69
Individual Tree Detection and Delineation.....	69
Tree Species Classification.....	70
UAS Regression Analysis and Biometrics	71
UAS Large Tree Survey.....	75
DISCUSSION.....	77
CONCLUSIONS	82
CHAPTER 3	84
ABSTRACT.....	84
BACKGROUND AND LITERATURE REVIEW	84
METHODS	93
Study Areas.....	93
Assessing Forest Health: Field and Photo Interpretation Survey	94
Assessing Forest Health: Digital Image Classification.....	96
Forest Health Accuracy Assessment.....	99
RESULTS	101
Airborne Imagery	101
UAS Imagery	103
DISCUSSION.....	106
CONCLUSIONS	110
CONCLUSIONS.....	111
LITERATURE CITED	116
APPENDICES	142
APPENDIX 1.	143
Google Earth Photo Interpretation Key	143
NAIP Photo Interpretation Key	144
UAS Photo Interpretation Key.....	145
Classification Features	146
Photo Interpretation Uncertainty.....	147
Automated Classification.....	147
APPENDIX 2.....	151
Stand Level Classification	151
Tree Level Classification	151

APPENDIX 3.....	153
Tree Health Survey Reference Trees	153
Classification Features	154

LIST OF TABLES

Table 1. Forest inventory plot sample sizes, for each composition class during both the nine composition class photo interpretation and generalized four class photo interpretation.	30
Table 2. Plot level forest composition thematic accuracy for UAS photo interpretations of 9 classes	32
Table 3. Plot level forest composition thematic accuracy for UAS photo interpretations of 4 classes.	33
Table 4. Unmanned Aerial Systems (UAS) qualitative assessment of photo interpretation uncertainty.....	35
Table 5. Unmanned Aerial Systems (UAS) qualitative assessment of photo interpretation uncertainty for at individual forest inventory plots of varying species composition (4 classes)..	37
Table 6. Individual tree detection accuracy for the Unmanned Aerial System (UAS) imagery segmentation.	38
Table 7. Reference data samples sizes by class for individual tree classifications using the UAS and NAIP	39
Table 8. Thematic map accuracy assessment error matrix for individual trees using the UAS imagery and the SVM algorithm for 8 classes.....	40
Table 9. Thematic map accuracy assessment error matrix for individual trees using the UAS imagery and the RF algorithm for 3 classes.....	41
Table 10. Impacts of digital classification training/testing split designs using the RF classifier, UAS Imagery, and 8 composition classes.....	46
Table 11. Forest biometric equations for the stand level characterizations of structure and composition.....	60
Table 12. Individual tree crown features (parameters) derived from both eCognition and ArcGIS software tools.....	66
Table 13. Individual tree detection (ITD) accuracy.....	70
Table 14. Species-based classification thematic map error matrix conducted on nine species completed using the random forest (RF) supervised classification algorithm.....	71
Table 15. Thematic accuracy error matrices for the classification of large trees.	76
Table 16. Google Earth Photo Interpretation Key for the 9 forest classes.	143
Table 17. NAIP Imagery Photo Interpretation Key for the 9 forest classes	144
Table 18. UAS Imagery Photo Interpretation Key for the 9 forest classes.....	145
Table 19. Classification features used for the supervised classification of the NAIP and UAS imagery.....	146
Table 20. Thematic (overall) accuracy for plot level photo interpretations using each of the three high-spatial resolution remotely sensed data sources.....	147

Table 21. Thematic map accuracy assessment error matrix for individual trees using the UAS imagery and the CART algorithm for 8 classes. 149

Table 22. Thematic map accuracy assessment error matrix for individual trees using the UAS imagery and the RF algorithm for 8 classes. 150

LIST OF FIGURES

Figure 1. Digital photogrammetry representations of a champion aspen tree	7
Figure 2. Location and Unmanned Aerial System (UAS) orthoimagery coverage of the nine study areas in Southeastern New Hampshire (NH).	17
Figure 3. Depiction of the forest stands for each of the seven study areas, located in Southeastern New Hampshire.....	57
Figure 4. Linear regression between field measured dbh and crown area estimated using the UAS tree segments.....	73
Figure 5. Linear regression between field measured dbh and crown radius estimated using UAS tree segments.....	73
Figure 6. Comparison of field-based inventory estimates and UAS-based inventory estimates of stand level characteristics.	75
Figure 7. Feature importance values for the random forests classification input features for large trees	77
Figure 8. Four woodland properties evaluated during our assessment of forest health.....	94
Figure 9. Mean Decrease in Impurity (MDI) image feature scores calculated using the NAIP imagery and random forests classifier.	102
Figure 10. UAS classification feature importance scores calculated using the MDI test.	105
Figure 11. Frequency distributions (i.e., sample sizes) plotted by diameter at breast height (dbh) size ranges.....	113
Figure 12. Feature importance for NAIP imagery classification of 8 composition classes.....	147
Figure 13. Feature importance for UAS imagery classification of 8 composition classes.....	148
Figure 14. Feature importance for both the UAS and NAIP imagery classification of 4 composition classes.....	150

ABSTRACT

CHARACTERIZING FOREST STANDS USING UNMANNED AERIAL SYSTEMS (UAS) DIGITAL PHOTOGRAMMETRY: ADVANCEMENTS AND CHALLENGES IN MONITORING LOCAL SCALE FOREST COMPOSITION, STRUCTURE, AND HEALTH

By

BENJAMIN T. FRASER

University of New Hampshire, September 2021

Present-day forests provide a wide variety of ecosystem services to the communities that rely on them. At the same time, these environments face routine and substantial disturbances that direct the need for site-specific, timely, and accurate monitoring/management (i.e., precision forestry). Unmanned Aerial Systems (UAS or UAV) and their associated technologies offer a promising tool for conducting such precision forestry. Now, even with only natural color, uncalibrated, UAS imagery, software workflows involving Structure from Motion (SfM) (i.e., digital photogrammetry) modelling and segmentation can be used to characterize the features of individual trees or forest communities. In this research, we tested the effectiveness of UAS-SfM for mapping local scale forest composition, structure, and health. Our first study showed that digital (automated) methods for classifying forest composition that utilized UAS imagery produced a higher overall accuracy than those involving other high-spatial-resolution imagery (7.44% - 16.04%). The second study demonstrated that natural color sensors could provide a highly efficient estimate of individual tree diameter at breast height (dbh) (± 13.15 cm) as well as forest stand basal area, tree density, and stand density. In the final study, we join a growing number of researchers examining precision applications in forest health monitoring. Here, we

demonstrate that UAS, equipped with both natural color and multispectral sensors, are more capable of distinguishing forest health classes than freely available high-resolution airborne imagery. For five health classes, these UAS data produced a 14.93% higher overall accuracy in comparison to the airborne imagery. Together, these three chapters present a holistic approach to enhancing and enriching precision forest management, which remains a critical requirement for effectively managing diverse forested landscapes.

INTRODUCTION

Numerous disturbances and resource management challenges are influencing 21st century forests which require our best efforts if these ecosystems are to retain their vital functions. Many studies in recent decades have focused on quantifying and qualifying the direct and indirect outputs of ecosystem functions, or ecosystem services, to support decision making in policy and natural resource management (Lindenmayer, *et al.*, 2000; Young, 2010; Asbeck, *et al.*, 2021). These services include such things as water quality, net primary productivity, carbon sequestration, nutrient cycling, flora and fauna, and recreation. Most evaluations value these services to be much higher than their input costs; some even suggest ecosystem services are worth several times that of global economies (Costanza, *et al.*, 1997; Nowak, *et al.*, 2008; Foody, 2015). While there is still noted uncertainty in their exact contribution to societies, one aspect that cannot be denied is that many ecosystem services are being overburdened and degraded in our current setting. Issues such as land cover conversion, climate change, and invasive species are negatively altering the projections of future environments, at both global and local scales (Foody, 2002; Ge, *et al.*, 2007; Ackerly, *et al.*, 2015). While we struggle with understanding these conservation concerns, factors such as increasing populations and urbanization create further demands on the remaining resources (Congalton, *et al.*, 1993; McKinney, 2006). It is also already known that local variations and sensitivities to change are what's driving vegetative cover change and lowered resilience (Townshend, *et al.*, 1991; Ackerly, *et al.*, 2015). Such fine scale variability may contribute to misleading assumptions if unacknowledged or unrecognized. This sensitivity to local scale forest diversity and management is especially true here in New England as a major portion of the forested landscape, greater than 80%, is under private

ownership and management (Janowiak, *et al.*, 2018). At global and regional scales, we are beginning to refine our models of which forest ecosystems remain, what their condition is, and what negative impacts are influencing them. During this analysis, we must establish a specific definition for what a forest is, so that we can accurately monitor their distributions. For example, in this research, we define forests based on the definition by The Food and Agriculture Organization of the United Nations (FAO). In this definition, “forest includes natural forests and forest plantations. It is used to refer to land with a tree canopy cover of more than 10 percent and area of more than 0.5 ha. Forests are determined both by the presence of trees and the absence of other predominant land uses...” (FAO, 2000). Using these understandings, we must then make every effort to effectively collect and communicate about the relevant characteristics of the forested landscape.

It is evident that most of the world’s forests have been heavily modified from their natural state (IPCC, 2000; Hansen, *et al.*, 2001; FAO, 2016; Vitousek, 2016). The degree of change has been reflected in recent research by Gunn *et al.*, (2019) who have shown that New England Forest Inventory and Analysis (FIA) plots estimate 40% of the forest land as being understocked with desirable trees. Present day forest inventory and monitoring require accurate and timely data on the most relevant attributes to remain cognizant of landscape patterns and development (Coppin and Bauer, 1996; Betchold and Patterson, 2005; Goodbody, *et al.*, 2017). Many of the relevant forest inventory attributes correspond directly or indirectly with biophysical properties at the forest stand level. Forest stands are homogenous groupings of trees and associated vegetation, which comprise similar soils and climatic conditions (Oliver and Larson, 1996; Hyyppä, *et al.*, 2000). The dynamics of forest stands have been studied extensively and are used to influence the strategies used to achieve management objectives (Oliver and Larson,

1996). At the national scale, monitoring programs such as the U.S. Forest Service FIA program continually sample permanent plots to analyze resource trends (Tomppo and Katila, 1991; Smith, 2002; Koch, *et al.*, 2015; Pause, *et al.*, 2016). At the local scale, frameworks such as Continuous Forest Inventory (CFI) (or other systematic network) plots, set out by conservation groups or universities are available, but often slightly less discoverable (Eisenhaure, 2018). While the inventory designs of many of these programs are being continually enhanced, field-based methods still require a considerable amount of time, money, and effort, to collect sufficient data. As Redford (1992) has stated, “while the presence of trees has long been used as a surrogate for conservation, the system could be destroyed or degraded from within. Ground-based inventories may be able to model trends over time, but they often leave many of the characteristics of the forest stand to be desired.”

A combination of advancements in fields such as computer science, statistics, signal theory, and mathematics have encouraged the application of remote sensing and Geographic Information Systems (GIS) to overcome some of the shortcomings of field-based, or in situ, sampling at various scales of analysis (Avery, 1969; Hogland, *et al.*, 2018). Over the past century, basic and applied research in both fields, and the aggregation of ideas with other disciplines has led to natural resource conservation becoming an increasingly data driven science (Michener and Jones, 2012). Remote sensing offers a potential enhancement of inventory methods, creating both a cost-effective alternative and the ability to make measurements based on the total area covered instead of from isolated samples (Coppin and Bauer, 1996; Kerr and Ostrovsky, 2003; Liu and Yang, 2015; Shen and Cao, 2017; Lu, *et al.*, 2018). GIS and Geographic Information Science offer ways of handling these data by supporting data storage, exploratory data analysis, spatial statistical analysis, and geovisualization (Narumalani, *et al.*,

1997; Burrough, 2001). After decades of development, GIS have integrated the tools from various disciplines which can then be used to repeatedly test models and resolve issues that are inherently spatial (Goodchild, 1992; Congalton, *et al.*, 1993; Burrough, 2001; Longley, *et al.*, 2015).

The harmonization of field-based inventories, remote sensing imagery, and GIS analysis allows forest managers to turn vast amounts of data into decision supporting information. While forests lend themselves well to broad-scale inventories, it is important to retain assessments at larger (local) scales, as well (Ackerly, *et al.*, 2015; Sonti, 2015). The scaling of data from the landscape scale, to the forest stand, to the individual tree, and tree sub-components remains a major challenge for spatial statistics (Hansen *et al.*, 2001; Fortin *et al.*, 2012; Michener and Jones, 2012). In recent years, this emphasis on fine scale forest characterization has expanded into a field known as precision forestry. Precision forestry encompasses geospatially driven, site-specific forest management that is economically, environmentally, sustainability mindful (Taylor, *et al.*, 2002; Šumarstvo and Pripadajuće, 2010; Goodbody, *et al.*, 2017). Collecting and validating data at a greater number of scales benefits these efforts. Novel remote sensing technologies have made progress towards collecting the desired data to conduct precision forestry (Lehmann, *et al.*, 2015; Lu, *et al.*, 2018; Hadas, *et al.*, 2019), but that remains only the first step of the process.

Unmanned Aerial Systems (UAS) have been attributed with renewing perspectives on each stage of geospatial analysis. From data collection, to pre-processing, specific feature classification and extraction, and accuracy assessments, UAS have connected fundamental principles to modern methods. While not technically novel technology, UAS still face an ambiguous definition and preferred reference as anything from Unmanned Aerial Vehicle

(UAV), to Remotely Piloted Aircraft (RPA), Aerial Robotics, or drones (Barnhart, *et al.*, 2012; Colomina and Molina, 2014; Nex and Remondino, 2014; Maturbong, *et al.*, 2019). Here, in agreement with other researchers, we suggest UAS as the best term, as it captures the understanding that there are many essential components to make up the ‘system’ (Dalamagkidis, *et al.*, 2008; Marshall, *et al.*, 2016; Fraser and Congalton, 2018). A marked transition from solely military development can be seen following the advent of micro-computers in the early 2000s (Marshall, *et al.*, 2016; Cummings, *et al.*, 2017). This progression to civilian use is not unlike many other forest engineering technologies (e.g., Global Positioning System (GPS), laser range finding, and aerial reconnaissance) (Horcher and Visser, 2004).

Further hardware refinement, software development and market demands have promoted a burst of UAS applications, allowing end-user participation with little barrier of access. The expansion of users and personalized systems is projected to continue at a rapid pace through the turn of the next decade, supported by ultra-high-resolution data collection, on-demand deployment, platform flexibility, and low operational costs (Tang and Shao, 2015; Day, *et al.*, 2016; Corte, *et al.*, 2020; Rudge, *et al.*, 2021). Today’s UAS operations include: historic building re-creations (Püschel, *et al.*, 2008), wildlife inventories (Jones, *et al.*, 2006; Baylis, *et al.*, 2016), precision agriculture (Zhang and Kovacs, 2012; Gago, *et al.*, 2015), public safety (Kakaes, *et al.*, 2015; Turner, *et al.*, 2017; Bullock, *et al.*, 2019), geomorphology (Westoby, *et al.*, 2012; Hugenholtz, *et al.*, 2013; James, *et al.*, 2017), and rangeland plant surveys (Hardin and Jackson, 2005; Gillan, *et al.*, 2020). More specific to forests, UAS have been applied at several spatial scales for real-time fire monitoring (Merino, *et al.*, 2012; Fernández-álvarez, *et al.*, 2019), forest structure characterization (Fritz, *et al.*, 2013; Iizuka, *et al.*, 2017), and forest health assessments (Lehmann, *et al.*, 2015; Michez, *et al.*, 2016; Otsu, *et al.*, 2019).

Within the U.S., the lack of a clear regulatory framework for UAS in the National Airspace System (NAS) to integrate with piloted aircraft, has been a significant yet recently diminishing obstacle (Dalamagkidis, *et al.*, 2008; Cummings, *et al.*, 2017). With a controversial history of military use and poor judgement being highlighted in civilian operations, serious concerns for safety, ethics, security, and privacy are relevant (Marshall, *et al.*, 2016). To best suit various requested uses of UAS, a specific class of small UAS (sUAS) were distinguished, and a Remote Pilot in Command license (Part 107) was created (FAA, 2021). The establishment of this program, along with collaborations with various governmental agencies, designated testing facilities, and improved safety systems have reduced, but not eliminated, the burden of exploiting these cutting-edge technologies.

One substantial innovation leveraged with UAS technologies is the maturation of Structure from Motion (SfM) (i.e., digital photogrammetry or Structure from Motion Multi-View Stereo) semi-automated workflows (Burns, *et al.*, 2015; Smith, *et al.*, 2016; Noordermeer, *et al.*, 2019; Xu, *et al.*, 2020). SfM modelling allows users to create ultra-high-spatial-resolution products from uncalibrated imagery. These 2-dimensional (2D) and 3D data products may include photogrammetric point clouds, digital elevation models, or orthomosaics (**Figure 1**). Using these products, fine scale features can be visually or digitally characterized more effectively. In association with the ability to model individual landscape objects, such as individual trees, automated image segmentation algorithms have expanded considerably in the last decade (Chen, *et al.*, 2018; Puliti, *et al.*, 2018; Abdullah, *et al.*, 2019; Lobo Torres, *et al.*, 2020). The combined effect of spatial modelling and segmentation is the ability to quantify features that were previously unavailable.

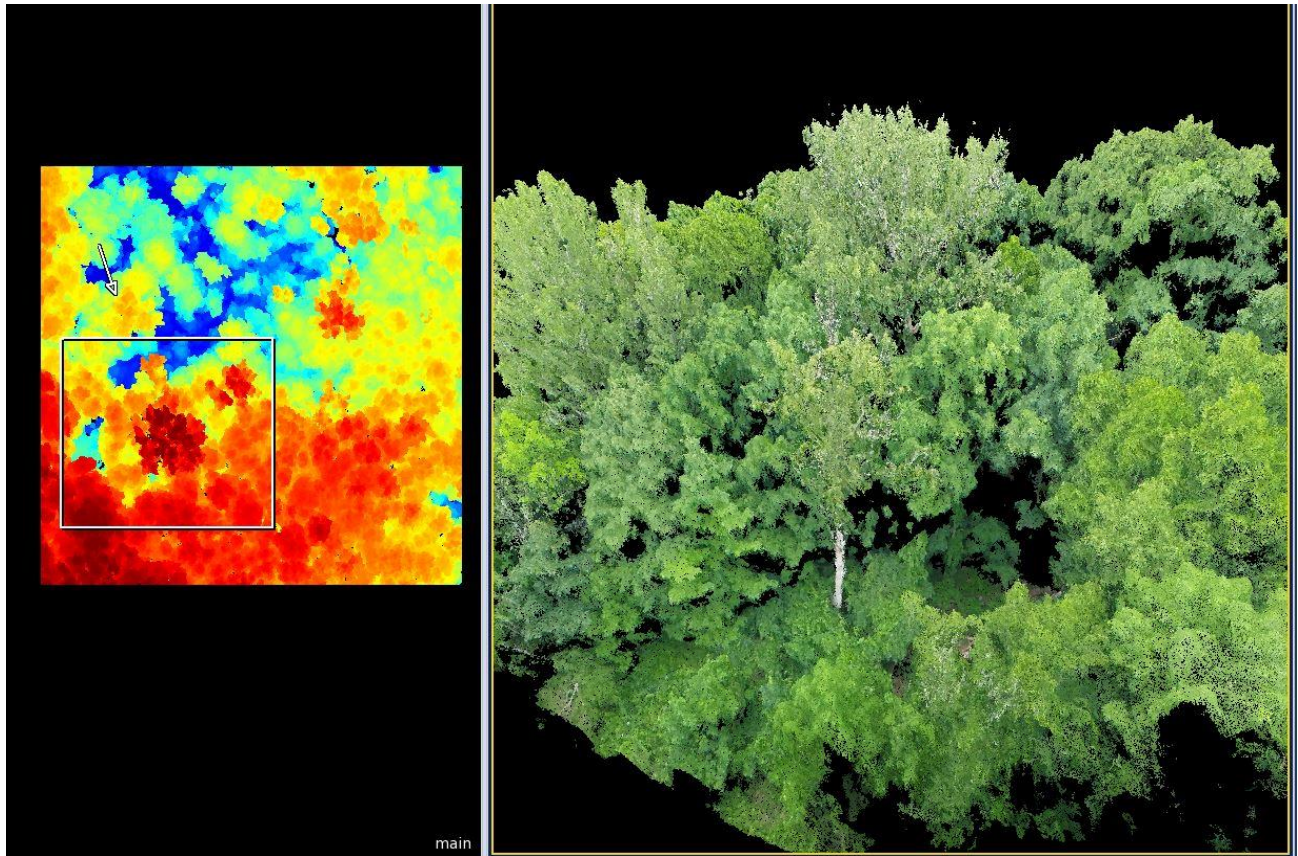


Figure 1. Digital photogrammetry representations of a champion aspen tree located at Kingman Farm, Madbury, NH. Left: Digital elevation model produced using Structure from Motion (SfM). Right: natural color photogrammetric point cloud.

The unification of technologies which contribute to UAS-SfM have presented both enhanced methods for acquiring vital forest ecosystem data, and new possibilities for integrating even further fields of knowledge. Although UAS-SfM was not designed for complex natural environments such as dense forests, its continued development may offer the chance to bridge gaps between local dynamics and broad-scale analyses (Harwin and Lucieer, 2012; Aguilar, *et al.*, 2019; Alvarez-Vanhard, *et al.*, 2020). However, understanding natural processes at the local level will require more than larger quantities of reliable data, more effective methods and communication must also be created (Lambin, *et al.*, 2001; Naidoo, *et al.*, 2008; Gunn, *et al.*, 2019). Therefore, the objectives of this research are to better characterize forest landscapes, by

focusing on the forest stand and individual trees. Several components of forest classification will be addressed to both update tools for guiding silvicultural management and establish novel methods of collecting data to inform larger-scale analyses (Oliver and Larson, 1996; Yurtseven, *et al.*, 2019). Both actions serve to define a niche for UAS by comparing these new methods to field-based practices and conventional remote sensing platforms. We are also testing these methods for exceptionally complex (structurally and compositionally) forests to ensure that the results are transferable to other natural environments (Nowacki and Abrams, 2015; Janowiak, *et al.*, 2018; Kirchhoefer, *et al.*, 2019). These forests represent ‘complex’ ecosystems due to their large number of species (i.e., compositionally complex) and high density of trees with overlapping canopies and diverse canopy architectures (i.e., structurally complex) (Ducey and Knapp, 2010; Harwin and Lucieer, 2012; Sankey *et al.*, 2017; Liang *et al.*, 2018).

This research will be divided into three sections that will be included in this dissertation as chapters and published separately as papers in peer-reviewed journals. The specific objectives for each section/chapter are as follows:

Objectives

CHAPTER 1

1. Compare digital (automated) and photo interpretation (manual) approaches for classifying fine scale forest composition using high-spatial resolution remotely sensed imagery.
 - a. Evaluate the photo interpretation accuracy and uncertainty for Google Earth, NAIP imagery, and UAS imagery.
 - b. Assess the digital classification of NAIP and UAS imagery using three supervised classification algorithms: CART, random forests, and SVM.

CHAPTER 2

1. Estimate forest stand biometrics derived from UAS-SfM models of Northeastern Forests.
 - a. Estimate tree specific dbh using crown geometry and UAS digital photogrammetry.
 - b. Calculate stand density using basal area and trees per acre by species.
 - c. Compare these UAS-based estimates to CFI plot field inventory measurements at the forest stand level.
2. Assess the detection of 'large' trees as economic and ecological indicators of forest condition.

CHAPTER 3

1. Determine the capability of UAS for classifying forest health at the individual tree level.
2. Compare the results of forest health classification using UAS to high-resolution, multispectral, airborne imagery.

CHAPTER 1: A Comparison of Methods for Determining Forest Composition from High-Spatial Resolution Remotely Sensed Imagery

ABSTRACT

Remotely sensed imagery has been used to support forest ecology and management for decades. In modern times, the propagation of high-spatial resolution image analysis techniques and automated workflows have further strengthened this synergy, leading to the inquiry into more complex, local-scale, ecosystem characteristics. To appropriately inform decisions in forestry ecology and management, the most effective and efficient methods should be adopted. For this reason, our research compares photo interpretation to digital (automated) processing for forest plot composition and individual tree identification. During this investigation, we qualitatively and quantitatively evaluated the process of classifying species groups within complex, mixed-species, forests in New England. This analysis included a comparison between three high-resolution remotely sensed imagery sources: Google Earth, National Agriculture Imagery Program (NAIP) imagery, and Unmanned Aerial Systems (UAS) imagery. We discovered that although the level of detail afforded by the UAS imagery spatial resolution (3.02 cm average pixel size) improved the photo interpretation results (7.87% - 9.59%) the highest thematic accuracy was still only 54.44% for the generalized composition groups. Our qualitative analysis of the uncertainty for photo interpreting different composition classes revealed the persistence of mislabeled hardwood compositions (including an early successional class) and an inability to consistently differentiate between 'pure' and 'mixed' stands. The results of digitally classifying the same forest compositions produced a higher level of accuracy for both detecting individual trees (93.9%) and labeling them (59.62% - 70.48%) using machine learning algorithms including Classification and Regression Trees, Random Forests, and Support Vector

Machines. These results indicate that digital, automated, classification produced an increase in overall accuracy of 16.04% over photo interpretation for generalized forest composition classes. Other studies, which incorporate multi-temporal, multispectral, or data fusion approaches provide evidence for further widening this gap. Further refinement of the methods for individual tree detection, delineation, and classification should be developed for structurally and compositionally complex forests to supplement the critical deficiency in local scale forest information around the world.

BACKGROUND AND LITERATURE REVIEW

The accurate identification of tree species is an important component of successful forest management (Shen and Cao, 2017; Zhao, *et al.*, 2020). For hundreds of years, societies have prepared land cover maps to better understand and manage the distribution of vegetation communities (Kuchler, 1976; Xie, *et al.*, 2008; Congalton, *et al.*, 2014). While the methodologies to produce such spatial representations have changed dramatically, it is apparent that these generalizations still serve as an important tool for solving a number of environmental problems (Martin, *et al.*, 1998; Foody, 2002; USGCRP, 2017). Many known drivers of ecosystem change and degradation stem from land cover and land use conversion at the local scale. For forested areas, this can mean a considerable reduction in neighboring area functionality and resource availability in addition to the influences of direct land cover transformation. With land cover maps, and especially forest cover type maps, serving to guide critical management decisions and research understanding, it is important that their representations are as reliable and as detailed as possible (Townshend, *et al.*, 1991; Zhao, *et al.*, 2020). Remotely sensed data have come to provide some of most accurate and cost effective

ways of producing such forest composition information (Avery, 1969; Shen and Cao, 2017). Modern high-spatial resolution imagery, with 1 meter or smaller pixels sizes, are becoming more attainable and as such are spurring a multitude of precision forestry applications (Ko, *et al.*, 2015; Maxwell, *et al.*, 2017; Berhane, *et al.*, 2018; Schepaschenko, *et al.*, 2019). Freely available high-resolution imagery from sources such as Google Earth provide users one such tool for compiling local scale information (Chen, *et al.*, 2015; He, *et al.*, 2017; Yadav and Congalton, 2017). Despite the undeniable benefits that this imagery provides, the best practices for using them to generate reliable and detailed forest cover information is yet undetermined.

For most research and management uses, raw imagery must be converted to information or classified (i.e., labeled or put into categories) to be effective for geospatial analysis. Classification involves the arrangement of objects into groups based on their relationship (Sokal, 1974). For land cover or land use classifications, the term thematic mapping could also be used (Pugh, 1997; Jensen, 2016). This arrangement of objects is a subjective, analytical, process which should be totally exhaustive, mutually exclusive, hierarchical, and defined by rules and labels to remain valid (Foody, 1999; Congalton and Green, 2019). The classification of remotely sensed imagery generates thematic maps (or layers) by distinguishing individual features based on a classification scheme. This creation of thematic maps is one of the most common applications of remotely sensed imagery (Foody, 2002; Verhulp and Niekerk, 2017). While there is a rich history of manually interpreted thematic layers, countless techniques have been developed using computer-based algorithms for reliably automating this procedure (Moessner, 1953; Avery, 1969; Holloway and Mengersen, 2018; Maxwell, *et al.*, 2018a; Schepaschenko, *et al.*, 2019). Identifying tree species through visual interpretation takes a trained specialist and remains time consuming for larger areas (Avery, 1969; Zhao, *et al.*, 2020). It is more common

today, that information on forest species is produced using automated approaches and high-resolution remotely sensed data (Schepaschenko, *et al.*, 2019; Zhao, *et al.*, 2020). To sufficiently handle the increasing amount of digital remotely sensed data, an approach called digital image processing has also been developed to analyze and explore the characteristics of the acquired imagery (Lillesand, *et al.*, 2015; Jensen, 2016; Maxwell, *et al.*, 2017).

The techniques for image classification are defined by several characteristics including simple or advanced, supervised or unsupervised, pixel-based or object-based (Otukey and Blaschke, 2010; Jensen, 2016). The first distinction, simple or advanced, specifies whether the algorithm integrates machine learning as a function for separating the defined classes. Following breakthroughs in computer science, classification algorithms used in thematic mapping began to integrate artificial intelligence (AI) or machine learning in the mid-1990s (Foody, 1999; Otukey and Blaschke, 2010; Maxwell, *et al.*, 2018b). Common and powerful examples of such classifications include decision trees (e.g., Classification and Regression Trees (CART) or random forests) and the support vector machine (SVM) algorithm (Breiman, 2001; Brown de Colstoun, *et al.*, 2003; Verhulp and Niekerk, 2017; Maxwell, *et al.*, 2018a). The second distinction, supervised or unsupervised, specifies whether the algorithm relies on training data to base its assignments (supervised classifications) or if the user defines some clustering parameters used to divide the sample units to maximize separability (unsupervised classifications) (Jensen, 2016). While conventional, supervised, algorithms are still used frequently for remote sensing image classification, machine learning methods have been found to generally perform better (Pal and Mather, 2005; Yu, *et al.*, 2014; Maxwell, *et al.*, 2018a). For the final distinction, pixel-based classifications (PBC) denote algorithms which operate on the smallest divisible unit of digital images, the pixel (Jensen, 2016). Object-based classifications (OBC) operate on homogenous

image primitives, also termed image areas, polygons, objects, or segments (Frauman and Wolff, 2005; Blaschke, 2010; Radoux, *et al.*, 2011). PBC relies heavily on spectral data to assign class labels, with only a few, more advanced, classification algorithms including ancillary information such as texture (Harris and Ventura, 1995; Lu and Weng, 2007; Fraser and Congalton, 2018). The increasing spatial resolution of remotely sensed data has caused subsequently greater challenges for positional registration and the heightened amount of detail in each pixel. Due to these challenges, classification methods have shifted towards using homogenous windows (e.g., 3x3 or 5x5 pixels) and/or image objects (Congalton and Green, 2019; Fraser and Congalton, 2019). OBC uses region-growing, thresholding, or clustering algorithms to segment images into more holistic units of analysis (Frauman and Wolff, 2005; Desclée, *et al.*, 2006). These image segments are commonly referred to as objects, polygons, areas, or primitives, in various disciplines. OBC incorporates greater context into each individual unit, such as size, compactness, spectral or geometric heterogeneity, and spectral averages, while maintaining user defined thresholds for between object variability (Coppin and Bauer, 1996). Like the preference for OBC over PBC, machine learning algorithms often allow for a greater number of inputs, reducing the reliance on spectral properties of individual pixels alone (Coppin and Bauer, 1996; Lehmann, *et al.*, 2015). Deciding between algorithms and classification approaches is a choice dictated by the specific needs of the project and the characteristics of the source imagery (Pugh, 1997; Lu and Weng, 2007).

To confront the constraints of time, money, and effort on site-specific (i.e., precision) forestry data collection, improved technologies need to be embraced (Šumarstvo and Pripadajuće, 2010; Hassaan, *et al.*, 2016; Baena, *et al.*, 2017; Goodbody, *et al.*, 2017). No longer considered ‘Dangerous, Dirty, and Dull contraptions’ (Barnhart, *et al.*, 2012), UAS have been

used in recent years for numerous high-precision applications (Lelong, *et al.*, 2008; Burns, *et al.*, 2015; Puliti, *et al.*, 2015; Goodbody, *et al.*, 2017; Gu and Congalton, 2021). Apart from the collection of raw imagery and videos, UAS imagery provides valuable information from 3-dimensional (3D) models created using Structure from Motion (SfM). The mathematical process behind SfM, or digital photogrammetry, provides a nearly autonomous workflow for reconstructing 3D surfaces from numerous 2D projections (images) (Verhoeven, *et al.*, 2012; Fonstad, *et al.*, 2013; Hugenholtz, *et al.*, 2013). The fundamental processing now in use has resulted from historic studies such as Ullman (Ullman, 1979), in which multiple representations of moving objects were used to form unique solutions of their 3D structure (Westoby, *et al.*, 2012; Bohlin, *et al.*, 2017, 2020). These algorithms are able to simultaneously calculate scene geometry, camera position, and camera orientation without the need of expensive, specialized, metric (i.e., calibrated) cameras (Westoby, *et al.*, 2012; Burns, *et al.*, 2015). UAS pairs well with this workflow given the ability to capture thousands of images, with the required overlap within a short amount of time.

In our study, we compared the capability of photo interpretation to digital processing for forest plot composition and individual tree identification using UAS and other high-spatial resolution remotely sensed imagery. A similar investigation by Holbling *et al.*, (2017), compared manual and semi-automated classification approaches for landslide mapping. They determined that while there were obvious trade-offs in the techniques, the final accuracy varied depending on the study site. In our analysis, we quantify the accuracy achieved when photo interpreting forest composition classes from three different sources of remotely sensed imagery (Google Earth, National Agriculture Imagery Program (NAIP), and Unmanned Aerial Systems (UAS)). We also provide a qualitative assessment of the uncertainty in forest composition mapping from

photo interpretation when using these image sources. To provide a comparison of these results with digital (automated) approaches, we quantified the individual tree identification accuracy achieved using the NAIP and UAS imagery. Three supervised classification algorithms were used for this test: CART, random forests, and SVM. This investigation provided a critical evaluation of the methods used to support local scale forest management, which for many parts of the world face a severe deficiency in coverage (Tang and Shao, 2015; Janowiak, *et al.*, 2018; Schepaschenko, *et al.*, 2019). We also specifically targeted UAS applications which can be adopted by a broad audience by implementing only natural color sensors and straightforward classification frameworks. Our research complements studies which have adopted multispectral, multi-temporal, Light Detection and Ranging (lidar), or hyperspectral approaches to UAS-based classifications of individual tree species (Sankey, *et al.*, 2017; Franklin and Ahmed, 2018; Gini, *et al.*, 2018; Xu, *et al.*, 2020). In doing so, we provided a novel investigation of the capability for UAS to enhance forest inventory assessments and extend the availability of structurally diverse and species rich forest species composition data and the most relevant methods to do so (Goodbody, *et al.*, 2017).

METHODS

Study Areas

A combination of nine forested properties, located in Southeastern New Hampshire were studied during this research. The properties included a total of 605.15 hectares (ha) of forested land comprising a variety of species compositions, forest successional classes, and stand structures (**Figure 2**). These sites were selected due to the availability of field-based inventory data (i.e., Continuous Forest Inventory (CFI) plots), and because of their limited management. The average size of these properties is 70.36 ha, while the smallest (Moore Fields) contains 17.2

ha of forested land cover. All but one of the properties, the Blue Hills Foundation lands, are owned and managed by the University of New Hampshire. These include: College Woods, Kingman Farm, Thompson Farm, Moore Fields, East Foss Farm, West Foss Farm, Dudley, and Burley-Demeritt (Woodlands, 2021). The Blue Hills study site is a contiguous forest, conservation lands, managed by the Harvard Forest.

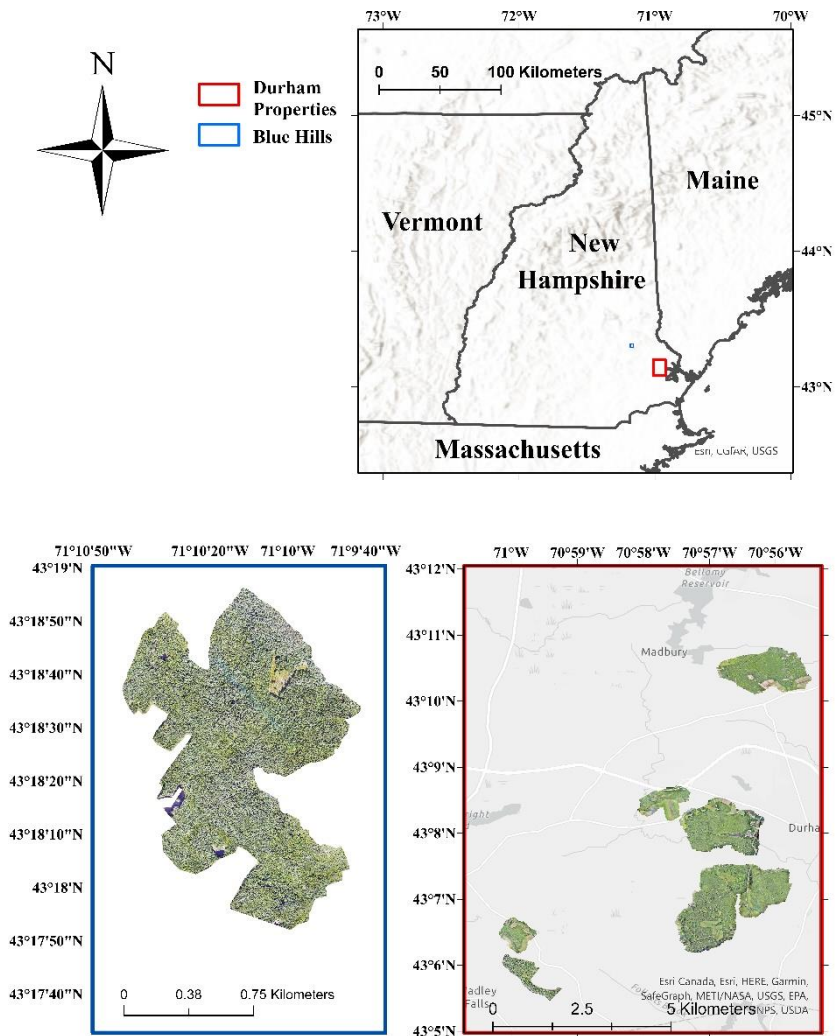


Figure 2. Location and Unmanned Aerial System (UAS) orthoimagery coverage of the nine study areas in Southeastern New Hampshire (NH). In Blue: The Blue Hills conservation lands in Strafford, NH. In Red: the eight University of New Hampshire (UNH) study areas located near Durham, NH.

Field Reference Data

Ground-based inventory designs are unique for each land manager. For UNH properties, forest inventory data are collected so that communities can be managed to maintain research integrity and characteristics of the broader New England region (Woodlands, 2021). Individual CFI plots are positioned systematically throughout each property with 1 plot per hectare (2.47 acres) (Eisenhaure, 2018). At each plot, an angle gauge methodology is used to elicit a probability proportional to size selection of each measured tree (Kershaw, *et al.*, 2016). The UNH woodlands office follows the regional recommendation of a basal area factor (BAF) $4.59 \text{ m}^2 / \text{ha}$ ($20 \text{ ft}^2 / \text{acre}$) inventory (Ducey, 2001; Eisenhaure, 2018). Any tree with a sufficient basal area and proximity from the plot center is recorded as a representative of the broader forest stand. Such methods give each plot a variable radius instead of a fixed size. Each selected tree had several biophysical measurements taken including: species name, diameter at breast height (dbh), collection date, and a silvicultural code (i.e., live or dead). Bearing and distance from the plot center were also recorded for all measured trees.

For several of the UNH woodlands included in this study, we elected to resample the plot locations and attributes ourselves to correct specific uncertainties. The newly resampled locations were chosen because the recorded positional accuracy appeared poor during exploratory data analysis and initial study (Fraser and Congalton, 2019). The GPS receivers now available include Wide Area Augmentation System (WAAS) positional averaging for improved registration with remotely sensed imagery. These study sites included College Woods, Kingman Farm, East Foss Farm, and Thompson Farm.

At the Blue Hills conservation lands in Strafford, NH, CFI plots follow a randomly generated distribution. Plot data, first collected in 2008, were distributed across upland forests

following a GIS analysis which removed areas within 50 m of parcel boundaries and non-forested land cover. To minimize spatial autocorrelation and capture a larger extent of the forest, a 50 m minimum spacing between plots was also defined. Individual inventory plots were resampled in 2010 and 2017, with the addition of 20 new plots in 2017. At each plot location, fixed area (20 x 20 m) plots were generated in which all trees taller than 1.4 m and with a dbh greater than or equal to 2.5 cm were measured (in cm). Vegetation recorded with a dbh smaller than 12.7 cm (5 inches) were filtered, however, to remove non-tree vegetation and present an estimate of species composition following a similar procedure as the other study sites.

The training data used for analysis of the digital classification approaches (i.e., individual tree classifications) in this study were generated from a combination of (1) ground-based inventory trees that were remeasured specifically for this analysis or (2) photo interpretations of CFI plot measured trees that were cross-referenced by two experienced, undergraduate technicians (Fraser and Congalton, 2021a). A high-precision EOS Arrow 200 RTK GPS with positional averaging was used to gather the locations of individual training trees for each class across several study areas (EOS, 2021). To ensure that a minimum number of both training and validation trees for each class were available, photo interpreters used a combination of the ground-based inventory trees, their local forestry knowledge (i.e., elements of photo interpretation for coniferous and deciduous trees), and specifically generated species-based training keys to generate additional reference data for several classes. For each class 70 reference trees were collected for use in both the NAIP and UAS supervised classifications. This reference data included each composition class found within our forest inventory plot classification scheme: white pine (*Pinus strobus*), Eastern hemlock (*Tsuga canadensis*), other conifers (e.g., red pine (*Pinus resinosa*)), American beech (*Fagus grandifolia*), oaks (*Quercus spp.*), red maple

(*Acer rubrum*), other hardwoods (e.g., shagbark hickory (*Carya ovata*)), and early successional forest species.

Remotely Sensed Imagery

To evaluate the use of photo interpretation for forest plot composition three image types were selected in this study. These are: Google Earth imagery, NAIP imagery, and UAS imagery. To evaluate the use of digital image analysis for forest plot composition and tree identification only the NAIP and UAS imagery were used. Our analysis began with evaluating photo interpretation because numerous research projects opt for photo interpretation of remotely sensed imagery as their source for reference data (e.g., Google Earth or airborne imagery) (Kirui, *et al.*, 2013; He, *et al.*, 2017; Oldoni, *et al.*, 2019; Schepaschenko, *et al.*, 2019). These data yield a synoptic view, can be cost effective, in modern times are high resolution, and in some cases provide multi-date or multispectral inferences. The Google Earth images are based on composites of natural color high-resolution satellite imagery with the most current, cloud free, and seamless appearance (Google Earth, 2021). For our study areas these included satellite imagery captured during the beginning of October 2018 and October 2020, with no specific sensor listed. The maximum resolution for the global coverage in Google Earth, however, is 15 m, with many areas featuring a much higher spatial resolution. The 2018 U.S. National Agriculture Imagery Program (NAIP) imagery maintains the same specifications as the imagery collected in 2016 (Maxwell, *et al.*, 2017; USDA, 2021). That is, New Hampshire was collected at a 60 cm spatial resolution with 4 spectral bands (blue, green, red, and near infrared (NIR)). For our study sites, NAIP imagery was collected between August 6th and October 16th, 2018.

Two fixed-wing unmanned aircraft, the senseFly eBee Plus and eBee X, deployed with natural color sensors were used to capture the UAS imagery for this research (senseFly, 2018,

2019a). The eBee Plus was deployed with its associated Sensor Optimized for Drone Applications (S.O.D.A.) while the eBee X was operated with the senseFly Aeria X sensor (senseFly, 2019b, 2019c). While the eBee X flight characteristics and camera quality are an improvement over the eBee Plus, hardware and logistical constraints required that several study areas were flown using the eBee Plus to ensure that summer leaf-on imagery (e.g., May – August in 2018, 2019, and 2020) could be captured. Both UAS were piloted using the eMotion flight management software (v3.15 and v3.19) (eMotion 2021). The preferred flight parameters were based on the results of previous research (Dandois, *et al.*, 2015; Fraser and Congalton, 2018). All missions were conducted with 85% forward overlap, 90% side overlap, winds perpendicular to the flight lines, consistent sun-angle and exposure, and flown at the Federal Aviation Administration (FAA) sUAS height limit of 121.92 m (400 ft) (Dandois, *et al.*, 2015; Puliti, *et al.*, 2015; Fraser and Congalton, 2018).

Following the collection of the UAS imagery, the individual image locations were post-processed using the National Oceanic and Atmospheric Administration (NOAA) Continuously Operating Reference Stations (CORS) network RINEX files and the given eBee flight log (NOAA, 2019). These positionally corrected images were then transferred to Agisoft MetaShape (v1.5.5.) for SfM modelling. Our processing workflow started with a “High Accuracy” image alignment to ensure that the maximum number of images could be aligned while still maintaining a precise alignment. Next, the “Ultra High” quality settings were selected to create the dense point cloud, digital elevation model (DEM), and orthomosaic. This maximum quality setting ensured that DEM was generated using the full resolution of the imagery, which is the foundation of the segmentation process in the next section (Gu, *et al.*, 2020). For each study area an ultra-high-resolution natural color orthomosaic and DEM were generated. These spatial data

products ranged in spatial resolution from 2.53 cm to 3.6 cm with an average pixel size (ground sampling distance) of 3.02 cm.

Classification Scheme

The characterization of New England Forest cover types is inherently difficult because of the density and species diversity of the trees (Nowacki and Abrams, 2015; Janowiak, *et al.*, 2018). Due to New England being a transition zone between boreal forests (to the north) and temperate hardwoods (to the south) there is a heterogeneous distribution of communities which must be captured even over small areas (Pugh, 1997). Several classification schemes exist for forest cover types in this region including Eyre (Eyre, 1980), Pugh, (1997), Justice et al., (2002), and MacLean et al., (2012). Each classification scheme uses the overstory tree species composition as a means of subdividing community types. The goal of our classification was to provide knowledge of the distribution of ecologically and economically similar forest stands. To best suit this goal and capture prominent and unique communities we adopted and modified the scheme given by Pugh, (1997). We began by defining forested land cover areas and individual trees. Here we used the definition by Anderson, (1976) as areas that have 10% or more aerial tree-crown density (coverage), capable of producing timber, and influential on the climate or water regime. Our definition of trees, based on the above forest-inventory methods, reflect woody vegetation with a minimum height of 3 m and a minimum diameter of 12.7 cm (5 inches). The first level of our classification hierarchy distinguishes Coniferous Forests, Mixed Forests, Deciduous Forests, and Early Successional Forests. Coniferous forests are forests which are dominated by tree species, comprising an overstory with greater than 66.6% basal area per unit area coniferous species. Mixed forests are forests which are dominated by tree species, comprising an overstory with less than or equal to 66.6% basal area per unit area and greater than or equal to 33.3% basal area per unit area coniferous species. Deciduous forests are forests which

are dominated by tree species, comprising an overstory with less than 33.3% basal area per unit area coniferous species. Lastly, early successional forests include forests which represent highly distinct tree composition and structure, are representative of unique ecosystem function and management, and are a key element of the New England landscape (King and Schlossberg, 2014). Here we include Birch (*Betula spp.*), Ash (*Fraxinus spp.*), and Aspen (*Populus spp.*) mixtures (not found in the previous classification scheme) within this ‘Early Successional’ category as an example of distinct early successional forests. The full definitions of each class within the next, more specific, level of forest classification are:

Coniferous (Softwood)

- **White Pine** - any forested land surface dominated by tree species, comprising an overstory canopy with greater than 70% basal area per unit area Eastern white pine.
- **Hemlock** - any forested land surface dominated by tree species, comprising an overstory canopy with greater than 70% basal area per unit area Eastern hemlock.
- **Mixed Conifer** - any forested land surface dominated by tree species, comprising other coniferous species besides white pine or Eastern hemlock (or a combined mixture of these species) that comprises greater than 66% basal area per unit area of the overstory canopy.

Mixed Forest

- **Mixed Forests** – any forested land surface dominated by tree species, comprising a heterogeneous mixture of deciduous and coniferous species each comprising greater than 20% basal area per unit area composition. Important species associations include eastern white pine and northern red oak (*Quercus rubra*), red maple (*Acer rubrum*), white ash (*Fraxinus americana*), eastern hemlock, and birches.

Deciduous (Hardwood)

- **Red Maple** – any forested land surface dominated by tree species, comprising an overstory canopy with greater than 50% basal area per unit area red maple.
- **Oak** – any forested land surface dominated by tree species, comprising an overstory canopy with greater than 50% basal area per unit area white oak (*Quercus alba*), black oak (*Quercus velutina*), northern red oak, or mixture of each.
- **American Beech** – any forested land surface dominated by tree species, comprising an overstory canopy with greater than 25% basal area per unit area American beech composition. This unique class takes precedence over other mentioned hardwood classes if present.
- **Mixed Hardwoods** - any forested land surface dominated by tree species, comprising other deciduous species besides red maple, oak, or American beech (or a combined mixture of these species) that comprises greater than 66% basal area per unit area of the overstory canopy.

Early Successional

- **Early Successional** - any forested land surface dominated by tree species, comprising an overstory composition that is highly distinct including areas dominated by early successional species such as paper birch (*Betula papyrifera*), white ash (*Fraxinus americana*) or aspen (*Populus spp.*).

Forest Composition from Photo Interpretation

Accuracy/Uncertainty from Photo Interpretation

At each CFI plot location, a 30 x 30 m fixed area, was registered to the plot center. Two trained, forest technicians interpreted and independently assigned a forest composition class to each NAIP, Google Earth, and UAS inventory plot sample. Any plot that was not interpretable in the imagery or was not labeled forest on any of the imagery sources was removed. This filtering of poor image quality locations resulted in a final sample size of 408 inventory plots. Each individual sample was interpreted a minimum of three times by each technician so that a combined consensus for each interpreter (rather than a single estimation) was determined. The majority composition, or mixture of classes, was then used to label the final plot composition for each source of imagery (see Fraser and Congalton, (2019)). A thematic map accuracy assessment error matrix was then used to quantitatively compare the plot level agreement for each imagery source to the field reference data (Congalton and Green, 2019). To aid the manual interpretation, training keys for each composition class were created for selected CFI plot locations for each image source. These training keys provided clear examples of each individual species and a distinct threshold between the forest classes. Additionally, both photo interpreters were trained using local reference imagery and the elements of photo interpretation regarding both coniferous and deciduous forest canopy characteristics. To ensure that each inventory plot was labeled

based on a consensus and not a single visual assessment, both interpreters classified each sample three times, leading to a total of six trials for each source of imagery. The consensus between these six trials were used to label the final composition for each inventory plot. The agreement (or conversely variability) between these six trials was investigated during our qualitative analysis of photo interpretation uncertainty.

Following the quantitative analysis of photo interpretation accuracy using each of the three remotely sensed imagery sources, we conducted a qualitative assessment of both specific and generalized composition class uncertainty. This qualitative assessment included a review a minimum of four inventory plots, randomly selected from each composition class. In total 36 of the original 408 plots were sampled. We then analyzed the variability and misclassification of such plots across each of the three interpretation trials that both photo interpreters conducted (6 in total). This test was completed for each of the three imagery sources so that similarities and differences in their ability to label individual classes could be better understood. We applied this qualitative analysis to both the more specific, 9-composition class scheme, and generalized, 4-composition class scheme.

Forest Composition from Digital Classification

Image Segmentation and Tree Detection

To evaluate the digital classification approaches, both the NAIP and UAS imagery were segmented and classified using three supervised classification algorithms. The Google Earth imagery was not classified using these methodologies as the data were only hosted within the Google Earth Pro software and therefore cannot be digitally processed.

We used a multiresolution segmentation technique, found within eCognition (v9.1) to delineate individual tree crowns on the NAIP imagery. A range of segmentation scale, shape, and compactness parameters were administered (e.g., Scale 10-600, Shape 0.1-0.7, Compactness 0.3-0.8). The results of these segmentation parameters were evaluated both qualitatively (i.e., visually) and quantitatively in comparison to manually digitized reference trees at several of our study areas. For the quantitative assessment, we calculated the over segmentation accuracy (Oa), under segmentation accuracy (Ua), and quality rate (QR) of each parameter combination for over 200 digitized reference trees. The goal of this segmentation was to provide pure tree species segments, which dictated that over segmentation took priority over the other evaluation metrics. Following the selection of an optimal parameter combination, individual tree crowns were delineated on the NAIP imagery. A total of 29 object level features (spectral, textural, and geometric attributes) were calculated for use in the supervised classification algorithms (see **APPENDIX 1**). Two of these features, the mean and the standard deviation of the near-infrared (NIR) band were unique to the NAIP imagery.

Segmentation of the UAS imagery was conducted using a marker-controlled watershed segmentation (MCWS) technique (Chen, *et al.*, 2018; Jianyu Gu, *et al.*, 2020). This MCWS workflow consisted of several stages, each reliant on the 3D tree crown data available for each study area. We began by creating an ultra-high-resolution canopy height model (CHM) based on the DEMs. A 2 m New Hampshire lidar bare earth dataset was used to adjust the SfM DEMs to height above elevation values (GRANIT, 2021). Next, we applied a Gaussian filter to this raster dataset to diminish excessive pits and peaks (i.e., noise) in the data (Panagiotidis, *et al.*, 2017; Chen, *et al.*, 2018; Gu, *et al.*, 2020). To begin the individual tree detection and delineation (ITDD) process, we applied a local maxima filter, with a fixed-window size, to the final filtered

CHM to establish the MCWS marker (i.e., individual tree crowns). A fixed, circular, window size of 45 cells (~1.65 m) was chosen for this step. This window size was selected during initial testing because it met our objective of avoiding under segmentation (omission error) as much as possible and for generating tree segments which represented only single species. Other similar studies for this region, selected larger fixed-window sizes for the purpose of determining the best performance for individual tree delineation as represented by QR at the expense of greater omission error (Gu, *et al.*, 2020; Fraser and Congalton, 2021a; Gu and Congalton, 2021). To quantify the individual tree detection error, we calculated the object detection rate (ODR), as well as the over detection (over segmentation or commission) and under detection (under segmentation or omission) by comparison with over 200 digitized reference trees (Mohan, *et al.*, 2017; Gu, *et al.*, 2020; Fraser and Congalton, 2021a). The next stage in the MCWS process consisted of masking the non-forested areas and large canopy gaps based on a minimum height threshold. A height threshold of 6 m was applied to the CHM prior to delineating the individual tree crowns (Hirschmugl, *et al.*, 2007). The final stage of the MCWS process applied the segmentation algorithm, which were initialized at the given markers and delineated tree boundaries using the height gradients from the CHM (Gu, *et al.*, 2020). Similar to the NAIP segmentation results, the final UAS tree segments were quantitatively and qualitatively evaluated against manually digitized reference trees using the Oa, Ua, and QR metrics (Chen, *et al.*, 2018). After this assessment of segmentation quality, 26 spectral, geometric, and textural features were generated for each tree segments using eCognition which were then available for use the digital classification approaches (see **APPENDIX 1**).

Automated Classifications

Three supervised classification algorithms were applied to tree segments generated from the NAIP and UAS data to label the segment into one of the classes in the classification scheme.

Multiple classification algorithms were implemented because of their often contradictory performance in other studies (Maxwell, *et al.*, 2018a). First, we applied a singular decision tree (CART) to determine if the complexity of our forests could be differentiated by a more simplistic classifier (Brown de Colstoun, *et al.*, 2003; Verhulp and Niekerk, 2017). Secondly, we applied a random forests (RF), ensemble classifier, made up of 500 decision trees to these same tree segments (Breiman, 2001; Maxwell, *et al.*, 2018a). We used the Gini index for this classification to control the decision tree splits (Loh, 2011; Krzywinski and Altman, 2017). For both decision tree-based classifications the mean decrease in impurity (MDI) was calculated for each of the included features to ensure an optimal confluence of input data could be enforced. In other words, individual features with the lowest scores could be pruned to both reduce the dimensionality of the classification and improve the overall accuracy. For the final supervised classification algorithm we implemented a support vector machine (SVM) classifier, based on the one-against-one form (Chapelle, *et al.*, 1999; Pal and Mather, 2005). A linear kernel was selected for the kernel function (Maxwell, *et al.*, 2018a). All three of these classifications were performed in Python using the Sickit-learn package and with all of the available geometric, spectral, and textural features (Leckie, *et al.*, 2003; Pedregosa, *et al.*, 2011; Gini, *et al.*, 2014; Franklin and Ahmed, 2018). Using this package, a number of procedures for selecting the training and validation samples were implemented. These included: (1) splitting the reference data to achieve a minimum validation sample size of 30 samples per class (i.e., 55% training and 45% validation); (2) splitting the reference data to achieve a minimum validation sample size of 30 samples per class and performing removing negatively influential features based on the MDI scores; (3) splitting the reference data to achieve a 65% training/ 35% testing split; and (4) conducting a permutation-based out-of-bag validation with 3% of the total sample size selected

for validation. We then elected to apply the procedure that achieved both the highest overall accuracy and maintained a statistically valid accuracy assessment (Congalton and Green, 2019). Each accuracy assessments for each of the classification methods and imagery sources was performed 10 times so that an average of their overall accuracy could be recorded.

RESULTS

Accuracy/Uncertainty in Photo Interpretation

The accuracy achieved when photo interpreting forest inventory plot level compositions using the Google Earth, NAIP, and UAS imagery was evaluated for both the nine class and four class composition schemes. The sample sizes and labels for these classes can be seen in **Table 1**. In total, 408 forest inventory plots were classified for each of the three imagery sources. A large portion of these plots, based on the field-inventory data were coniferous (a combination of white pine, Eastern hemlock, and mixed conifer composition classes).

Table 1. Forest inventory plot sample sizes, for each composition class during both the nine-composition class photo interpretation and generalized four class photo interpretation.

Photo Interpretation Sample (Inventory Plot) Sizes								
WP	EH	MC	MF	OAK	RM	AB	MH	ES
85	10	44	131	40	23	10	37	28
Conifer			MF	Deciduous				ES
139			131	110				28

Plot level classification accuracies using the each of the three high-resolution imagery sources were low given the species complexity of these forests (see **APPENDIX 1**). The overall accuracy for interpreting 9 classes using the Google Earth imagery was 29.9%. Classes such as

AB, EH, RM, and OAK, showed the lowest thematic accuracies. When generalized to only four classes, the overall accuracy using the Google Earth imagery increased to only 44.85%.

Interpreting these same plots using the NAIP imagery resulted in a similar performance. Our nine class thematic accuracy was 31.86%, while the generalized 4-class assessment resulted in an overall accuracy of 46.57%. Both the nine class and four class interpretation accuracies were higher when using the highest spatial resolution UAS imagery. The forest inventory plot compositions reached an overall accuracy of 39.46% for 9 classes (**Table 2**) and 54.44% for 4 composition classes (**Table 3**).

Table 2. Plot level forest composition thematic accuracy for UAS photo interpretations of nine classes

Field (Reference) Data												
		WP	EH	MC	MF	AB	RM	OAK	MH	ES	TOTAL	USERS ACCURACY
		UAS Photo Interpretation	WP	51	1	17	13	0	1	0	1	1
	EH	2	1	1	3	1	0	0	1	0	9	11.11%
	MC	5	3	3	9	0	1	0	1	2	24	12.5%
	MF	22	2	20	65	2	8	14	12	8	153	42.48%
	AB	0	0	2	0	3	0	0	1	0	6	50.0%
	RM	0	0	0	3	1	5	3	3	0	15	33.3%
	OAK	2	0	1	10	1	1	17	10	4	46	36.96%
	MH	2	3	0	25	2	5	6	6	3	52	11.54%
	ES	1	0	0	3	0	2	0	2	10	8	55.56%
TOTAL		85	10	44	131	10	23	40	37	28	161/408	
PRODUCERS ACCURACY		60.0%	10.0%	6.8%	49.62%	40.0%	21.74%	42.50%	16.22%	35.71%		OVERALL ACCURACY 39.46%

Table 3. Plot level forest composition thematic accuracy for UAS photo interpretations of four classes.

		Field (Reference) Data				TOTAL	USERS ACCURACY
		C	MF	D	ES		
UAS Photo Interpretation	C	84	26	3	3	116	72.41%
	MF	44	65	38	8	115	41.94%
	D	10	38	63	7	118	53.39%
	ES	1	2	6	10	19	52.63%
TOTAL		139	131	110	28	222/408	
PRODUCERS ACCURACY		60.43%	49.62%	57.27%	35.71%		OVERALL ACCURACY 54.44%

We conducted a qualitative assessment of the uncertainty incurred during the photo interpretation of complex, mixed-species, forests. Our assessment included the labeling of plot level composition across Google Earth, NAIP, and UAS imagery. **Table 4** shows a subsample of 36 plots where the results of the field data are compared to the photo interpretation results. For example, we see that the first OAK plot (**Table 4**), comprised of 81.2% OAK, with the remainder of the composition (18.2%) being American beech. With the proportion of OAK being greater than 50%, based on the field data, each of the interpretations should have also labeled the plot as OAK, however, there were several instances in which the interpreter labeled the plot as mixed hardwoods (MH). A MH classification would indicate that the plot was visually interpreted as having greater than 66% deciduous composition, while also consisting of less than

50% OAK composition and less than 20% AB composition. The final Eastern hemlock (EH) plot, containing 85.7% EH, was mislabeled once as mixed forest (MF) and twice as mixed conifer (MC). These interpretations indicated that the interpreters did not recognize a composition containing greater than 70% EH. For each of the four AB plots, and six interpretation trials each, these plots were only mislabeled as coniferous dominated once. The most common misclassification of AB plots was MH. This misclassification of AB as MH indicated that both interpreters did not recognize forest compositions containing greater than 20% AB. Photo interpretations conducted using the Google Earth imagery showed large amounts of uncertainty for all plots other than those heavily dominated by mixed forest (MF). Of the 36 plots that were included in this analysis, only three reported a consensus (4 or more labels in agreement) for the correct forest composition. The NAIP imagery photo interpretations fared slightly better. For these assessments, most classes were identified correctly labeled at least once. Composition classes such as WP, MH, and Early Successional (ES) were correctly identified more often with the NAIP imagery than the Google Earth imagery. Still, only five of the 38 plots were interpreted with a majority agreement for the correct composition. When interpreting the UAS imagery, there was a noticeable decrease in the uncertainty for identifying individual species (e.g., American beech and red maple). MH, however, showed a noticeable drop in successful identifications, when using the UAS imagery. Although individual classes were correctly identified more often, there was still a low percentage of classes which formed an agreement for the correct forest composition. Six of the 36 plots (16.7%) interpreted using the UAS imagery resulted in a majority agreement for correct composition class.

Table 4. Unmanned Aerial Systems (UAS) qualitative assessment of photo interpretation uncertainty for at individual forest inventory plots of varying species composition (9 classes) across six trials. Note: the green box indicates agreement with the field data while the red box indicates disagreement. The two photo interpreters are referenced as ‘J’ and ‘H’ with their three trials labeled each as ‘1’, ‘2’, and ‘3’.

Unmanned Aerial Systems (UAS) Photo Interpretation Uncertainty: 9 Composition Classes							
Field Data	Field-based Composition (%)	J-1	J-2	J-3	H-1	H-2	H-3
WP	87.5% WP, 6.3% EH, 6.3% AB	WP	MC	MC	WP	MC	MC
WP	75% WP, 12.5% RM, 12.5% MH	WP	MC	MC	WP	MC	MC
WP	83.3% WP, 8.3% OAK, 8.3% ES	MF	MF	MF	WP	MF	MF
WP	91.7% WP, 8.3% RM	WP	MC	WP	WP	MC	WP
EH	75% EH, 25% WP	WP	WP	WP	MC	WP	WP
EH	90% EH, 10% ES	EH	MF	MF	EH	EH	MC
EH	85.7% EH, 14.3% ES	EH	WP	EH	MC	MF	EH
EH	85.7% EH, 14.3% ES	MF	MC	EH	EH	EH	MC
MC	41.7% EH, 41.7% WP, 8% RM, 8% MH	MF	MC	EH	MC	WP	MF
MC	44.4% WP, 33.3% EH, 22.2% BB	EH	MC	EH	MC	MC	EH
MC	69.23% WP, 15.4% ES, 7.7% MH, 7.7% OAK	WP	WP	MC	WP	WP	WP
MC	45.5% WP, 27.3% EH, 27.3% OAK	MC	MF	WP	WP	MF	MC
MF	60% EH, 40% ES	EH	MF	MF	EH	EH	MF
MF	50% WP, 33.3% OAK, 8.3% MH, 8.3% RM	MH	MF	MF	MF	MF	MC
MF	54.5% WP, 45.5% OAK	MF	WP	WP	MF	MC	MC
MF	62.5% WP, 37.5% OAK	OAK	MF	MH	MF	OAK	MH
OAK	81.2% OAK, 18.2% AB	OAK	MH	MH	OAK	OAK	MH
OAK	66.7% OAK, 33.3% MH	MH	MH	MH	OAK	MF	EH
OAK	60% OAK, 20% RM, 20% WP	OAK	MH	MH	MH	MF	OAK
OAK	66.7% OAK, 33.3% EH	OAK	OAK	RM	OAK	OAK	OAK
RM	100% RM	MH	RM	MH	RM	MH	EH
RM	50% RM, 50% MH	ES	ES	ES	WP	ES	RM
RM	77.8% RM, 11.1% EH, 11.1% OAK	MH	RM	RM	RM	RM	AB
RM	60% RM, 20% WP, 20% OAK	MF	OAK	OAK	RM	RM	MH
AB	44.4% OAK, 33% AB, 22.2% EH	AB	OAK	OAK	AB	MH	EH
AB	33.3% MH 25% AB, 16.7% EH, 16.7% RM, 16.7% ES	AB	ES	AB	AB	AB	MH
AB	66.7% AB, 33.3% OAK	MF	MH	MH	AB	MH	RM
AB	40% AB, 20% RM, 20% MH, 20% ES	RM	MH	OAK	AB	OAK	OAK
MH	50% MH, 25% OAK, 25% EH	MH	MH	MF	OAK	MH	MF
MH	33.3% MH, 22.2% OAK, 22.2% ES, 11.1% EH, 11.1% RM	OAK	MH	MH	OAK	MC	MH
MH	37.5% RM, 25% MC, 25% ES, 12.5% OAK	OAK	MH	OAK	MF	MH	MF
MH	50% RM, 16.7% EH, 16.7% ES, 16.7% MH	MF	AB	AB	MF	AB	MH
ES	100% ES	ES	EH	ES	MF	EH	EH
ES	100% ES	MH	ES	AB	MF	ES	ES
ES	100% ES	OAK	MH	MH	MF	MH	MH
ES	100% ES	ES	ES	ES	WP	MH	ES

We also assessed the uncertainty in photo interpretations when the forest classes were generalized to conifer forest (C), deciduous forest (D), mixed forest (MF), and early successional forest (ES). For the Google Earth and NAIP interpretation assessments of forest composition, there was a less obvious contrast between the uncertainty incurred in labeling four classes and the uncertainty in labeling nine classes. Much of the misclassification for both imagery sources resulted in commission to the MF class, instead of a similar species dominance. Using the Google Earth imagery, nine of the 36 inventory plots were labeled correctly, based on a majority agreement. With the NAIP imagery, 11 of the 36 plots reported a majority agreement for the correct forest composition. Below in **Table 5**, we see the plot level interpretations using the UAS imagery. Classes such as WP, OAK, and American beech (AB) have fewer misclassifications at this level of generalization. The third ES plot, containing a 100% ES basal area composition was still mislabeled as deciduous during all trials. The third WP plot (third from the top) was incorrectly labeled MF during five of the six trials, despite containing only 8.3% OAK and 8.3% ES composition. Many of the MF classes were incorrectly labeled as either coniferous or deciduous dominated. Using the UAS imagery to photo interpret four generalized forest composition classes at the plot level resulted in the lowest amount of uncertainty. Overall, 28 of the 36 (77.78%) were labeled with a consensus for the correct forest composition.

Table 5. Unmanned Aerial Systems (UAS) qualitative assessment of photo interpretation uncertainty for at individual forest inventory plots of varying species composition (4 classes) across six trials. Note: the green box indicates agreement with the field data while the red box indicates disagreement. The two photo interpreters are referenced as ‘J’ and ‘H’ with their three trials labeled each as ‘1’, ‘2’, and ‘3’.

Unmanned Aerial Systems (UAS) Photo Interpretation Uncertainty: 4 Composition Classes							
Field Data	Field-based Composition (%)	J-1	J-2	J-3	H-1	H-2	H-3
C	87.5% WP, 6.3% EH, 6.3% AB	C	C	C	C	C	C
C	75% WP, 12.5% RM, 12.5% MH	C	C	C	C	C	C
C	83.3% WP, 8.3% OAK, 8.3% ES	MF	MF	MF	C	MF	MF
C	91.7% WP, 8.3% RM	C	C	C	C	C	C
C	75% EH, 25% WP	C	C	C	C	C	C
C	90% EH, 10% ES	C	MF	MF	C	C	C
C	85.7% EH, 14.3% ES	C	C	C	C	MF	C
C	85.7% EH, 14.3% ES	MF	C	C	C	C	C
C	41.7% EH, 41.7% WP, 8% RM, 8% MH	MF	C	C	C	C	MF
C	44.4% WP, 33.3% EH, 22.2% BB	C	C	C	C	C	C
C	69.23% WP, 15.4% ES, 7.7% MH, 7.7% OAK	C	C	C	C	C	C
C	45.5% WP, 27.3% EH, 27.3% OAK	C	MF	C	C	MF	C
MF	60% EH, 40% ES	C	MF	MF	C	C	MF
MF	50% WP, 33.3% OAK, 8.3% MH, 8.3% RM	D	MF	MF	MF	MF	C
MF	54.5% WP, 45.5% OAK	MF	C	C	MF	C	C
MF	62.5% WP, 37.5% OAK	D	MF	D	MF	D	D
D	81.2% OAK, 18.2% AB	D	D	D	D	D	D
D	66.7% OAK, 33.3% MH	D	D	D	D	MF	C
D	60% OAK, 20% RM, 20% WP	D	D	D	D	MF	D
D	66.7% OAK, 33.3% EH	D	D	D	D	D	D
D	100% RM	D	D	D	D	D	C
D	50% RM, 50% MH	ES	ES	ES	C	ES	D
D	77.8% RM, 11.1% EH, 11.1% OAK	D	D	D	D	D	D
D	60% RM, 20% WP, 20% OAK	MF	D	D	D	D	D
D	44.4% OAK, 33% AB, 22.2% EH	D	D	D	D	D	C
D	33.3% MH 25% AB, 16.7% EH, 16.7% RM, 16.7% ES	D	ES	D	D	D	D
D	66.7% AB, 33.3% OAK	MF	D	D	D	D	D
D	40% AB, 20% RM, 20% MH, 20% ES	D	D	D	D	D	D
D	50% MH, 25% OAK, 25% EH	D	D	MF	D	D	MF
D	33.3% MH, 22.2% OAK, 22.2% ES, 11.1% EH, 11.1% RM	D	D	D	D	C	D
D	37.5% RM, 25% MC, 25% ES, 12.5% OAK	D	D	D	MF	D	MF
D	50% RM, 16.7% EH, 16.7% ES, 16.7% MH	MF	D	D	MF	D	D
ES	100% ES	ES	C	ES	MF	C	C
ES	100% ES	D	ES	D	MF	ES	ES
ES	100% ES	D	D	D	MF	D	D
ES	100% ES	ES	ES	ES	C	D	ES

Image Segmentation and Tree Detection

Quantitative metrics (Oa, Ua, and QR) were used to determine an optimal set of multiresolution segmentation parameters to delineate individual tree crowns within the NAIP imagery. The optimal selection of segmentation parameters included a scale parameter of 10, a shape of 0.2, and a compactness of 0.5. Measuring the correspondence of these tree segments to 230 reference trees resulted in an Oa of 0.382, a Ua of 0.849, and a QR of 0.657.

For the MCWS of the UAS CHM and orthomosaic, we began by assessing the individual tree detection accuracy. A total of 231 samples were used for this assessment (**Table 6**). The 45-cell fixed window size led to an overall detection accuracy of 93.9%. This detection rate is a combination of the 231 reference trees that were detected as a singular canopy (correct or 1:1 detection) and those that were detected as multiple trees. In other words, only 6.1% of the reference trees were not detected (under detection or omission error). While a smaller window size did eventually remove the omission error, it caused every tree to be heavily over segmented. A larger window size increased the omission error (under detection) to greater than 10%.

Table 6. Individual tree detection accuracy for the Unmanned Aerial System (UAS) imagery segmentation.

Correct Detection	Over Detection (Commission Error)	Under Detection (Omission Error)	Total
85	132	14	231
36.80%	57.14%	6.1%	Overall Detection Accuracy 93.9%

Continuing through the MCWS process, we quantitatively evaluated the final segmentation results against these same 231 reference samples (Chen, *et al.*, 2018). These UAS tree segments resulted in a Oa of 0.73, a Ua of 0.523, and a QR of 0.6438.

Automated Classification

Both the NAIP and UAS imagery were evaluated for their effectiveness in identifying individual trees using three supervised digital classification algorithms. The sample sizes for each of the eight composition classes for both imagery sources are included in **Table 7**. Since these are for labeling individual trees, the mixed forest class is not possible.

Table 7. Reference data samples sizes by class for individual tree classifications conducted using the UAS and NAIP automated approaches.

Individual Tree Reference Data Sample Sizes								
	WP	EH	OC	ES	OH	OAK	RM	AB
NAIP	97	76	90	79	77	135	95	77
UAS	102	77	85	74	88	152	97	77

Individual tree digital classifications using the segmented NAIP imagery were generated using the CART, RF, and SVM classifiers. Following the examination of feature importance scores (see **APPENDIX 1**), we removed the gray level co-occurrence matrix (GLCM) contrast, GLCM dissimilarity, border index and gray level difference vector (GLDV) contrast for the NAIP imagery CART and RF classifications. This removal resulted in an increase in overall accuracy of 1.13% and 1.55% for CART and RF respectively. The overall accuracy of labeling 8 classes for the three classifiers were 21.44% (CART), 29.23% (RF), and 29.36% (SVM).

The digital classification of eight composition classes using UAS imagery resulted in higher overall accuracies for each of the three supervised classifiers. For this imagery, the least

important features were asymmetry, density, shape index, radius of the short ellipsoid, and compactness (see **APPENDIX 1**). The removal of these features improved the overall accuracies between 0.235% (CART) and 1.33% (SVM). The overall accuracies for eight composition classes using the UAS imagery, based on an average of 10 iterations were 33.27% (CART), 46.67% (RF), and 46.90% (SVM) (**Table 8**). These UAS thematic accuracies are, on average, a 15.60% increase over the same methods when using the NAIP imagery.

Table 8. Thematic map accuracy assessment error matrix for individual trees using the UAS imagery and the SVM algorithm for 8 classes.

Field (Reference) Data											
		WP	EH	OC	AB	RM	OAK	OH	ES	TOTAL	USERS ACCURACY
UAS Imagery Using the SVM Classifier	WP	36	4	6	0	1	1	7	2	57	63.16%
	EH	2	16	3	13	4	6	3	7	54	29.63%
	OC	5	1	20	1	2	2	3	2	36	55.56%
	AB	0	6	2	14	2	2	3	3	32	43.75%
	RM	1	2	0	1	18	2	4	3	31	58.06%
	OAK	0	4	2	4	7	49	13	9	88	55.68%
	OH	2	1	4	0	6	4	6	1	24	25.0%
	ES	0	1	1	2	4	2	1	6	17	35.29%
TOTAL		46	35	38	35	44	68	40	33	165/339	
PRODUCERS ACCURACY		78.26%	45.71%	52.63%	40.0%	40.91%	72.06%	15.0%	18.18%		OVERALL ACCURACY 48.67%

The overall classification accuracies for both the NAIP and UAS imagery increased when the eight classes were collapsed to conifer, deciduous, and early successional. We again evaluated the feature importance for both the NAIP and UAS image classifications (see **APPENDIX 1**), to determine the optimal feature selection for classifying coniferous, deciduous, and early successional cover types. Both imagery sources showed a consensus for the most important (e.g., greenness and brightness) and least important (e.g., border index and compactness) features. The NAIP imagery correctly classified on average 45.32% of the tree segments using the CART algorithm. Using the RF and SVM algorithms, the average overall accuracies increased to 53.58% and 52.69% respectively. Classifying these same image segments using the UAS imagery produced average overall accuracies of 59.62% (CART), 70.48% (RF) (**Table 9**) and 68.59% (SVM).

Table 9. Thematic map accuracy assessment error matrix for individual trees using the UAS imagery and the RF algorithm for three classes.

Field (Reference) Data						
		C	D	ES	TOTAL	USERS ACCURACY
UAS Imagery Using the RF Classifier	C	86	18	18	122	70.49%
	D	27	126	34	187	67.38%
	ES	6	8	11	25	44.0%
	TOTAL	119	152	63	229/334	
PRODUCERS ACCURACY		72.27%	82.89%	17.46%		OVERALL ACCURACY 68.56%

DISCUSSION

Analysis of Photo Interpretation Uncertainty

The qualitative analysis of photo interpretation uncertainty showed regular progression in the ability to differentiate composition classes within complex forests. When classifying more specific composition classes (i.e., 9 groups) we saw that all three remotely sensed imagery sources struggled to provide a consensus across six interpretation trials. Such a consensus is needed to provide both an accurate and confident label for the composition of each inventory plot. The UAS imagery also showed slightly less variability in the identification of more pure species classes, in comparison to the Google Earth and NAIP imagery. The perceived ability to identify individual species however, also led to a lower percentage of plots labeled as mixed hardwoods or mixed conifers. Other classes, such as EH, demonstrated that even with nearly absolute plot composition (> 85%) there was a significant amount of confusion and misclassification with other species. Such classes likely require further training or revision of the classification scheme (Avery, 1969; Zhao, *et al.*, 2020). When the forest composition was generalized to only four classes, all three imagery sources showed a considerable reduction in misclassifications. While there was still some confusion between specific mixtures or dominance, many of the plots for each source of imagery could be identified at least in these basic compositional groups. Additional classification rules such as forming a hierarchical classification by first identifying the plot as coniferous, deciduous, mixed, or other forest could have bridged this gap in misclassifications (Verhulp and Niekerk, 2017). One potential source of confusion in the labeling of these inventory plots could have been the presence and visual perception of large trees. Large trees are known to disproportionately account for stand structure and function (Whitman and Hagan, 2007; Fraser and Congalton, 2021a). A few large trees (or even a single tree in some cases) could have accounted for a large portion of the perceived plot

composition based on the synoptic view of the photo interpreter. These same trees, however, may not be representative of the same compositional dominance when measured using the variable plot radius design that we used to collect the field-based reference data. This research was conducted within the transition forest region of New England forests (Janowiak, *et al.*, 2018). These mixed specific forests comprise a rich diversity of hardwood species at local scales but also contain a common white pine and Eastern hemlock component. The lower spatial resolution Google Earth and NAIP imagery may suffer from this tendency for species mixtures, as both result in a large amount of MF commission error, even during the labeling of on four composition classes. Lastly, certain classification scheme edge cases (e.g., a plot with 33% coniferous composition which could be interpreted as deciduous dominated or MF depending on the interpreter) were found during this qualitative analysis.

When looking at the overall thematic accuracies for the Google Earth, NAIP, and UAS plot level interpretations we formed several important insights. For both the 9-class composition accuracy and the 4-class composition accuracy, the Google Earth and NAIP imagery produced approximately equal results (\pm approximately 2%). Both sources of imagery demonstrated a considerable amount of commission error for the MF class. The NAIP imagery acquisition (influencing phenology) and image characteristics were not consistent, leading to challenges in interpretations across study areas (Maxwell, *et al.*, 2017). Further spatial data exploration and pre-processing before using the NAIP imagery could be integrated to influence species classification success. Despite the increased spatial resolution to only 3.02 cm using the UAS imagery however, the highest overall accuracy achieved using photo interpretation was still only 54.44%. As with other studies, specific hardwood classes and early successional species

mixtures (ES) showed a high amount of thematic classification error (Franklin and Ahmed, 2018).

Analysis of Digital Classifications

Despite watershed segmentation being one of the most common and powerful methods for delineating tree crowns given the availability of 3D data, the visual assessment of tree segment quality was never absolute for all species (Chen, *et al.*, 2018; Gu, *et al.*, 2020). Our individual tree detection accuracy produced a final omission error of 6.1%, similar to other studies conducted using remotely sensed data (Shen and Cao, 2017; Xu, *et al.*, 2020). During the manual refinement of the digital classification training samples, it was observed that many tree segments still contained some portion of a species mixture. The occurrence of mixed-species tree segments was especially common for the large coniferous trees, which displayed the lowest classification accuracy. The individual segments for these large coniferous trees commonly absorbed neighboring sub-dominant canopy deciduous trees. A more advanced segmentation technique could be adopted in future studies to better produce pure tree segments (Gu and Congalton, 2021)

Turning to the automated individual tree classification results, the UAS imagery produced on average a 15.65% increase in overall accuracy over the NAIP imagery when comparing the same classification algorithms and composition classes. Digital classification of the NAIP imagery, as with the interpretation analysis likely suffers from inconsistencies in collection date and spectral characteristics (Maxwell, *et al.*, 2017). The highest overall accuracy for eight classes was achieved using the UAS imagery and the SVM classifier, at 46.90%. This classification accuracy represents a 7.44% higher accuracy than photo interpretations at the plot

level, for the more discrete classification scheme. Both the NAIP and UAS imagery supervised classifications still result in low accuracies for more specific classes such as EH and RM, however. In the automated classification of generalized (3) classes, we again observed an increase in performance for the UAS imagery over the NAIP imagery. The accuracy of the UAS imagery was on average 15.70% higher for the three supervised algorithms in comparison with the NAIP imagery. The highest overall accuracy for the 3-class automated classification was produced using the UAS and the RF algorithm, at 70.48%, which is an increase over the four-class photo interpretation accuracy of 16.04%. Achieving a higher overall accuracy for eight classes using the SVM algorithm and for three classes using the RF algorithm is not inconsistent with other findings. Many studies have either evaluated the results of multiple machine learning algorithms or found that the best classifier is application dependent (Belgiu and Drăgu, 2016; Maxwell, *et al.*, 2018a; Wessel, *et al.*, 2018). As part of our initial testing, we compared various procedures for training and validating these individual tree classifications (**Table 10**). These methods included: (1) splitting the reference data to achieve a minimum validation sample size of 30 samples per class; (2) splitting the reference data to achieve a minimum validation sample size of 30 samples per class and performing removing negatively influential features; (3) splitting the reference data to achieve a 65% training/ 35% testing split; and (4) conducting a permutation-based out-of-bag validation with 3% of the total sample size selected for validation. Based on both the performance and statistical validity, we applied the second method for each of the digital classification evaluations (Holloway and Mengersen, 2018; Congalton and Green, 2019).

Table 10. Impacts of digital classification training/testing split designs using the RF classifier, UAS Imagery, and eight composition classes.

Individual Tree Classification Accuracies using the RF classifier, UAS Imagery, and 8 and 3 Composition Classes.				
	55% Training / 45% Testing	55% Training / 45% Testing with Feature Reduction	65% Training / 35% Testing	Out-of-Bag (OOB) Validation
Minimum Sample Size	30 per Class	30 per Class	26 Per Class	Permutations of 3% from the total
Average Accuracy 8 Classes	45.84%	46.67%	43.07%	45.84%
Average Accuracy 4 Classes	64.01%	70.48%	65.36%	65.51%

Similar studies, employing the use multispectral and multi-temporal UAS have been known to produce higher overall accuracies. In Gini et al., (2018) accuracies were produced which ranged from 58% to 87%. These findings, however, were for the classification of several hardwood species within a private nursery, which is different from the species-rich, New England forests evaluated here. Xu et al., (2020) produced comparable accuracies for 8 subtropical species (conifer and deciduous) by incorporating both multispectral imagery and use of the photogrammetric point cloud. For the classification of eight, conifer and deciduous, species they found a 65% overall accuracy and an 80% overall accuracy for labeling only coniferous and deciduous species. The inclusion of multispectral bands and indices, or simply an increase in spectral resolution, would likely increase the classification accuracy when using the UAS imagery (Zaman, *et al.*, 2011; Candiago, *et al.*, 2015; Gini, *et al.*, 2018; Otsu, *et al.*, 2019). One of the most important features, as reported in **Figure 2** and **Figure 4**, for the NAIP imagery individual tree classifications was the NIR band. Numerous studies have outlined the importance of NIR reflectance in tree species classification (Fassnacht, *et al.*, 2016; Maxwell, *et al.*, 2017; Hernandez-Santin, *et al.*, 2019). Our results however, show that natural color photogrammetric

sensors, which provide a more efficient and sometimes more effective platform for surveying contiguous forests, can be used with a decrease in accuracy of approximately 10% (Fraser and Congalton, 2018). One important factor for this success was selection and reduction in classification features (Mishra, *et al.*, 2018). Our MDI test and subsequent feature reduction, while only resulting in a 2% difference in classification accuracy here, will become more important as the number of features and spectral complexity is increased (Persad and Armenakis, 2017; Holloway and Mengersen, 2018). Lastly, image segmentation quality improvements could be explored to enhance individual tree classification. High-resolution image segmentation techniques and individual tree detection and delineation methods are being developed at a rapid pace (Pal and Pal, 1993; Chen, *et al.*, 2018; Yan, *et al.*, 2018; Lobo Torres, *et al.*, 2020; Gu and Congalton, 2021). The ability to accurately detect and delineate the range of tree species and crown morphologies present in this landscape would provide more representative training samples for each species and therefore enhance the potential of each classification algorithm.

Future Perspectives

Future research should continue to investigate the best methods for adopting UAS for fine scale (i.e., precision) forest management (Tang and Shao, 2015; Franklin and Ahmed, 2018; Janowiak, *et al.*, 2018). Data fusion techniques, such as the integration of both satellite and UAS data (Effiom, *et al.*, 2019), or optical and lidar (Sankey, *et al.*, 2017; Shen and Cao, 2017), present methods for overcoming the limitations of UAS digital photogrammetry and achieving high accuracies for individual tree identification. Advanced classification algorithms may also present a variety of methods for better handling of the data dimensionality. However, such techniques would require a far greater amount of training data and technical expertise to

complete (Holloway and Mengersen, 2018; Maxwell, *et al.*, 2018a). The extension of forest composition data from one location for classification of another could provide several advantages to forest managers, such as semi-automated classifications, considerable gains in time, cost reductions, and lower expert user knowledge required when given proper consideration for potential sources of uncertainty (Leukert, *et al.*, 2004). Unlike satellite-based generalizations of forest composition data across study sites, UAS are not prone to the same dissimilarities in image characteristics (Pax-Lenney, *et al.*, 2001; Leukert, *et al.*, 2004; Verhulp and Niekerk, 2017). Instead, UAS applications face a myriad of rapidly evolving computer vision and data science challenges and solutions (Michener and Jones, 2012). The development of these disciplines and tools is hoped to lead to achieving sufficient tree level accuracies, which can then be aggregated to the plot or forest stand levels.

CONCLUSIONS

Trends in automated and semi-automated forest classifications using high-resolution remotely sensed data have made the thematic classification of individual trees a realistic aspiration. In this study, we evaluated, both qualitatively and quantitatively, the application of Google Earth, NAIP, and UAS imagery for plot composition and individual tree identification. For this analysis, we compared photo interpretation and digital processing approaches. Our results indicated that supervised, machine learning, classifiers outperformed photo interpreters for specific (+ 7.44%) and generalized (+ 16.04%) species composition. While photo interpretation is commonly applied for broad scale inferences of forest composition, the uncertainty for labeling more specific classes as well as the costs required to train interpreters makes fine-scale assessments impractical. Our results indicate that automated, machine learning,

approaches can be an effective alternative for local scale forest surveys, even with only single-date natural color imagery. In comparison with other research, the inclusion of multi-temporal imagery, multispectral imagery, or more advanced segmentation techniques would likely increase this divide even further. Subsequent studies should continue to examine diverse forests and geospatial analysis techniques for delineating the trees within them.

CHAPTER 2: ESTIMATING PRIMARY FOREST ATTRIBUTES AND RARE COMMUNITY CHARACTERISTICS USING UNMANNED AERIAL SYSTEMS (UAS): AN ENRICHMENT OF CONVENTIONAL FOREST INVENTORIES

ABSTRACT

The techniques for conducting forest inventories have been established over centuries of land management and conservation. In recent decades, however, compelling new tools and methodologies in remote sensing, computer vision, and data science have offered innovative pathways for enhancing the effectiveness and comprehension of these sampling designs. Now, with the aid of Unmanned Aerial Systems (UAS) and advanced image processing techniques we have never been closer to mapping forests at field-based inventory scales. Our research, conducted in New Hampshire on compositionally complex, mixed-species forests, utilized natural color UAS imagery for estimating individual tree diameters (diameter at breast height (dbh)) as well as stand level estimates of Basal Area per Hectare (BA/ha), Quadratic Mean Diameter (QMD), Trees per Hectare (TPH), and a Stand Density Index (SDI) using digital photogrammetry. To strengthen our understanding of these forests, we also assessed the ability of UAS to map the presence of large trees (i.e., > 40 cm in diameter). We assessed the ability of UAS digital photogrammetry to identify large trees in two ways: (1) using the UAS estimated dbh and the 40 cm size threshold and (2) using a random forests supervised classification and a combination of spectral, textural, and geometric features. Our UAS-based estimates of tree diameter reported an average error of 19.7% to 33.7%. At the stand level, BA/ha and QMD were overestimated by 42.18% and 62.09% respectively, while TPH and SDI were underestimated by 45.58% and 3.34%. When considering only stands larger than nine ha however, the overestimation of BA/ha at the stand level dropped to 14.629%. The overall classification of large trees, using the random forests supervised classification achieved an overall accuracy of

85%. The efficiency and effectiveness of these methods offer local land managers the opportunity to better understand their forested ecosystems. Future research into individual tree crown detection and delineation, especially for co-dominant or suppressed trees, will further support these efforts.

BACKGROUND AND LITERATURE REVIEW

The alteration of forest stand dynamics by mechanisms such as anthropogenic climate change, landscape fragmentation, land cover change, and overutilization have driven the need to revise our conventional forest management tools and procedures with modern technologies without forgetting silvicultural fundamentals. With the support of more contemporary workflows, forestry professionals can make more effective decisions. The main objective of many forest inventories is to quantify the size, structure, and distribution of observed tree species (Smith, 2002; Eisenhaure, 2018). Numerous plot sampling designs have been established and refined over the centuries based on silvicultural practices and evolving technologies (Husch, *et al.*, 1972; Betchold and Patterson, 2005; Kershaw, *et al.*, 2016; Zhou, *et al.*, 2018; Cao, *et al.*, 2019). However, field-based campaigns are still severely limited in terms of their temporal and spatial scales. These inventory designs also do not often record the full suite of forest attributes, which could be useful for managing and understanding the dynamics of forest communities.

For many researchers and land managers, forest characterization has been achieved through sampling designs which quantify stand basal area and tree density (Stage and Rennie, 1994; Cade, 1997; MacLean and Congalton, 2012; Shang, *et al.*, 2020; Xu, *et al.*, 2020). Basal area, or the cross-sectional areas of a tree at breast height, is used to define size classes, and therefore, inferring stand dynamics such as resource availability and competition (Oliver and Larson, 1996; Cade, 1997; Kershaw, *et al.*, 2016). Tree density, a measure of the number of trees

per unit area (e.g., hectare), provides insight regarding stand biomass, carbon accumulation, species diversity, growth, and mortality (Ducey and Knapp, 2010; Forrester, 2014). Both of these variables are often key elements collected during timber cruises and permanent plot frameworks (i.e., Continuous Forest Inventory (CFI) and Forest Inventory and Analysis (FIA)) (Leckie, *et al.*, 2003). From these variables, indirect estimations or broad trends in biomass, carbon stock, economic value, and other ecosystem services can be drawn (Frolking, *et al.*, 2009; Boisvenue and White, 2019; Saeed, *et al.*, 2019; Gunn, *et al.*, 2020). Forest managers are becoming increasingly aware of the resources provided by forest ecosystem functions outside of those typically measured (i.e., economic value or abundance of wood) (FAO, 2016; Lausch, *et al.*, 2017). To manage forest stands for alternative characteristics, either indirect estimates must be made (with accepted uncertainty), or additional effort must be made to take supplementary measurements in the field. For this purpose, many ecological researchers have turned to using indicators (Gatica-Saavedra, *et al.*, 2017; Lausch, *et al.*, 2017; Asbeck, *et al.*, 2021).

Indicators provide access to otherwise unavailable attributes, representing a more complete understanding of community condition and function although at often a higher cost of sampling. They are also important due to the inability to both sample every desired stand feature and sample across a large enough area (Juutinen and Mönkkönen, 2004; Whitman and Hagan, 2007). However, selection of the most appropriate indicator is no simple task. Using imperfect representation can quickly lead to error in understanding and management (Lindenmayer, *et al.*, 2000; Lausch, *et al.*, 2016).

Vascular plants have served as cost-effective indicators of community dynamics (Kuchler, 1976; Juutinen and Mönkkönen, 2004). Large diameter trees have been widely recognized as important indicators. These trees comprise most of the stand structure and

dynamics across tropical and temperate forests (Whitman and Hagan, 2007; Lutz, *et al.*, 2012). Large diameter trees are defined in several different ways, usually dependent on the region or forest community type and the tree species (Lindenmayer, *et al.*, 2012; Lutz, *et al.*, 2018). Lutz *et al.*, (2018) recommends an upper percentile (e.g., 99th percent) of the observed tree size distribution. Such definitions, however, can be biased when considering unevenly sized populations. Better suited is the definition for New England forests proposed by Whitman and Hagan (2007), and followed by Ducey *et al.*, (2013) which classifies large trees as those greater than or equal to 40 cm (15.748 inches) diameter at breast height (dbh). These large trees, both living and dead, have been successfully used as indicators of old growth and late-successional forests (Whitman and Hagan, 2007; Lutz, *et al.*, 2013). Living large trees create both timber and non-timber value, through culturally and spiritually important qualities (Lutz, *et al.*, 2012). Large dead trees remain as keystone elements within the ecosystem for decades due their ecosystem services, including nutrient cycling and wildlife habitat (Lindenmayer, *et al.*, 2012; Jones, *et al.*, 2018). However, the presence of large trees alone cannot be used to define old growth forests. The density of large trees can, however, provide a signal for the ecological and economic status of the stand (Congalton, *et al.*, 1993; Oliver and Larson, 1996). Even in low stem densities, large trees control much of the forest community carbon storage and biomass (Lutz, *et al.*, 2012; Ducey, *et al.*, 2013; Lutz *et al.*, 2018). Low stem densities, restricted sampling extents, and between plot variability have challenged most attempts to understand the presence or absence of large diameter trees. Although it seems an obvious choice to implement remote sensing to locate and quantity large tree presence, many platforms lack the combined spatial, spectral, and temporal resolution to reliably generate estimates (He, *et al.*, 1998; Berni, *et al.*, 2009; Guimarães, *et al.*, 2020).

Remote sensing has a long history of collaboration with forest inventory and management, with photogrammetric mapping and aerial surveys in use for nearly 100 years (Spurr, 1948; Colwell, 1955; Husch, *et al.*, 1972; Hinkley and Zajkowski, 2011; Pause, *et al.*, 2016; Liang, *et al.*, 2019). Advanced tools and techniques such as Light Detection and Ranging (LiDAR) and radar sensors present current users with promising results (Vierling, *et al.*, 2008; Jensen, 2016; Chen, *et al.*, 2017; Lausch, *et al.*, 2017; Muhamad-Afizzul, *et al.*, 2019). Many of these cutting-edge technologies, however, bring with them barriers such as hardware and software costs or the need for additional specialized knowledge. Additionally, they often do not provide the temporal or spatial resolution to map individual trees or scales which would be best suited for individual landowners (Janowiak, *et al.*, 2018). To ensure operationally feasible management, remote sensing systems must find compelling ways to estimate a variety of forest attributes while maintaining workflows that can be adapted to diverse projects and users.

Since their proliferation in the early 2000's, Unmanned Aerial Systems (i.e., UAS, UAV, or drones) have made vast strides in their ability to monitor and model forests (Falkowski, *et al.*, 2009; Hinkley and Zajkowski, 2011; Lu, *et al.*, 2018; Corte, *et al.*, 2020). UAS offer the potential to further reduce the moderate amounts of uncertainty in estimating forest attributes from high-resolution manned aircraft or satellite imagery (Leckie, *et al.*, 2003; Taylor, *et al.*, 2016; Hogland, *et al.*, 2018). The expanded adoption of UAS can also provide managers with better qualitative and quantitative information at large scales, while maintaining relatively low levels of uncertainty (Lindenmayer, *et al.*, 2000; Goodbody, *et al.*, 2018; Corte, *et al.*, 2020). Technological advances including Structure from Motion (SfM), segmentation algorithms for automated individual tree detection and delineation, and increases in battery performance have paved the way for the general adoption of this platform (Cummings, *et al.*, 2017; Kuželka and

Surovy, 2018). While there are noted improvements in spatial data resolution and associated processing techniques the use of high-resolution imagery is not without its inherent challenges measuring complex stand structure and composition (Fritz, *et al.*, 2013; Goldbergs, *et al.*, 2018).

Here we used UAS to estimate individual tree dbh, as well as stand basal area and density, and compared these results to field based measurements. Additionally, we provided a new perspective on the challenges of species-based mapping through the classification of individual large trees (Franklin and Ahmed, 2018). Similar studies, such as Iizuka *et al.*, (2017) have demonstrated a strong relationship between crown area or crown width and tree diameter, although for predominantly coniferous forests. Ramalho de Oliveria *et al.*, (2021) demonstrated that both UAS-LiDAR and UAS photogrammetry methods could achieve tree detection accuracies higher than 90% among tree plantations. Many other studies, such as Goodbody *et al.*, (2017) have compared UAS photogrammetric measurements to other remotely sensed data for the measurement of tree height. Our research instead focused on complex, mixed-species forests, with two primary objectives focused on enhancing the power of local scale land managers. These objectives are:

- 1. Estimate forest stand biometrics from UAS-SfM models of Northeastern Forests.**
 - a. Estimate tree specific dbh using crown geometry and UAS digital photogrammetry.**
 - b. Calculate stand density using basal area and trees per acre by species.**
 - c. Compare these UAS-based estimates to CFI plot field inventory measurements at the forest stand level.**
- 2. Assess the detection of ‘large’ trees as economic and ecological indicators of forest condition.**

METHODS

Study Areas

To conduct the analysis for our first objective, estimating forest stand biometrics using UAS-SfM, seven woodland properties located in Southeastern New Hampshire were studied (**Figure 3**). In total, 466 hectares (ha) were quantified, representing a mixture of forest community types and ages. Each of these sites were selected based on their availability of field-based inventory data within 5 years of when the woodlot could be sampled using our UAS. All of the properties (College Woods, Kingman Farm, East Foss Farm, Moore Fields, Dudley, and Burley-Demeritt), other than the Blue Hills study area are managed by the University of New Hampshire (UNH) for their naturalness and research integrity. The Blue Hills Foundation lands are contiguous forests, managed by the Harvard Forest as conservation lands. Due to logistical constraints with the UAS, only 118.64 ha out of the original 1034.78 ha of upland forests within the Blue Hills conservation lands were used in this study. These seven properties were stratified into 44 forests stands, with an average stand size of 10.59 ha, based on the available forest inventory data, using the methods described in the next section.

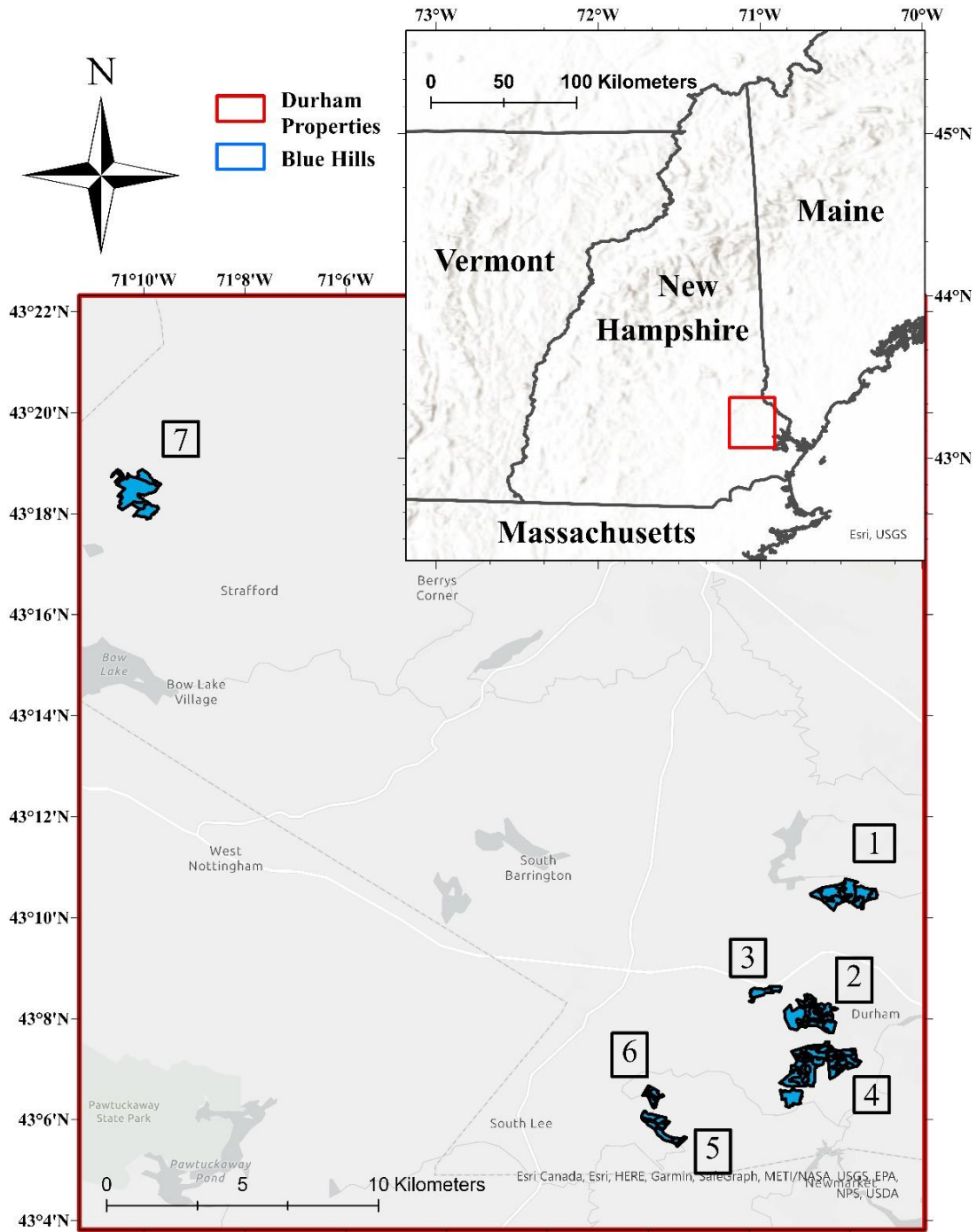


Figure 3. Depiction of the forest stands for each of the seven study areas, located in Southeastern New Hampshire. In numbered order (1) Kingman Farm (97.2 ha), (2) College Woods (111.6 ha), (3) Moore Fields (17.2 ha), (4) East Foss Farm (59.9 ha), (5) Burley- Demeritt (43.9 ha), (6) Dudley (17.5 ha), and (7) Blue Hills (118.6 ha).

For our second objective, quantifying the presence of large trees, we revisited two of our original study areas: College Woods and Kingman Farm. These study areas were selected due to their proximity, known presence of large trees, and diversity of forest stand types. For these two properties, seven forest stands were selected to conduct our large tree analysis. These included three predominantly coniferous stands, two mixed forest stands, and two deciduous stands. These stands reflected approximately 103 ha of forest and a minimum of 100 sampled trees in each of the coniferous, deciduous, and mixed forest stand types.

Field Data Collection

CFI plot parameters were measured across UNH woodlands using a systematic grid sampling design. These plots were distributed on a grid spacing of 1 plot per hectare. At each plot location, a variable radius plot (using horizontal point sampling) was established (Eisenhaure, 2018). Measured trees were identified using a basal area factor (BAF) $4.95 \text{ m}^2/\text{ha}$ (BAF $20 \text{ ft}^2/\text{acre}$) angle gauge. For each measured tree, the species, dbh, and a silvicultural code (i.e., living or dead status) was recorded. Each measured tree was also numbered and geolocated using a bearing and distance from the plot center.

To improve the positional accuracy of the original CFI plot center locations, based on the uncertainty discovered in Fraser and Congalton, (2019) the plot centers for several sites were re-collected during the 2018-2020 summer field seasons. These sites included: College Woods, Kingman Farm, and East Foss Farm. During this recollection, a wide area augmentation system (WAAS) enabled GPS and location averaging was utilized.

For the Blue Hills conservation land forests, field inventories were conducted in 2008, 2010, and 2017. In 2008, 100 inventory plots were randomly distributed across the conservation

lands upland forests and measured, with a 50-m minimum buffer between plots to increase their distribution. These same 100 plots were then remeasured in 2010 and 2017. In 2017, an additional 20 new plots were generated. At each plot, overstory vegetation measurements were made for all trees taller than 1.4 m and having a dbh greater than or equal to 2.5 cm. This data was filtered so that only trees with a dbh greater than or equal to 12.7 cm (5 inches) were retained. This filtering ensured that non-tree vegetation would be removed and so that the calculations of forest stand composition, based on basal area, would more closely match the sampling design of the other study areas.

Using the provided forest inventory data, forest stands were delineated into nine mutually exclusive community types. These community types included: White Pine (*Pinus strobus*), Eastern Hemlock (*Tsuga canadensis*), Other Conifer, Mixed Forest, Red Maple (*Acer rubrum*), Oak (*Quercus spp.*), American Beech (*Fagus grandifolia*), Other Hardwoods, and Other Forest. The full definitions for these forest communities can be found in **Appendix 2**. This stand delineation was accomplished using the majority class composition of the individual forest inventory plots, based on species basal area proportions, aggregated in their local area. Additionally, high-resolution image interpretation conducted by trained and experienced forest technicians familiar with the study sites was used to digitize specific boundaries (see Fraser and Congalton, (2019)).

For each of these forest stands, the aggregated CFI plot measurements were used as the basis for calculating stand level attributes which served as the field-based reference data for our first objective. These stand level attributes are summarized in **Table 11**.

Table 11. Forest biometric equations for the stand level characterizations of structure and composition.

Forest Parameter	Equation	Variables
Cross-sectional Area (CA) of individual trees	$CA = dbh^2 * 0.00007854$	dbh = diameter at breast height
Basal Area per Hectare (BA/ha)	$BA/ha = \frac{(Number\ of\ Trees * BAF)}{Number\ of\ Plots}$	BAF = Basal Area Factor
Trees Per Hectare (TPH)	$\frac{\sum TF_i}{Number\ of\ plots}$	TF_i = Tree Factor of Tree i
Quadratic Mean Diameter (QMD or \bar{d}_Q)	$\bar{d}_Q = \sqrt{\frac{BA/ha}{TPH * 0.00007854}}$	
Stand Density Index (SDI)	$SDI = TPH * \left(\frac{QMD}{25.4}\right)^{1.605}$	1.605 and 25.4 are constants

Basal area is a useful characteristic for defining the composition of forest stands (Kershaw, *et al.*, 2016). The Quadratic Mean Diameter (QMD) complements basal area as a description of stand composition and provides an additional level of insight for those looking to quantify stand volume (Curtis and Marshall, 2000; Kershaw, *et al.*, 2016). Stand density (SDI), and stocking, are used to depict the production quality of a given site (i.e., a measure of the sites production efficiency or quality) (Woodall, *et al.*, 2005; Kershaw, *et al.*, 2016).

Using the delineated stand maps, seven forest stands located throughout the Kingman Farm and College Woods study sites were used to collect field-based reference data on large trees. This stratification allowed for the evaluation of large trees across divergent forest communities (Whitman and Hagan, 2007; Ducey, *et al.*, 2013). These forest stands included a variety of coniferous, hardwood, and mixed forest types. For each of these forest stands, the original CFI plot data was reviewed for the presence of large trees. From these CFI plot records, all trees with a dbh greater than or equal to 37 cm (14.57 inches) were remeasured during the

2020 field season. Trees smaller than 40 cm in dbh were included in this sampling so that the classification accuracy of trees below the size threshold of ‘large’ would be evaluated. A new tree-specific position was recorded using our high-precision GPS and a new dbh measurement was taken. An EOS Arrow 200 GPS (EOS, 2021) was used to collect this position, which is reported to reach centimeter level accuracy. From our use below the dense canopy, the GPS receiver reported a 1.54 m average confidence, which would provide an approximate estimate of the tree location given the known difference between the tree stem and crown apex (Fuchs, 2003). From these data, approximately 459 trees were sampled for this second research objective, 45 of these trees were snags and 64 had a dbh smaller than 40 cm. The dbh of these trees ranged from 17.272 cm to 130.81 cm. The point locations of individual trees were manually edited in ArcGIS when necessary to better correspond with tree crowns visible within the UAS orthoimagery. GPS points which could not be matched to tree crowns based on their dbh or species were removed, resulting in a final count of 393 reference trees.

UAS Data Collection and Processing

The UAS imagery collected for this study was captured using a combination of two fixed-wing aircraft and two natural color sensors. These aircraft included the senseFly eBee Plus and its newer iteration, the senseFly eBee X, from Parrot (senseFly, 2018, 2019a). Both UAS were controlled using pre-programmed autonomous mission planning software (eMotion versions 3.15 and 3.19) (eMotion, 2021). The results of previous studies were used to select the flight parameters, including flying only on days with consistent sun-angle and exposure, flying when winds were light and perpendicular to the flight lines, and flying at altitudes near the maximum allowed by the Federal Aviation Administration (FAA) Part 107 guidelines of 121.92 m (400 ft) (Dandois, *et al.*, 2015; Puliti, *et al.*, 2015; Fraser and Congalton, 2018). All missions

were set to have 85% forward overlap and 80% side overlap to aid the modeling of the complex forest landscape (Fraser and Congalton, 2018, Fraser and Congalton, 2019). The internal Real Time Kinematic (RTK) feature of both aircraft was enabled during all missions so that the image capture locations could be post processed to a higher precision before SfM modeling. The two sensors deployed by these aircraft included (1) the Aeria X, natural color camera and (2) the Sensor Optimized for Drone Applications (SODA) natural color camera (senseFly, 2019b, 2019c). Due to its improved hardware characteristics, the Aeria X sensor was used whenever possible, however the SODA was used to capture several of the study sites due to logistical and technical constraints.

A number of best practices have discussed for UAS-SfM software choice and settings, but with constant refinements and no established output standards there remains some flexibility in this procedure (Dandois, *et al.*, 2015; James, *et al.*, 2017; Fraser and Congalton, 2018). Agisoft MetaShape (previously ‘Agisoft PhotoScan’) v1.5.5. was used for all SfM modeling. The processing workflow selected first the “High Accuracy” image alignment, and then the “Ultra High” quality settings for the dense point cloud formation, digital elevation model (DEM) generation, and orthomosaicking. These selections ensured that the full resolution of the original imagery was used during the Structure from Motion Multi-View Stereo (SfM-MVS) processing. This also provided a far greater amount of detail in the DEMs, which was necessary for establishing the segmentation process (Gu, *et al.*, 2020). For each image collection date, the SfM outputs included an ultra-high-resolution natural color orthoimage and an ultra-high-resolution DEM.

Individual Tree Detection and Delineation

Our original individual tree detection and delineation (ITDD) procedure consisted of applying a multiresolution segmentation to the orthoimagery and relying on their spectral, textural, and geometric principals to segment individual tree canopies. After several iterations of this method however, even the best results, quantitatively and visually, displayed poor performance. Instead, a marker-controlled watershed segmentation (MCWS) approach, outlined in Gu et al., (2020), was used to achieve far more realistic individual tree segments (Panagiotidis, *et al.*, 2017). For our approach, we utilized an ultra-high-quality canopy height model (CHM) for each study area due to its performance during initial testing. To create each of the CHMs, we began by normalizing the heights to above ground elevation values by subtracting the New Hampshire 2m lidar bare earth dataset using a common datum and vertical coordinate system (GRANIT, 2021). We then applied a low pass (Gaussian) filter to the resulting layer to reduce the notable presence of noise (i.e., excess pits and peaks) (Panagiotidis, *et al.*, 2017; Chen, *et al.*, 2018; Gu, *et al.*, 2020). A local maxima operation was applied to this final CHM in ArcGIS Pro version 2.7 to identify the individual treetops (i.e., markers for MCWS). The fixed window size for this operation was set to the average size of the reference tree crowns, approximately 4.5 m, based on the results of similar studies (Hwang and Lee, 2011; Gu, *et al.*, 2020). To evaluate the performance of the individual tree detection and mitigate biases for the under detection of sub-dominant trees which is occurs with remotely sensed imagery acquired from above, we calculated the object detection rate of the final treetops in comparison to our field reference data (Leckie, *et al.*, 2003; Hirschmugl, *et al.*, 2007; Yang, *et al.*, 2017). We also compared the tree detection error (commission and omission rate) for this 4.5 m fixed window size to both larger and smaller window sizes on a subset of our data to ensure the most accurate representation of individual tree canopies (i.e., optimal detection of singular trees). The identified treetops were

then compared to digitized reference trees to calculate the individual tree detection accuracy (i.e., object detection rate or ODR) as well as the rate of over detection and under detection (Mohan, *et al.*, 2017; Gu, *et al.*, 2020). For the College Woods and Kingman Farm study sites, two iterations of reference tree segments were on-screen digitized by trained and experienced field technicians using the species, size, and location information from our field inventory. These reference trees were distributed throughout both of these properties and represented the full range of tree sizes and species visible in the imagery. We then used the intersection of these two independent sample sets as reference polygons to validate the accuracy of our MCWS. This produced a total of 237 reference polygons.

A two-stage algorithm written in Python was used to complete the MCWS (Gu, *et al.*, 2020). The first stage involved masking non-forest areas and large canopy gaps. This mask set a minimum height threshold of 3 m (~10 ft) for all image segments. Due to the presence of pits and smoothed regions within some of the CHM canopy gaps, an additional greenness index threshold was calculated from the orthoimagery and applied to this mask. A conservative greenness index threshold was used to retain connected portions of lower canopy vegetation, still present in the imagery, but remove isolated or understory remnant vegetation. The second stage of the algorithm applied the MCWS segmentation. This algorithm started with the identified treetops, and delineated individual tree boundaries using the height gradients found within the CHM (Gu, *et al.*, 2020).

The accuracy of these final individual tree segments was evaluated both quantitatively and qualitatively. An overlap index (OI) was used to determine the corresponding best match between the digitized reference polygons and the canopy segments to support our quantitative evaluation of the image segments (Chen, *et al.*, 2018; Gu, *et al.*, 2020). During this empirical

evaluation of the segmentation quality, three matching indices were calculated. Both an Over-segmentation index (Oa) and Under-segmentation index (Ua) were calculated to determine the degree to which the segments corresponded with individual trees (Clinton, *et al.*, 2010; Chen, *et al.*, 2018). Over-segmentation was prioritized over under-segmentation while comparing the results of various segmentation parameters, due to its influence on species classification (Chen, *et al.*, 2018). The final empirical evaluator that we calculated was a Quality Rate (QR) index. The QR index measures the geometric correspondence between the reference polygon and the segmented trees, with a result of 0 indicating a complete match (Weidner, 2008; Chen, *et al.*, 2018; Gu, *et al.*, 2020). A final, visual assessment was conducted following each empirical assessment of segmentation quality to ensure that the crown edges represented in the orthoimagery matched the highest performing quantitative results (Chen, *et al.*, 2018).

Tree Species Classification

For each of the final tree segments (canopies), a variety of spectral, geometric, and textural attributes were calculated using eCognition Developer (v9.1). These attributes, shown in **Table 12**, were used as both the species classification parameters and for the secondary classification framework for large trees.

Table 12. Individual tree crown features (parameters) derived from both eCognition and ArcGIS software tools.

Classification Features		
Spectral	Geometric	Textural (all directions)
Greenness Mean of Brightness band Mean of red band Mean of green band Mean of blue band Std. Dev red band Std. Dev. green band Std. Dev. blue band Intensity	Area (Pixels) Length/Width Asymmetry Border index Compactness Density Radius of largest enclosed ellipse Radius of smallest enclosed ellipse Roundness Shape Index Area (m2) Radius (minimum bounding circle radius) *Area (m2) and Radius calculated in ArcGIS	GLCM Homogeneity GLCM Contrast GLCM Dissimilarity GLCM Entropy GLCM Mean GLCM Correlation GLDV Mean GLDV Contrast *GLCM = Gray Level Co-Occurrence Matrix *GLDV = Grey Level Difference Vector
*Greenness= $\frac{(\text{Mean Green} - \text{Mean Red}) + (\text{Mean Green} - \text{Mean Blue})}{(2 * \text{Mean Green}) + (\text{Mean Red}) + (\text{Mean Blue})}$		

Our species classification was completed using a Random Forests supervised classification algorithm in Python (Pedregosa, *et al.*, 2011). This classification scheme included: White Pine, Eastern Hemlock, Other Conifer, American Beech, Red Maple, Oak, Other Hardwood, Other Forest, and Snag. The full definitions of these classes can be seen in **Appendix 2**. An additional sampling of individual reference trees, gathered through a blend of field inventory and photo interpretation, was used to generate reference data for this classification. A

minimum of 30 training and 30 validation trees, located throughout several of the study areas, were used for each class. The Gini index was used to control the impurity of the individual decision tree splits (Loh, 2011; Krzywinski and Altman, 2017). A measure of variable importance was also generated using the mean decrease in impurity (MDI) to ensure the performance of the algorithm (Breiman, 2001). The thematic accuracy of this species-based classification was evaluated using a thematic map accuracy assessment error matrix (Congalton and Green, 2019).

UAS Regression Analysis and Biometrics

A linear regression was used to empirically model estimates of dbh from the UAS data. Both the crown area and crown radius of individual tree segments were examined for their relationship (i.e., fit) to field-based measurements of dbh (Lamson, 1987; Lockhart, *et al.*, 2005). Crown area was calculated for all of the individual tree segments based on their geometry in ArcGIS. Crown radius was derived from the radius of the minimum bounding circle for each segment. The relationship between UAS tree canopies (segments) and field-based measurements of dbh included 393 reference trees. This data was split, with a consideration for species diversity, size diversity, and stand composition diversity, so that 75% of the reference samples were used to build the regression models and 25% were used to validate its accuracy. Both the crown area and crown radius models were examined for all species, coniferous species, and deciduous species independently (Minor, 1951; Bonnor, 1964; Kershaw, *et al.*, 2016). The Pearson's coefficient (r) was used to determine the strength of the relationship (Snedcor and Cochran, 1980). Additionally, the validation trees were used to generate a root mean square error (RMSE) for the best fitting regression model to determine if this data fell within the 2% to 18% confidence interval expected from field-based measurements of dbh (Bohlin, *et al.*, 2012).

Using this new relationship for dbh derived from the UAS data, the dbh for all of the detected trees for our seven study sites was calculated. From this variable, stand level attributes such as basal area per hectare, TPH, QMD, and SDI were calculated using the same fundamental equations as the field inventory assessment with two adjustments (Ducey and Knapp, 2010; Ducey, *et al.*, 2013; Kershaw, *et al.*, 2016). The first adjustment was that these estimates of stand level characteristics were made using all of the observed trees within each stand, and not just the independent field sampling plots. Second, to calculate the total observed stand basal area and then basal area per hectare, individual tree segments which were smaller than 3 m^2 or 500 pixels were removed using a semi-automated method based on visual inspection of the orthoimagery and then implementing a filter in ArcGIS Pro. This process removed small and erroneous image objects, located mostly around canopy gaps and edges, which did not represent tree canopies and would positively bias the total stand basal area. The accuracy for these UAS-based forest inventory estimates were assessed based on their percent difference from the field-based estimates for each stand.

UAS Large Tree Survey

To meet our second objective, the quantification of large tree presence, we again used the geometry of the individual tree segments (crowns) identified in the last section. With these tree canopies, two distinct methods were used to categorize large and small trees. First, we used the best fitting regression equation from objective one to estimate the dbh of each of our reference trees from their crown geometry. This dbh was then cross-referenced with the validation trees to determine their agreement in classification for large and small trees (i.e., greater than or less than 40 cm dbh). Trees with an estimated dbh smaller than 40 cm were labeled as small, while trees with an estimated dbh greater than or equal to 40 cm were labeled as large. Our second method

consisted of a supervised classification of large and small trees using the random forests classifier, similar to the original species-based classification. This random forests classification was established using the same training and validation samples as the estimated dbh regression (Congalton and Green, 2019). Each of the features calculated for the original species-based classification (29 features) were reapplied for the purpose of defining large and small trees. The species of each reference tree was also used as an additional feature for this classification. This secondary, thematic, classification was evaluated using a thematic map accuracy assessment error matrix (Congalton and Green, 2019)

RESULTS

UAS-SfM Modelling

The spatial resolution of the SfM-MVS orthoimagery and CHMs ranged from 2.53 cm to 3.6 cm. The average spatial resolution was 2.94 cm. In total 14 spatial models were created; one orthoimage and one CHM for each of the seven study areas using the Ultra-High-quality setting in Agisoft MetaShape.

Individual Tree Detection and Delineation

A total of 237 digitized reference trees from College Woods and Kingman Farm were used to quantify the overall tree detection accuracy based on our selected, optimal window size. Alternate window sizes and segmentation parameters were evaluated but found to be less accurate for overall detection accuracy. **Table 13** shows the overall detection accuracy for individual trees, as well as the rate of over detection (commission error) and under detection (omission error). Of these trees, 64.56% were correctly identified and delineated as a singular canopy. The percentage of over detected (i.e., over segmented) trees, 18.14%, and under detected

(under segmented) trees, 17.3%, were roughly balanced. The overall detection rate was 82.7%.

This is a combination of the trees detected with a singular canopies (i.e., "correct detection") and those that were falsely detected as multiple trees (i.e., over detected).

Table 13. Individual tree detection (ITD) accuracy, including the rates of commission and omission error as well as the overall detection accuracy.

Individual Tree Detection		Field (Reference) Data			
		Correct Detection	Over Detection (Commission Error)	Under Detection (Omission Error)	TOTAL
UAS Detected	Total	153	43	41	237
	Accuracy Percentage	64.56%	18.14%	17.3%	OVERALL Detection 82.7%

The geometric accuracy of the final tree segments were compared to these same digitized reference trees using the Oa, Ua, and QR indices. This resulted in an Oa of 0.2103, a Ua of 0.3741, and a QR of 0.49796. In the effort to obtain the most accurate delineation of individual trees, we tested the influence of applying an additional multiresolution segmentation to these tree segments. This would further interject spectral information into the segmentation process. All tests however, resulted in a minimum of a 0.86% decrease in the QR, which would negatively affect the resulting estimates of dbh.

Tree Species Classification

Our species-based classification, including nine classes, resulted in an overall accuracy of 56.10% (**Table 14**). Classes such as snags, white pine, and other conifer displayed the highest producer's and user's accuracies. Alternatively, classes such as other forest, other hardwoods,

and red maple resulted in the lowest user’s accuracies with 36.11%, 37.84%, and 43.75% accuracies, respectively. This was echoed in the producer’s accuracies, with each of these classes as well as the oak class showing increased rates of commission error.

Table 14. Species-based classification thematic map error matrix conducted on nine species: American beech (AB), Eastern hemlock (EH), oaks, other conifers (OC), other forests (OF), other hardwoods (OH), red maple (RM), snags, and Eastern white pine (WP). Classification was completed using the random forests (RF) supervised classification algorithm.

Random Forests Classification		Field (Reference) Data										
		AB	EH	OAK	OC	OF	OH	RM	SNAG	WP	TOTAL	USERS ACCURACY
UAS Data	AB	23	4	9	0	2	0	0	0	0	38	60.05%
	EH	6	16	8	3	0	1	2	0	3	39	41.03%
	OAK	6	2	44	6	8	6	4	0	0	76	57.89%
	OC	2	6	2	32	0	0	0	0	3	45	71.11%
	OF	6	1	9	0	13	5	2	0	0	36	36.11%
	OH	1	1	9	2	4	14	4	1	1	37	37.84%
	RM	2	0	11	2	4	7	21	0	1	48	43.75%
	SNAG	0	0	0	1	0	0	1	33	5	40	82.50%
	WP	2	5	1	3	1	1	1	3	34	51	66.67%
TOTAL		48	35	93	49	32	34	35	37	47	230/410	
PRODUCERS ACCURACY		47.92 %	45.71 %	47.31 %	65.31 %	40.63 %	41.18 %	60.00 %	89.19 %	72.34 %		OVERALL ACCURACY 56.10%

UAS Regression Analysis and Biometrics

To model the relationship between crown geometry and dbh, two regression models were examined. First, the relationship between crown area and dbh was modeled (**Figure 4**) for all species, then coniferous and deciduous species independently. Crown area resulted in an *r* value

of 0.2816 overall, with deciduous and coniferous species reaching r values of 0.1517 and 0.3603. The second regression modelled the relationship between crown radius and dbh (**Figure 5**). All three trend lines for this model had a better overall fit than those of the crown area regression. The combined species r value reached 0.3792, while deciduous and coniferous species had values of 0.3895 and 0.4686. In comparing these two models, deciduous species in both cases showed a worse fit than did coniferous species. The equation for the line of combined species crown radius to dbh is given below in **Equation 1**. This equation gave the best overall fit for all species, and was used as the basis for the stand level biometric estimation in the next section. In this equation ‘x’ is the crown radius of an individual tree segment, and ‘Y’ is the trees dbh.

Equation 1. UAS-based estimation of diameter at breast height (dbh) derived from the segmentation of individual tree crown radius.

$$Y = 3.26057x + 36.05689$$

Using this equation, we compared the UAS estimated dbh for our validation trees to the field-measured dbh. This comparison resulted in a RMSE of 13.15 cm, which is equivalent to an error of 19.7% to 33.7% based on the average size of our measured trees (based on one standard deviation from the mean).

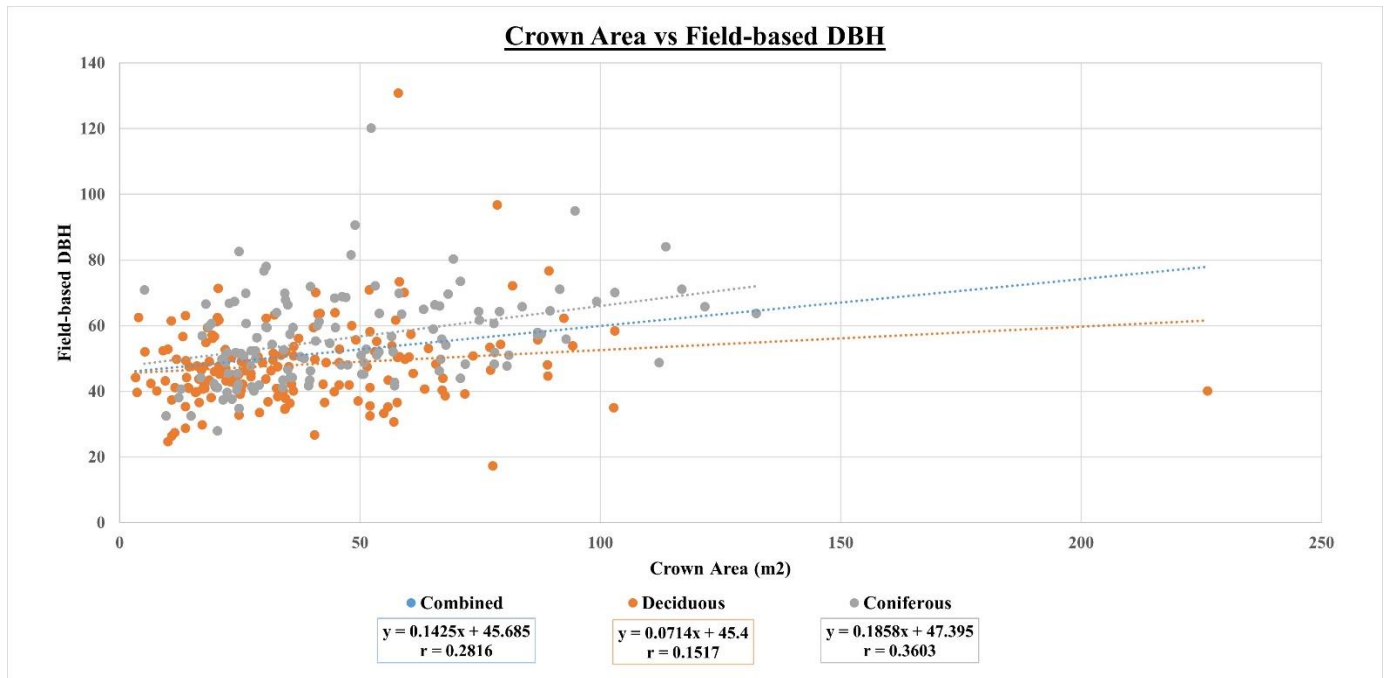


Figure 4. Linear regression between field measured dbh and crown area estimated using the UAS tree segments. Three trend lines and their respective equations are displayed for all species combined, as well as deciduous species and coniferous species independently.

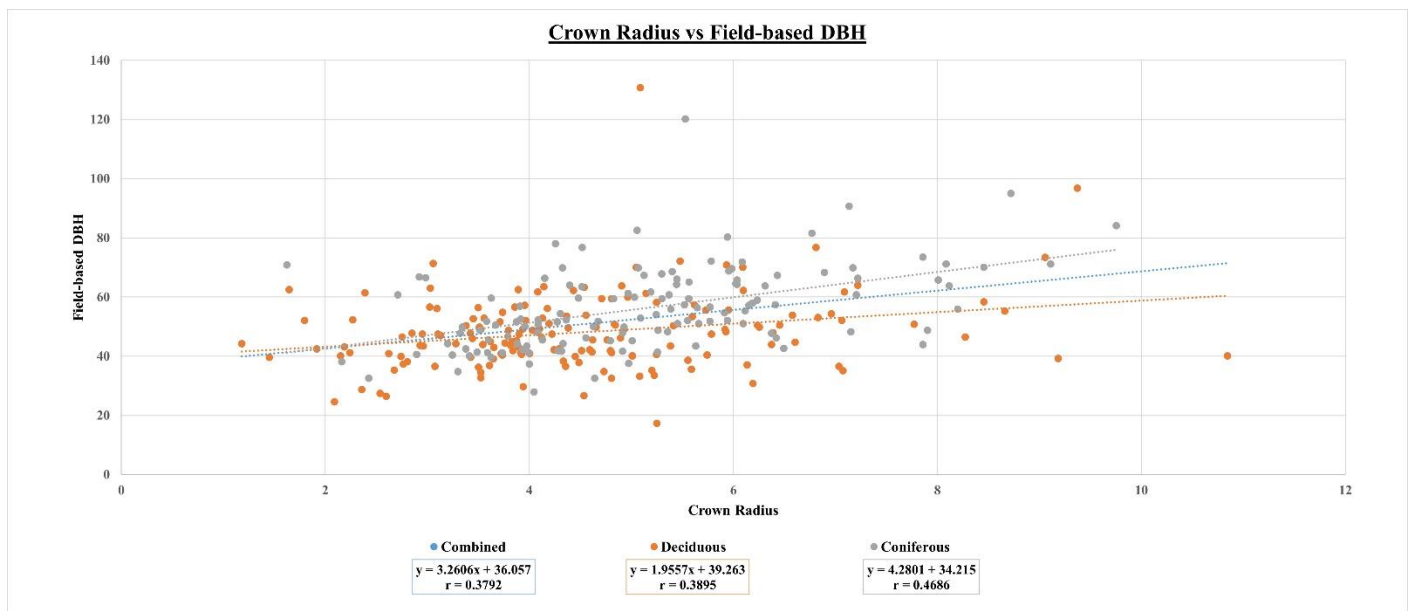


Figure 5. Linear regression between field measured dbh and crown radius estimated using UAS tree segments. Three trend lines and their respective equations are displayed for all species combined, as well as deciduous species and coniferous species independently.

To understand the accuracy for estimating stand level characteristics, the crown radius to dbh regression equation above was used to calculate the basal area of individual tree segments. In conjunction with this, TPH was determined based on the detection of treetops in each stand, and both were used to derive estimates of QMD and SDI which could be compared to field-based reference data. **Figure 6**, below, shows our comparison between UAS estimates of BA/ha, TPH, QMD, and SDI. In this figure, 100% on the y-axis denotes the UAS-based estimate for a given stand is equivalent to the field inventory estimate for the given attribute (e.g., 100% of the reference data value). The estimates of BA/ha showed that the UAS on average was 42.18% higher (142.181% or + 8.59 m^2 / ha) than field-based measurements. On the other hand, TPH estimates were 45.58% lower than the field-based estimates at 54.417% (322 vs 626.5 TPH). This overestimation of BA/ha and underestimation of TPH were reflected in the other comparisons which resulted in overestimations of 62.081% for QMD (+14.99 cm) and an underestimation of 3.337% for SDI (-6.01).

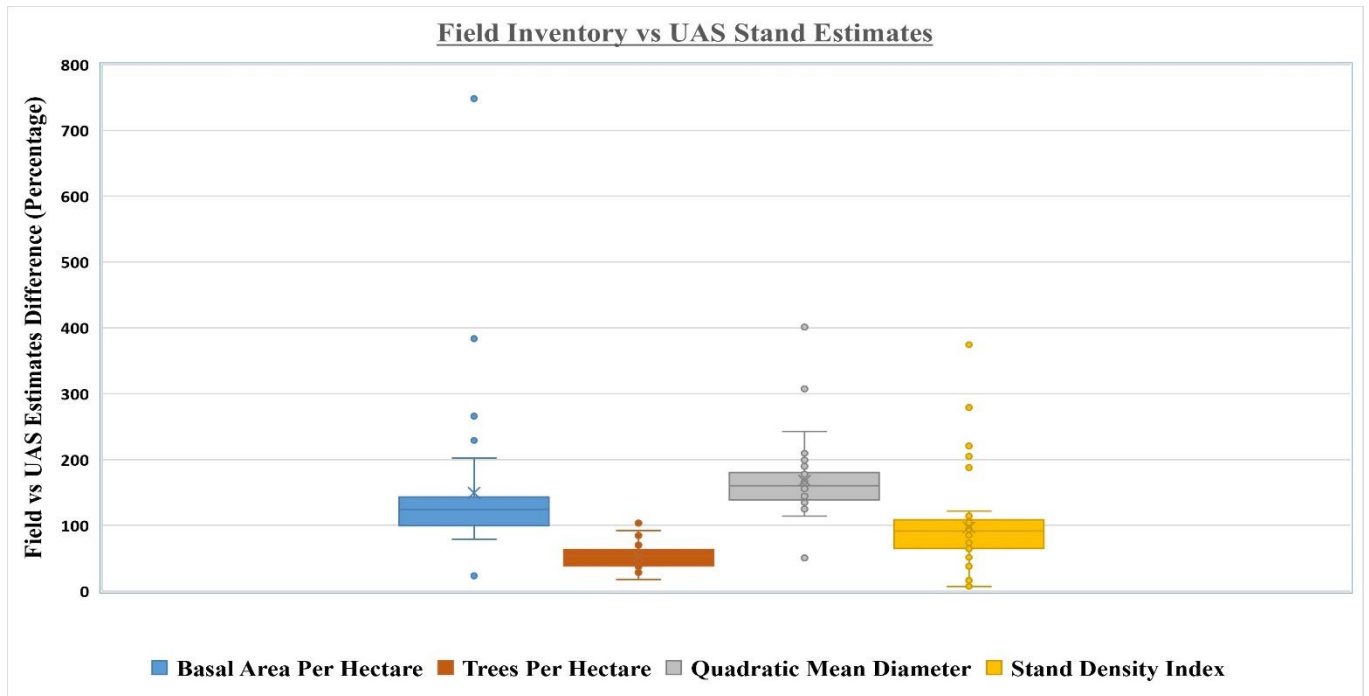


Figure 6. Comparison of field-based inventory estimates and UAS-based inventory estimates of stand level characteristics including: Basal Area per Hectare (BA/ha), Trees per Hectare (TPH), Quadratic Mean Diameter (QMD), and Stand Density Index (SDI). The y-axis is based on the estimation of the UAS data when compared to the field-measured reference for each stand; 100% on this axis denotes that these estimates are equivalent in value, while 200% would denote that the UAS-based estimate was twice that of the reference data.

UAS Large Tree Survey

Two methods were used to quantify the accuracy of large tree classification using the UAS tree segments (**Table 15**). The first consisted of classifying trees as large, greater than or equal to a 40 cm dbh, based on their estimated dbh from the crown radius regression model discussed above. For the 100-validation trees measured and classified based on our field reference data, 84% were correctly classified as large trees. In addition, all 16 trees that were smaller than 40 cm in diameter (100% of these samples) were also classified as large based on the UAS data. The second method to classify trees as large or small included applying a random forests supervised classification to the same training ($n = 293$) and validation ($n = 100$) trees as the regression model. This supervised classification utilized the same input features as the

species-based classification (**Table 12**) with one addition, a numeric code for the known species identification. This random forests classification resulted in an overall accuracy of 85%. The slight increase in classification accuracy was the result of the successful classification of one small sugar maple (*Acer saccharum*) tree.

Table 15. Thematic accuracy error matrices for the classification of large trees. (A) Using the linear regression equation for dbh based on the segmented crown radius and (B) using a random forests supervised classification.

A: Linear Regression: Large Trees		Field (Reference) Data			
		LARGE	SMALL	TOTAL	USER ACCURACY
UAS Data	LARGE	84	16	100	84.00%
	SMALL	0	0	0	100%
	TOTAL	84	16	100	
	PRODUCERS ACCURACY	100%	0%		OVERALL ACCURACY 84/100 84.00%
B: Random Forests: Large Trees		Field (Reference) Data			
		LARGE	SMALL	TOTAL	USER ACCURACY
UAS Data	LARGE	84	15	99	84.85%
	SMALL	0	1	0	100%
	TOTAL	84	16	100	
	PRODUCERS ACCURACY	100%	6.25%		OVERALL ACCURACY 85/100 85.00%

Figure 7 shows the feature importance of all 30-image object features implemented for the supervised random forests classification of large trees. These feature importance values are calculated using the MDI. Crown radius (0.0585) followed by the greenness index (0.0493) and crown area in m^2 (0.0467), displayed the highest feature importance. Many of the additional geometric and textural features displayed the lowest feature importance.

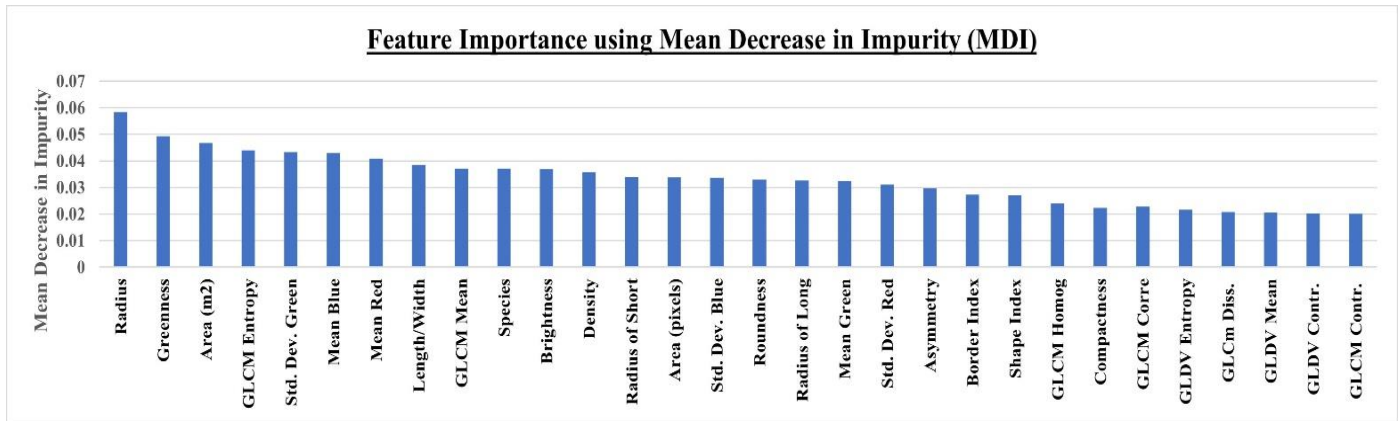


Figure 7. Feature importance values for the random forests classification input features for large trees based on the mean decrease in impurity (MDI) index.

DISCUSSION

The quantification of forest stand and individual tree characteristics using remote sensing has been a topic of interest for several decades (Gillis, *et al.*, 2005; Bohlin, *et al.*, 2012; Kuželka and Surový, 2018; Goodbody, *et al.*, 2020). Our first objective investigated the ability for UAS-SfM photogrammetry to estimate individual tree diameter as well as stand level characterizations of BA/ha, TPH, QMD, and SDI. In addition to this, we utilized a random forests supervised classification to examine individual tree species and in support of our second objective, a survey of large tree presence using UAS.

The overall classification accuracy for our nine-class (species) system was 56.10%. Classes that were highly distinct, such as white pine and snags, reported both high producer's

and user's accuracies. Other classes such as other forest and other hardwoods showed the worst performance. The class for Eastern hemlock also showed poor performance, likely because of their poor reconstruction in the SfM models for some regions of the orthoimagery and DEMs which was realized during the visual exploration of the data and canopy delineation procedures. The results of quantifying dbh for individual trees using crown geometry demonstrated a relatively low precision (± 13.15 cm) and fit ($r = 0.3792$). This contrasts with a study by Iizuka et al., (2017) which demonstrated a strong relationship between canopy geometry and field-measured dbh, especially for crown width ($r = 0.7786$). Their study, however, was conducted using predominantly coniferous species (e.g., *Chamaecyparis obtuse*) in a low species diversity area while our study had a complex mixture of dense conifers and deciduous trees. In **Figure 5**, we see the presence of several large outlier trees, with low crown radius values, that were over segmented. These training trees were recorded with diameters ranging up to 130 cm.

Segmentation has been a large concern when considering the modeling of large trees using only optical, natural color imagery. Our approach utilized an MCWS algorithm, following multiple testing cycles. For example, when performing this same MCWS algorithm on medium-quality SfM data products, we achieved a slightly higher individual tree detection accuracy, however, there was a subsequent 9% decrease in the segments QR which negatively impacted each of the dbh regression models. More recent, region growing, segmentation algorithms have been published which show promising results for this same procedure (Gu and Congalton, 2021). The complexity of these Northeastern, mixed-species forests present a challenge, however. The diversity of tree canopy appearances has led to a continual pursuit for the improved identification and delineation of trees within closed canopy forests (Kuželka and Surový, 2018; Liu, et al., 2019). The correct identification and extraction of small trees in particular is noted as a source of

uncertainty for the classification of large and small trees, which will be further reflected on in the next section. Lastly, several studies have recognized that site-specific and species-specific allometric equations based on crown geometry have achieved good performance for measuring indirect forest characteristics (Rautiainen, *et al.*, 2008; Pretzsch, *et al.*, 2015; Pretzsch, 2019; Rudge, *et al.*, 2021). Future research will explore methods for improving species-based classifications and the increases in accuracy found by adapting species-specific equations for tree crown-dbh mathematical models.

Based on the regression equation for crown radius, our UAS-based estimates of tree diameter showed an average difference of 19.7% to 33.7% when compared to field reference data. In a study by Wieser *et al.*, (2017) UAS-lidar measurement errors for tree diameter ranged from 9% for trees between 20 and 30 cm in diameter to 1.8% for trees larger than 40 cm in diameter. This study was conducted on pre-alpine alluvial forests in Austria (Wieser, *et al.*, 2017). Corte *et al.*, (2020) established a similar result for UAS-lidar with the measurements of individual tree diameter reaching an RMSE of 11.3% on a eucalyptus plantation (*Eucalyptus benthamii*). While our results have not yet reached those of UAS-lidar, the affordability and technical accessibility of our photogrammetric framework provide a strong incentive for its use in local scale management. Our results for stand level estimations showed an overestimation of BA/ha (42.181%) and QMD (62.088%) while TPH and SDI were underestimated by 46.439% and 3.309%. The underestimation of tree density using UAS-SfM is not uncommon. Goldbergs *et al.*, (2018) analyzed the detection rate of individual trees using SfM point cloud. Their results showed that dominant and co-dominant trees had a detection accuracy of approximately 70% while suppressed trees resulted in a detection accuracy under 35%. The complexity of our multi-canopy forests make the comparison of field-based and remote sensing inventory measurements

challenging. In a study by Ramalho de Oliveira et al., (2021) the detection accuracies of individual trees, within a loblolly pine (*Pinus taeda*) plantation in central Florida, reached 96% and 92% for UAS-lidar and UAS photogrammetry, respectively. Recognizing that the UAS-based estimations of tree diameter tended to exaggerate their actual sizes, we implemented a filtering of tree segments that were smaller than 500 pixels or 3 m². Identified treetops that were delineated as only a few pixels during the MCWS were registered as trees with a minimum dbh of 36.057 cm using **Equation 1**. This caused the initial estimates of total stand basal area and BA/ha to be two to three times higher. Lastly, we considered the influence of stand size of these inventory characteristics. Most of the stands that are shown as outliers in **Figure 6** are smaller than 10 ha in size. For example, a stand at the Dudley study area that was 5.77 ha in size resulted in the greatest overestimation of BA/ha with a calculation of 748.05% of the field-based value. This translated into an overestimation of QMD and SDI of 401.2% and 374.5% respectively. Stand size can present a considerable source of variability in the estimation of forest characteristics, with moderate stability not being reached for some remote sensing data sources until the stand size is 10 to 20 ha or larger (Hyypä and Hyypä, 2001). Several mechanisms may be involved in this trend in estimation error including; (1) that the accuracy of the reference (field-based) measurements may be improved with the inclusion of more inventory plots; (2) larger stands may exhibit less variability (i.e., more homogenous area) for the remote sensing estimates; or (3) the small differences in stand boundary may be more impactful for the smallest of stands (Hyypä and Hyypä, 2001). When comparing only stands larger than nine ha ($n = 19$), the overestimation of BA/ha reduced from 42.181% to 14.629%, with a subsequent boost to the precision of these estimations. This resulting overestimation of 14.6% for BA/ha at the stand

level more closely coincides with the results of other studies using photogrammetric measurements (Bohlin, *et al.*, 2017).

Exploring the results of our second objective, an evaluation of large tree mapping, we set a 40 cm dbh size threshold as the definition of large trees. Large trees represent a key ecosystem component, even in low densities (Ali, *et al.*, 2019; Kebrle, *et al.*, 2021; Yuan, *et al.*, 2021). Our random forests classification performed slightly better than the estimated dbh regression model for crown radius. These inflated overall accuracies of 85% and 84%, for the random forests and regression classifications, would likely decrease with the availability of a larger sample size of small trees as the classification accuracy of both models for this class was less than 10%. Previous studies have acknowledged the difficulty in surveying or tracking changes in large tree presence in the field (Lutz, *et al.*, 2012; Harris, *et al.*, 2021). While many recent studies have investigated the function of large trees in various habitats, few reflect on the accuracy or cost of estimating their presence and distribution (Hartel, *et al.*, 2018; Jones, *et al.*, 2018). As discussed above, more research is also needed to adopt these methods for the assessment of small or non-dominant trees in dense canopy stands (Goldbergs, *et al.*, 2018). These trees, located lower in the forest canopy, represent a considerable source of uncertainty when employing photogrammetric methods (citation).

While the quality of the segmentation results, i.e., individual tree delineation, is a primary source of uncertainty for these applications, the challenge of defining a standard segmentation practice for specific forest cover types is not easily overcome (Kuželka and Surový, 2018; Gu and Congalton, 2021). Future research should look at the benefits of multi-temporal workflows or the fusion of natural color sensors with lidar point clouds or hyperspectral imagery. This addition of data sources however brings to question the feasibility of not only collecting, but

understanding and processing such products, in a way, which would be adaptable for managing local-scale forests. The flexibility and efficiency of UAS-photogrammetry using SfM, and modern individual tree crown delineation methods makes it a fundamental target for updating and extending forest inventories (Panagiotidis, *et al.*, 2017; Ganz, *et al.*, 2019; Shang, *et al.*, 2020). These methods must remain approachable for local scale management, to remain applicable to a significant percentage of woodlands throughout this region (Morin, *et al.*, 2015; Janowiak, *et al.*, 2018).

CONCLUSIONS

Today's forests require detailed and up-to-date information to support local-scale management. Our research investigated the proficiency for UAS natural color imagery, integrating refined Structure from Motion (SfM) and advanced segmentation algorithms, for the estimation of individual tree and stand level characteristics. In our first objective, we estimated individual tree diameters within complex forests using their segmented crown radius. This resulted in an average error of 19.7% to 33.7%. At the stand level, this regression model resulted in overestimations of basal area per hectare, quadratic mean diameter, and the stand density index, while trees per hectare was underestimated. The results of this stand level assessment was improved when considering only stands larger than nine ha. Bringing the accuracy of our UAS methods closer to other studies conducted using photogrammetry and those which utilized lidar sensors. For the second objective, our assessment of large trees presented a high overall accuracy for both the crown radius regression model and random forests classification, 84% and 85% respectively. This classification, however, further highlighted in inability of UAS photogrammetry for identifying and delineating small or suppressed trees with this class receiving an accuracy of less than 10% for both methodologies. A major principal of this

research was the accuracy of the individual tree detection and delineation, which is rapidly progressing. The results of this study provide an additional exploration of complex forest photogrammetry using modern software and hardware technology as well as a relatively accessible framework for local scale management, which will lead to a greater understanding of our forested landscape

CHAPTER 3: Monitoring Fine-Scale Forest Health using UAS-SfM Multispectral Models

ABSTRACT

Forest disturbances, driven by pests, pathogens, and discrete events, have led to billions of dollars in lost ecosystem services and management costs. To understand the patterns and severity of these stressors across complex landscapes there must be an increase in reliable data at scale compatible with management actions. Unmanned Aerial Systems (UAS or UAV) offer a capable platform for collecting local scale (e.g., individual tree) forestry data. In our study, we evaluate the capability of UAS multispectral imagery for differentiating healthy, stressed, and degraded individual trees throughout mixed-species forests. We also make a comparison of these results to freely available high-resolution airborne imagery. During these investigations, several approaches to classifying forest health classes using the random forests and support vector machine (SVM) machine learning algorithms are applied. Using the random forests classifier, the UAS imagery correctly classified five forest health classes with an overall accuracy of 65.43%. When these classes were generalized to healthy, stressed, and degraded trees, the accuracy improved to 71.19%. Using similar methods, the high-resolution imagery achieved an overall accuracy of 50.50% for the five health classes, a reduction of 14.93%. Further analysis into the precise calibration of UAs multispectral imagery, a refinement of image segmentation methods, and the fusion of these data with more widely distributed remotely sensed imagery would further enhance the potential of these methods.

BACKGROUND AND LITERATURE REVIEW

Forest disturbances, coupled with invasions by foreign pests and pathogens, have come to dramatically alter vegetation systems. These discrete events transform physical structure,

ecosystem processes, and resource allocations which comprise a significant role at local and global scales and across both natural and developed environments (Oliver and Larson, 1996; Frohking, *et al.*, 2009; Coleman, *et al.*, 2018; Wilson, *et al.*, 2019). Examples of prevalent forest disturbance include fires, flooding, windstorms, droughts, overharvesting, pollution, fragmentation, and biological invasions. Invasions by insects and pathogens threaten the stability of forest ecosystems, events that are projected to increase (Aukema, *et al.*, 2011; Pontius, *et al.*, 2017). Private landowners and local governments most heavily endure the degradation and ecosystem change caused by these biological invasions (Aukema, *et al.*, 2011; Hassaan, *et al.*, 2016; Lausch, *et al.*, 2017). In conjunction with distinct disturbance events, continuous stress from anthropogenic activities have had a measured impact (Lausch, *et al.*, 2016). Managing forests for peak growth requires not only a combination of nutrients, light, temperature, and moisture but also the absence or diminished presence of threats and invasions (Kopinga and Burg, 1995; Lausch, *et al.*, 2016; Pan, *et al.*, 2018). Reconciling forest disturbances and stress requires understanding where it occurs and what influences it may have at several spatial and temporal scales. Despite such a need for information, forest disturbance and health assessments are still a task often left to the limited number of land managers and conservation resources. Unfortunately, even in the simplest of environments, forests present complex interactions of cause and effects which further hinder research and management. Individual tree species are known to display differences in their response to changes in resource availability or stand dynamics (Oliver and Larson, 1996; Lausch, *et al.*, 2016; Gerhards, *et al.*, 2019).

The definition of ‘forest health’ requires a multifaceted consideration of scales ranging from the individual tree branch to the entire forest ecosystem while including both biotic and abiotic factors. Lausch *et al.*, (2016) defines forest health most simply, at the tree scale, as “the

absence of disease or damage.” Ward and Johnson, (2007) provide two more complete definitions for forest health. First, “a measure or condition of forest ecosystem robustness, including rates of growth and mortality, crown condition or vigor, and the incidence of damage” (Steinman, 2004; Ward and Johnson, 2007). Second, forest health is defined as “a capacity to supply and allocate water, nutrients, and energy in ways that increase or maintain productivity while maintaining resistance to biotic and abiotic stresses” (McLaughlin and Percy, 1999; Ward and Johnson, 2007). With both the complexity of natural processes to observe (both the internal functions and external interactions of trees) and the potential for influences and responses to coalesce, forest health presents a uniquely difficult challenge for adequate monitoring (Lausch, *et al.*, 2016; Meng, *et al.*, 2016).

In New England forests there are numerous regionally important tree species that are facing devastating disturbances. These species include eastern white pine (*Pinus strobus*), ash (*Fraxinus spp.*), oaks (*Quercus spp.*), eastern hemlock (*Tsuga Canadensis*), and American beech (*Fagus grandifolia*), among others. For hundreds of years, white pine has played a central role for northern U.S. and Canadian forest ecosystem services (Broders, *et al.*, 2015). In recent decades, combinations of several fungal pathogens and air pollutants have caused measurable disturbances to white pine (Broders, *et al.*, 2015). This phenomenon, now known as white pine needle damage (WPND) or white pine needle cast, was discovered to be most prominently caused by the fungus (*Canavirgella banfieldii*). WPND is expected to increase in severity and distribution given its current geographic extent and the projected climate scenarios (Broders, *et al.*, 2015; Wyka, *et al.*, 2017). The value of ash species stems from their fast growth and wood density, because of which they are a basis for many timber products (Poland and McCullough, 2006). Since 2002 however, emerald ash borer (EAB) (*Agrilus planipennis*) has devastated over

15 million ash trees, costing the U.S. economy an estimated \$30 billion (Poland and McCullough, 2006; Pontius, *et al.*, 2017). Oaks provide both commercial value as priority timber products and numerous wildlife resources (Tirmenstein, 1991; Carey, 1992). Throughout New England however, disturbance events stimulated by gypsy moths (*Lymantria dispar dispar*) are threatening the future of their resources at alarming rates (Pasquarella, *et al.*, 2018). Eastern hemlock present several resources for wildlife due to their dense stand structure and food provisioning (Carey, 1993). Hemlocks represent a common feature of the New England forested landscape. Nearly as ubiquitous as these host trees, hemlock woolly adelgid (HWA) has devastated the region's populations. Following invasion, HWA has been known to severely impair over 90% of hemlock trees (Orwig and Foster, 1998; Simoes, *et al.*, 2019). Beech trees provide food for both wildlife and humans, an excellent source of fuelwood, lumber for many wood products, and even medicine as a source creosote (Burns and Honkala, 1990). Due to infestations of beech scale (*Cryptococcus fagisuga*) (i.e., beech bark disease), entire stands of trees are being impacted.

Due to the variability in responses to disturbance that various tree species exhibit, it is difficult to quantify and communicate how such negative trends could be mitigated (McCune, 2000; Pause, *et al.*, 2016). The rapid progression of change and mortality caused by many of these disturbances has come to outpace the critical obtainment of reliable information using in situ (i.e., field-based) methods (Tucker, *et al.*, 1985; Goetz and Dubayah, 2011; Zaman, *et al.*, 2011; Lausch, *et al.*, 2017). Field-based methods for the early detection of forest stress involve either visual assessments of crown vigor, or the analysis of soil and foliar biophysical properties to evaluate photosynthetic activity (Lausch, *et al.*, 2016). Crown vigor assessments focus on the defoliation, thinning, and dieback of tree crowns in relation to expected site development (Innes,

1998; Hallett, *et al.*, 2006, 2018; Pontius and Hallett, 2014; Wyka, *et al.*, 2017). Well defined guides created by the U.S. Forest Service (USFS) provide methods for classifying crown vigor classes based on defoliation, transparency, and discoloration charts (Pontius and Hallett, 2014; Hallett, *et al.*, 2018; HTHC, 2021). These methods can be standardized and compared across study areas to monitor the severity of the disturbances. Alternatively, foliar analysis using spectroscopy has become far more accessible in recent years. Field spectrometers and lab-based chlorophyll fluorescence measurements give evidence for pre-visual decline in leaf activity (Kopinga and Burg, 1995; Pontius and Hallett, 2014; Lausch, *et al.*, 2017; Guidi, *et al.*, 2019). Both methods are routinely applied to protect global forest ecosystems. A comprehensive evaluation of forest health including multiple observations or measurements is needed for effective monitoring (Frolking, *et al.*, 2009; Gatica-Saavedra, *et al.*, 2017; Lausch, *et al.*, 2017).

To observe, or measure, a reduction in forest health using remote sensing requires choosing a well-fitting indicator (Noss, 1999; Lindenmayer, *et al.*, 2000; Juutinen and Mönkkönen, 2004; Pause, *et al.*, 2016). Choosing such an indicator is often one of the first steps in a forest health assessment (Meng, *et al.*, 2016). At both the individual tree level and at the level of forest stands or landscapes these indicators measure conditions, or the changes in them using a range of variables. These variables include crown vigor (Pontius, *et al.*, 2017; Grulke, *et al.*, 2020; Schrader-Patton, *et al.*, 2021), structural characteristics such as tree height, growing stock, or crown size (Pause *et al.*, 2016), phenology, water content, defoliation (Royle and Lathrop, 1997; Wyka, *et al.*, 2017), canopy discoloration, and fragmentation (Lausch, *et al.*, 2016; Bigler and Vitasse, 2021). Two prevailing techniques exist for conducting these assessments of forest health using modern, high-resolution, imagery: (1) aerial surveys or (2) digital image classification.

Aerial visual surveys using piloted aircraft provide excellent scales of observation, with potentially highly accurate results. The methods for conducting these surveys are well-defined and broadly adopted, allowing trained personnel to detect both tree species and disturbance type (e.g., disease or defoliation cause) even among complex forests (Broders, *et al.*, 2015; Coleman, *et al.*, 2018). Still, these surveys are restricted due to their: cost, inability to fly on-demand, insufficient temporal frequency for observing all types of disturbance, and limitation of only detecting areas that already show signs of invasion or stress. Close range digital remote sensing and satellite imagery classification allows users to precisely monitor long-term stress and change using indicators (Pause, *et al.*, 2016; Lausch, *et al.*, 2017). Digital imagery with modern hardware often assimilates the use of signal theory and increased spectral dimensionality for obtaining information from measured reflectance (Hoffbeck and Landgrebe, 1996). A primary example of this is chlorophyll fluorescence measurements, which assess the photosynthetic efficiency, or variation in it (stress), to determine vegetation status or health (Lausch, *et al.*, 2017; Guidi, *et al.*, 2019). When a plant becomes stressed, due to the impacts of some stressors, it is said to be ‘chlorotic’ which most results in a reduction in photosynthetic activity and is marked by a shift towards greater amounts of green and red reflectance (Horsley, *et al.*, 2002; Jensen, 2016). Both healthy and stressed leaves can be identified based on the internal and external structures of the leaf (e.g., chlorophylls and xanthophyll) and their responses to electromagnetic energy (Gago, *et al.*, 2015; Jensen, 2016). From small handheld devices to multimillion-dollar platforms, sensors are being developed and applied that can detect stress or changes in photosynthetic efficiency (i.e., metabolism) before visible indications are available (Chaerle and Van Der Straeten, 2000; Lausch, *et al.*, 2017). These remote sensing spectral responses are tested against laboratory analyses to distinguish between true and observed

reflectance (i.e., defining necessary radiometric corrections) (Hoffbeck and Landgrebe, 1996; Näsi, *et al.*, 2016; Choi, *et al.*, 2019). Once the true reflectance from a given sensor is defined, statistical relationships between spectral response and various biotic traits can be empirically modeled (Lausch, *et al.*, 2017; Lu, *et al.*, 2018). For example, many spectral band indices have been developed which can be used to interpret changes in vegetation status or condition (Royle and Lathrop, 1997; Pontius, *et al.*, 2017; Lu, *et al.*, 2018). The Normalized Difference Vegetation Index (NDVI), including modified versions, and forms of visible vegetative indices (VVI) represent two of the most readily applied methods (Kerr and Ostrovsky, 2003; Goodbody, *et al.*, 2018; Otsu, *et al.*, 2019; Zhang, *et al.*, 2020). The formula for NDVI and two common VVI can be seen below (**Equations 2, 3, and 4**).

Equation 2. Normalized Difference Vegetation Index (NDVI)

$$NDVI = \frac{(NIR-Red)}{(NIR+Red)}$$

Equation 3. Visible Vegetation Index (VVI).

$$VVI = \left[\left(1 - \left| \frac{Red-Red_0}{Red+Red_0} \right| \right) \left(1 - \left| \frac{Green-Green_0}{Green+Green_0} \right| \right) \left(1 - \left| \frac{Blue-Blue_0}{Blue+Blue_0} \right| \right) \right]$$

Equation 4. Normalized Green Red Difference Index (NGRDI).

$$Normalized\ Green\ Red\ Difference\ Index\ (NGRDI) = \frac{(Green-Red)}{(Green+Red)}$$

More advanced sensors, such as Goddard's LiDAR Hyperspectral and Thermal Imager (G-LiHT), bring together hyperspectral imaging and 3D laser scanner reconstructions to form fusion datasets. G-LiHT and comparable sensors are able to map vegetation communities, invasive species presences, natural disturbances, and carbon cycles (Lausch, *et al.*, 2017; Liu, *et*

al., 2017; Gerhards, *et al.*, 2019; Zhao, *et al.*, 2020). Multi-sensor data fusion has become more prominent in recent decades. However, challenges such as spectral intercalibration, temporal discontinuity, and positional misregistration must be managed when adopting these methods (Jenerowicz, *et al.*, 2017; Berra, *et al.*, 2019; Alvarez-Vanhard, *et al.*, 2020). Regardless of which platform and sensor is deployed, there remains two primary procedures for monitoring forest health using digital remotely sensed data. The first method is called image differencing which uses a time series analysis to diagnose patterns of change in an area. This method can be reliable but is sensitive to misregistration and calibration errors (Coppin and Bauer, 1996; Royle and Lathrop, 1997; Desclée, *et al.*, 2006). The second method is image classification. Image classification uses spectral responses, and any additional geospatial data, to distinguish distinct biotic traits (Royle and Lathrop, 1997; Jensen, 2016). Like aerial visual surveys, these digitally classified remotely sensed images can be still limited by temporal infrequencies, inflexible deployment conditions, cost, and cloud coverage (Jenerowicz, *et al.*, 2017; Berra, *et al.*, 2019; Næsset, *et al.*, 2019). Therefore, the question remains of how to best harmonize these evolving technologies with operational feasibility.

Unmanned Aerial Systems (UAS) have become a noteworthy platform for bringing geospatial sciences and technologies into the hands of more diverse stakeholders. Although UAS have had a long history of military development, consumer market demands and concurrent technological innovations have made this platform both economic and adaptive (Marshall, *et al.*, 2016; Fraser and Congalton, 2018). Several studies have used normal color or modified normal color consumer-grade cameras onboard UAS to measure vegetation biophysical properties with high precision (Lelong, *et al.*, 2008; Gini, *et al.*, 2014; Lehmann, *et al.*, 2015; Lu, *et al.*, 2018). Other studies have applied UAS for estimating attributes of individual trees and forest stands

(Tang and Shao, 2015; Michez, *et al.*, 2016; Liang, *et al.*, 2019; Zhou and Zhang, 2020). These efforts directly assist the need for large-scale (i.e., individual tree or management unit size) data which can be used for disturbance monitoring and decision making (Poland and McCullough, 2006; Kattenborn, *et al.*, 2019; Smigaj, *et al.*, 2019; Revill, *et al.*, 2020). Our study further defines a niche for UAS forest health assessments, between that of advanced data fusion techniques and more limited yet operational aerial surveys. Our goal is to provide a means for large-scale (local) land managers to have a more complete understanding of their forests, by supplementing in situ surveying. By providing information on the presence and abundance of stressed or degraded trees forest managers can more quickly react to lowered resource availability or diminished ecosystem function (Grulke, *et al.*, 2020). For this reason, we investigated the ability to classify coniferous and deciduous tree health classes, instead of targeting a specific disturbance event. To accomplish this, we evaluated the ability of simple multispectral sensors onboard UAS for distinguishing healthy, stressed, and degraded trees in complex, mixed-species, forests. Specifically, our objectives were:

- 1. Determine the capability of UAS for classifying forest health at the individual tree level**
- 2. Compare the results of forest health classification using UAS to high-resolution, multispectral, airborne imagery**

METHODS

Study Areas

Four woodland properties, managed by the University of New Hampshire (UNH) were employed in this research. These properties included: Kingman Farm, Thompson Farm, College Woods, and Moore Fields (**Figure 8**) and represent a total of 304.1 hectares (ha) of forests located near the main UNH campus. These study sites were chosen due to the availability of previous forest inventory records and for having a known presence of forest disturbances (e.g., WPND, HWA, EAB, and beech bark disease) (Eisenhaure, 2018; Woodlands, 2021).

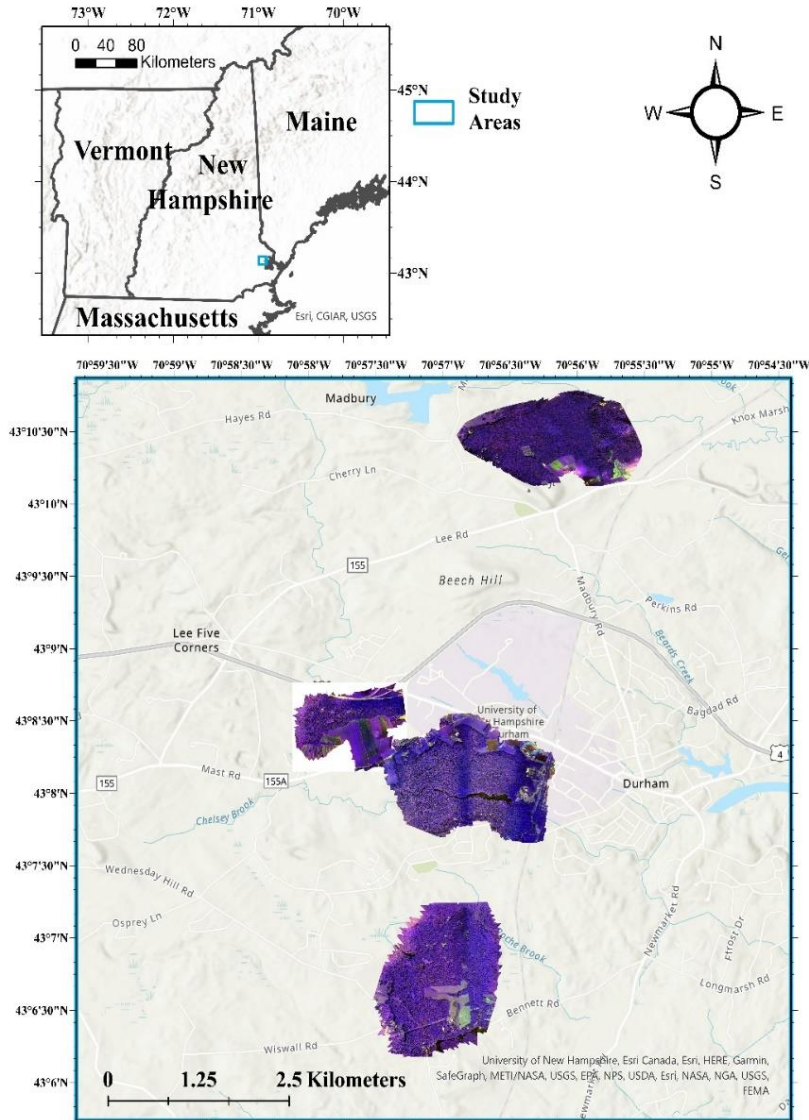


Figure 8. Four woodland properties evaluated during our assessment of forest health. Each property is shown using the multispectral (False Color Composite) orthoimagery generated from our Unmanned Aerial System (UAS) imagery.

Assessing Forest Health: Field and Photo Interpretation Survey

Field-based sampling was conducted to provide reference data for each forest health class. At each study area, we visited preexisting continuous forest inventory (CFI) plots to locate a variety coniferous and deciduous species (Eisenhaure, 2018; Fraser and Congalton, 2021a). These species included: Eastern white pine (*Pinus strobus*), Eastern hemlock (*Tsuga canadensis*), red pine (*Pinus resinosa*), American beech (*Fagus grandifolia*), red maple (*Acer*

rubrum), white ash (*Fraxinus americana*), and Northern red oak (*Quercus rubra*). Each individual tree was positionally located using a high-precision EOS Arrow 200 RTK GPS (EOS, 2021). The positional error, as reported by the device during sampling, ranged between 0.48 m and 3.19 m. Additional trees, were located for each health class while traversing the miles of trials distributed throughout each of the properties. To assess the health of each sampled tree, a team of two researchers used visual guides of crown vigor and degradation (Pontius and Hallett, 2014; Pontius, *et al.*, 2017). These visual charts and classifications are based on Pontius and Hallett, (2014) and supplemental practices suggested in Broders et al., (2015) and Innes (1998). This procedure was adopted due to the ease of implementation and available training. Using these charts, data on fine twig dieback, leaf discoloration, leaf defoliation, crown vigor, crown transparency, and crown light exposure (see Pontius and Hallett, 2014 or Hallett and Hallett, 2018 for definitions) were entered into the Healthy Trees Healthy Cities app (HTHC, 2021). This app then summarized the full suite of tree health attributes, using standardized variables (Z-scores) which were calculated using the mean and standard deviation of regional, species-specific, observations for each attribute (Green, 1979; Pontius and Hallett, 2014; Hallett and Hallett, 2018). For the final step, this app translated this comprehensive, species-specific, Z-scores for each tree into a 10-part, numeric, classification system, with lower values representing healthier trees (Pontius and Hallett, 2014; Hallett and Hallett, 2018).

For our analysis, we collapsed this 10-part classification system into five distinct forest health classes:

- **Coniferous (C)** – Healthy coniferous trees (e.g., eastern white pine or eastern hemlock) identified as having minimal or no signs of stress, which are calculated using the stress index as classes 1, 2, or 3.
- **Deciduous (D)** – Healthy deciduous trees (e.g., American beech, white ash, or Northern red oak) identified as having minimal or no signs of stress, which are calculated using the stress index as classes 1, 2, or 3.
- **Coniferous Stressed (CS)** – Stressed coniferous trees, displaying moderate or severe reductions in crown vigor, which are calculated using the stress index as classes 4 through 9.
- **Deciduous Stressed (DS)** – Stressed deciduous trees, displaying moderate or severe reductions in crown vigor, which are calculated using the stress index as classes 4 through 9.
- **Degraded/Dead (Snag)** – Coniferous or deciduous trees identified as stress class 10 (dead) which represent the most degraded of each health attribute.

A minimum of 20 samples for each of these five classes were collected during our field-inventory. Using these field samples, interpretation guides for each class were established (see **Appendix 3**). These guides were then used by a trained forest technician, in addition to ultra-high-resolution, multispectral UAS imagery, to photo interpret additional reference samples. Photo interpretation was conducted to provide a minimum of 70 samples for each forest health class providing for a more evenly distributed sample throughout the study areas.

Assessing Forest Health: Digital Image Classification

Airborne Imagery

To examine the performance of digitally classifying these five forest health classes using freely available, high-resolution, remotely sensed imagery our first analysis was conducted using 2018 National Agriculture Imagery Program (NAIP) imagery. These images were collected at a 60 cm spatial resolution, with 4 spectral bands (blue, green, red, and near infrared (NIR) (USDA, 2021). To provide an evaluation of individual trees, these images were segmented using a

multiresolution segmentation algorithm within eCognition (v9.1). The segmentation parameters, as refined in our previous study (Fraser and Congalton, 2021b), were: Scale 10, Shape 0.2, and Compactness 0.5. These parameters provided an over segmented result, which was necessary for digitally classifying individual trees. For each image object, 30 object level features were calculated including: spectral, textural, and geometric attributes, as well as three spectral indices (NDVI, NGRDI, and the Greenness Index). These spectral indices were selected due to their given association with plant stress (Louhaichi et al., 2001; Gago, *et al.*, 2015; Lu, *et al.*, 2018; Otsu, *et al.*, 2019). The equations for NDVI and NGRDI are given above (**Equations 2** and **4**) while the equation for the Greenness Index is presented here (**Equation 5**).

Equation 5. Greenness Index.

$$\text{Greenness Index} = \frac{(\text{Mean Green} - \text{Mean Red}) + (\text{Mean Green} - \text{Mean Blue})}{(2 * \text{Mean Green}) + (\text{Mean Red}) + (\text{Mean Blue})}$$

UAS Imagery

UAS imagery were collected using a combination of two aircraft, the senseFly eBee X and its predecessor the eBee Plus (senseFly, 2018, senseFly, 2019a). To obtain natural color imagery, the eBee Plus was operated with its associated Sensor Optimized for Drone Applications (S.O.D.A.) while the eBee X utilized the senseFly Aeria X sensor (senseFly, 2019b, 2019c). These sensors provided the photogrammetric basis for the marker-controlled watershed segmentation (MCWS) described in the next section as well as uncalibrated blue, green, and red spectral bands. Multispectral UAS imagery was collected using the Parrot Sequoia+. This five-lens sensor system is comprised of a natural color sensor (not used in this study), as well as independent green (550 ±40 nm), red (660 ±40 nm), NIR (790 ±40 nm), and red edge (735 ±10 nm), lenses (senseFly, 2021). All missions were conducted using the eMotion flight management

software (eMotion, 2021). The flight parameters for all missions consisted of 85% forward overlap between images, 90% side overlap, consistent sun-angles and cloud exposures, and flying heights of 121.92 m (400 ft) above the ground (Dandois, *et al.*, 2015; Puliti, *et al.*, 2015; Fraser and Congalton, 2018). Prior to missions conducted using the Parrot Sequoia+ sensor, a radiometric calibration target was used to adjust the camera reflectance to absolute measurements (senseFly, 2021). During post-processing, individual image locations were positionally corrected using the National Oceanic and Atmospheric Administrations (NOAA) Continuously Operating Reference Stations (CORS) and the aircrafts flight logs (NOAA, 2019). The positionally corrected images were then brought into Agisoft MetaShape (v 1.5.5.) for Structure from Motion Multi-View Stereo (SfM-MVS) modelling. For each study area, a set of both natural color and multispectral images were processed using the provided SfM workflow within this software. We selected the “High Accuracy” image alignment option, then the “Ultra High” setting for each of the remaining modelling steps (Fraser and Congalton, 2018; Gu, *et al.*, 2020; Fraser and Congalton, 2021b). An ultra-high-resolution digital elevation model (DEM) was generated from the natural color imagery to support the segmentation process. Two orthomosaics (i.e., orthoimages) were produced for each property; one from each of the natural color and multispectral workflows.

The UAS imagery was segmented using a MCWS technique outlined in Gu *et al.*, (2020) (Chen, *et al.*, 2018; Fraser and Congalton, 2021a). First, a canopy height model (CHM) for each of the four study areas was created by subtracting a 2 m New Hampshire lidar bare earth model from the UAS DEMs (GRANIT, 2021). A Gaussian (low pass) filter was then applied to these CHMs to remove residual noise in the data (Panagiotidis, *et al.*, 2017; Chen, *et al.*, 2018; Gu, *et al.*, 2020). To establish the individual treetops (i.e., ‘markers’), a fixed, circular, window size of

4.5 m was used to identify the local maxima. This window size was found to provide a more accurate single tree delineation in previous studies (Gu, *et al.*, 2020; Fraser and Congalton, 2021a; Gu and Congalton, 2021). An object detection rate (ODR) and segmentation Quality Rate (QR) for these data and study areas are defined in our previous study, Fraser and Congalton (2021a). Following the individual tree detection and delineation (ITDD) process, we created a composite of the natural color and multispectral UAS imagery for each study area. A nearest neighbor raster resampling tool, within ArcGIS Pro (v 2.8.0), was used to resample the higher spatial resolution natural color imagery to match the respective study areas multispectral imagery (Alonzo, *et al.*, 2014; Hogland, *et al.*, 2018; Chandel, *et al.*, 2020). This resampling ensured we retained spatial data consistency during the classification process (García, *et al.*, 2018; Alvarez-Vanhard, *et al.*, 2020; Gu and Congalton, 2021). These composite images were then used to generate 36 image object features in eCognition (**see Appendix 3**).

Forest Health Accuracy Assessment

For the forest health assessment of both the NAIP and UAS imagery, the final check of the reference trees was conducted using photo interpretation and manual (on-screen) editing. Points that could not be matched to corresponding species (i.e., nearby image objects) in either set of imagery were removed. The final sample size for each forest health class for each set of imagery are in **Table 16**.

Table 16. Reference data sample sizes for each forest health class for both the NAIP and UAS imagery digital classifications.

	Coniferous	Coniferous Stressed	Deciduous	Deciduous Stressed	Dead/Degraded
NAIP	87	70	84	71	79
UAS	90	70	84	73	91

To quantify the accuracy of classifying for health classes using each source of imagery, we adopted thematic map accuracy assessment error matrices (Congalton and Green, 2019). A number of accuracy assessment (i.e., training and validation data splitting methods) and classification techniques were applied to analyze the results generated from the UAS and NAIP imagery. For the NAIP imagery, all tests were performed using a random forests (RF) supervised classification algorithm (Breiman, 2001; Maxwell, *et al.*, 2018b; Fraser and Congalton, 2021a). For the UAS imagery, in addition to using the RF classification algorithm, the support vector machine (SVM) algorithm was also employed (Chapelle, *et al.*, 1999; Pal and Mather, 2005). This secondary algorithm was included due to the often case-specific superior classification performance found between these two techniques (Maxwell, *et al.*, 2018b; Wessel, *et al.*, 2018; Fraser and Congalton, 2021b). When using the RF classification algorithm, the following analyses were applied: (1) a standard cross-validation with a split of 55% training data and 45% validation data; (2) this same approach with a 50% training and validation data split; (3) splitting the training and validation data 55%/45% but with the removal of the least important image features (i.e., feature reduction); (4) performing the validation using an out-of-bag (OOB) permutation; (5) classifying coniferous and deciduous tree health classes independently; and (6) collapsing the forest health classes into only 'healthy' (a combination of coniferous and deciduous trees), 'stressed', and 'degraded.' Two additional tests were applied to the UAS image classification, using the RF algorithm, to investigate the influence of the redundant image bands included when making a composite of the natural color and multispectral imagery. Each evaluation was performed a minimum of 10 times, so that an average overall accuracy could be produced. For both the NAIP and UAS imagery, a mean decrease in impurity (MDI) test was used to quantify the importance of individual spectral, geometric, and textural image features.

The SVM classifier was applied only to the UAS imagery. This classification included a standard cross-validation, with a split of 55% training and 45% validation data (similar to the first RF classification analysis above). This SVM classification was also completed 10 times, so that an average overall classification accuracy could be compared to the RF classification results.

RESULTS

Airborne Imagery

Our first assessment of forest health using digitally classified thematic layers was implemented using the freely available NAIP imagery. The individual classification results from each method and averaged (10 trials) overall accuracies can be seen in **Table 17**. In this table, we see that the highest overall accuracy, when including all five classes, was achieved using a 55%, 45% training and validation sample split and the removal of the least important image features (i.e., feature reduction) (**Figure 9**). The out-of-bag (OOB) accuracy for this same method resulted in a 10.7% lower overall accuracy. When the forest health classes were generalized to only ‘healthy’, ‘stressed’, and ‘degraded’, the overall accuracy reached 70.62%. This average accuracy is also similarly achieved when classifying coniferous (72.5%) and deciduous (66.3%) classes independently. In **Table 18**, we provide an example error matrix created using the 55% training sample size and feature reduction method, with five classes, to further understand the difference in accuracy between this approach and the accuracy achieved using the generalized (3) classes.

Table 17. NAIP imagery classification accuracies for each random forests classification method. The highest accuracy for our five-class scheme is highlighted in green.

	55% Training Split	50% Training Split	55% Training and Feature Reduction	55% Training Out-of-Bag	Coniferous Only	Deciduous Only	Healthy/Stressed/Degraded
1	0.5568	0.5153	0.5227	0.4093	0.7196	0.6698	0.7102
2	0.5	0.5051	0.4943	0.3907	0.729	0.6604	0.7102
3	0.5568	0.5051	0.4545	0.4093	0.729	0.6509	0.7443
4	0.517	0.5204	0.5	0.386	0.7102	0.6509	0.6875
5	0.4886	0.4847	0.4659	0.4093	0.729	0.6604	0.7102
6	0.5057	0.4796	0.4375	0.3814	0.7383	0.6227	0.6761
7	0.4602	0.5102	0.7943	0.4093	0.7102	0.6604	0.75
8	0.4886	0.5051	0.4716	0.3907	0.6822	0.6887	0.7045
9	0.5	0.4643	0.4261	0.3953	0.757	0.6509	0.6818
10	0.4487	0.5051	0.483	0.3953	0.7477	0.717	0.6875
Average	0.50224	0.49949	0.50499	0.39766	0.72522	0.66321	0.70623

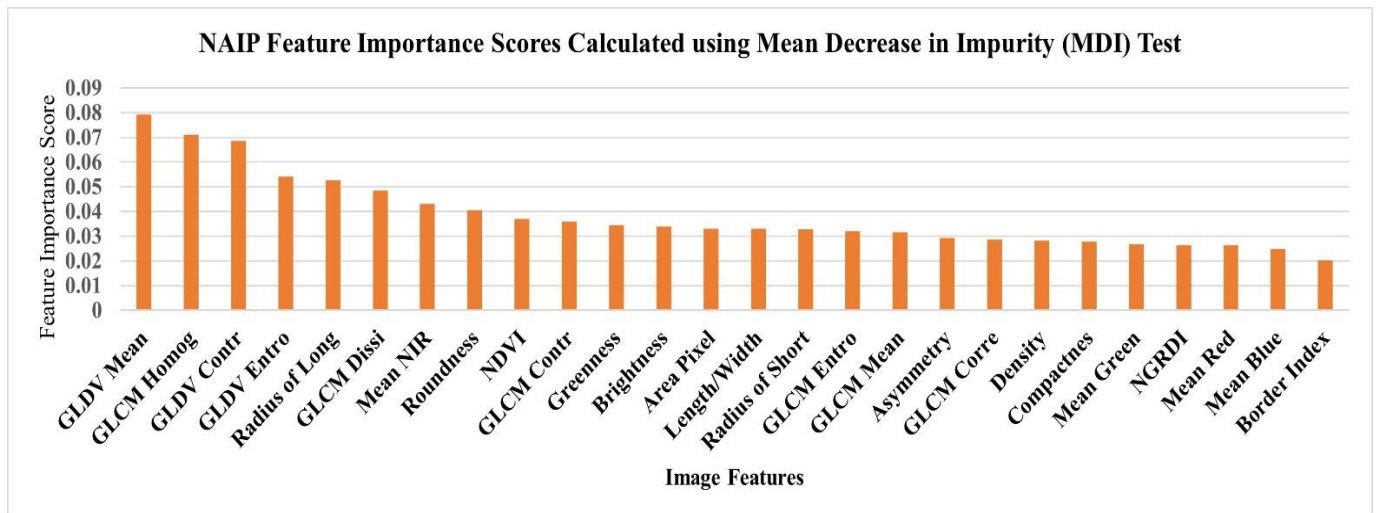


Figure 9. Mean decrease in impurity (MDI) image feature scores calculated using the NAIP imagery and random forests classifier.

Table 18. Forest health thematic map accuracy assessment error matrix produced using the NAIP imagery, random forests (RF) supervised classification algorithm, and feature reduction digital classification method. The classes represented in this error matrix include: Coniferous (C), Deciduous (D), Coniferous Stressed (CS), Deciduous Stressed (DS), and Snag (Dead/Degraded).

		Field (Reference) Data					TOTAL	USERS ACCURACY
		C	D	CS	DS	Snag		
NAIP Imagery Using the RF Classifier	C	27	8	5	8	2	50	54.0%
	D	6	19	1	3	0	29	65.52%
	CS	2	1	12	8	4	27	44.44%
	DS	2	8	6	8	0	24	33.33%
	Snag	2	2	7	5	30	46	65.21%
TOTAL		39	38	31	32	36	96/174	
PRODUCERS ACCURACY		69.23%	50.0%	38.71%	25.0%	83.33%		OVERALL ACCURACY 55.17%

UAS Imagery

The UAS-SfM processing for this study generated a natural color (SODA) and multispectral (Sequoia) orthomosaic for each of the four properties. These spatial models comprised pixel sizes (i.e., ground sampling distances or spatial resolution) ranging from 11.6 cm to 13.2 cm for the multispectral imagery. The average spatial resolution was 12.55 cm. A number of supervised, digital, classification techniques were employed to assess forest health classes (**Table 19**). In this table, we see that the highest average overall accuracy was produced using a 55% training, 45% validation, sample split and the OOB evaluation method (65.43%). This result was only slightly higher, 0.376%, than the 55% training and feature reduction method. This feature reduction was based on the MDI scores found using this method (**Figure 10**). We additionally applied these classification methods without the SODA green and red bands, and again without any of the SODA bands. Both iterations produced a slight decrease in

the average overall accuracy. When exchanging the random forests classifier for the SVM classifier, the overall accuracy lowered by approximately 8%. Lastly, when generalizing the health assessment to ‘healthy’, ‘stressed’ and ‘degraded’ trees, the overall accuracy reached 71.19%. When examining one of the error matrices produced using the five-class health assessment (**Table 20**) we see that some of the misclassification was the result of confusion between coniferous and deciduous classes.

Table 19. UAS imagery classification accuracies for each random forests and SVM classification method. The highest accuracy for our five-class scheme is highlighted in green.

	55% Training Split	50% Training Split	55% Training and Feature Reduction	Without green and red (SODA)	Without SODA Bands	55% Training Out-of-Bag	Coniferous Only	Deciduous Only	SVM	Healthy/Stressed/Degraded
1	0.6685	0.6225	0.6522	0.6685	0.6576	0.6637	0.7876	0.7232	0.5761	0.7609
2	0.6359	0.6373	0.6304	0.6522	0.6196	0.6592	0.7522	0.7321	0.6087	0.701
3	0.6413	0.6814	0.6141	0.6413	0.6359	0.6637	0.8053	0.7679	0.587	0.7174
4	0.6304	0.6618	0.6793	0.6793	0.6685	0.6592	0.7522	0.7946	0.5489	0.7228
5	0.6359	0.652	0.663	0.6413	0.6087	0.6771	0.7876	0.7768	0.5543	0.701
6	0.625	0.6373	0.6359	0.5978	0.5987	0.6099	0.7788	0.6696	0.5924	0.7065
7	0.6685	0.6029	0.6413	0.6467	0.6467	0.6457	0.7964	0.7054	0.5543	0.6848
8	0.6685	0.6667	0.6737	0.6033	0.663	0.6323	0.7611	0.6607	0.5707	0.7174
9	0.6413	0.652	0.6739	0.6304	0.6576	0.6637	0.7788	0.7232	0.5435	0.6902
10	0.6576	0.6324	0.6413	0.5924	0.6902	0.6682	0.8407	0.7232	0.5652	0.7174
Average	0.64729	0.64463	0.65051	0.63532	0.64465	0.65427	0.78407	0.72767	0.57011	0.71194

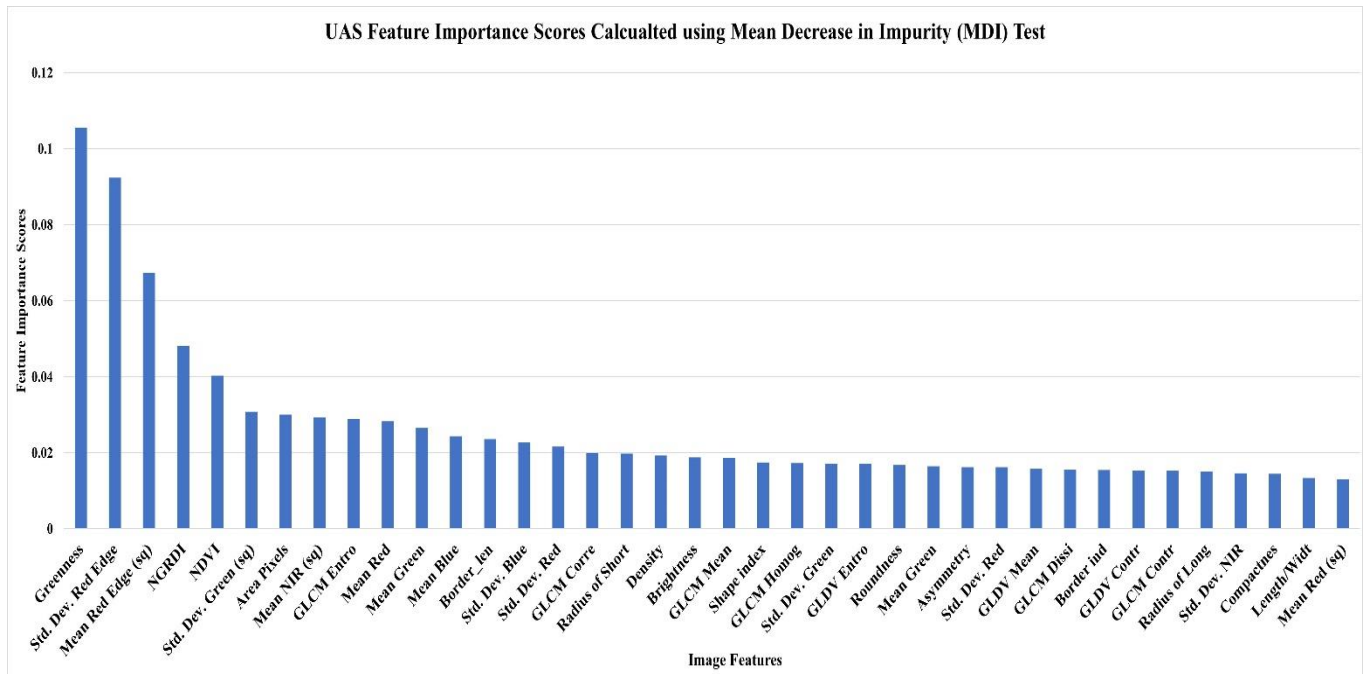


Figure 10. UAS classification feature importance scores calculated using the MDI test.

Table 20. Forest health thematic map accuracy assessment error matrix produced using the UAS imagery, random forests (RF) classifier, and feature reduction digital classification method. The classes represented in this error matrix include: Coniferous (C), Deciduous (D), Coniferous Stressed (CS), Deciduous Stressed (DS), and Snag (Dead/Degraded).

		Field (Reference) Data						
		C	D	CS	DS	Snag	TOTAL	USERS ACCURACY
UAS Imagery Using the RF Classifier	C	30	1	8	7	4	50	60.0%
	D	7	31	0	13	0	51	60.78%
	CS	3	0	18	4	0	25	72.0%
	DS	1	6	3	6	5	21	28.57%
	Snag	0	0	2	3	32	37	86.49%
TOTAL		41	38	31	33	41	117/184	
PRODUCERS ACCURACY		73.17%	81.58%	58.06%	18.18%	78.05%		OVERALL ACCURACY 63.59%

DISCUSSION

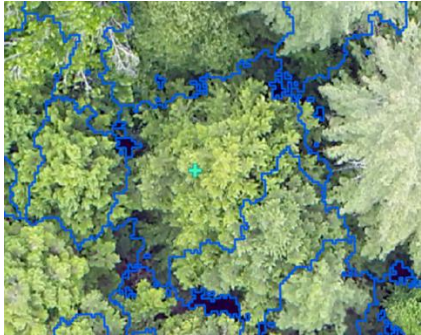
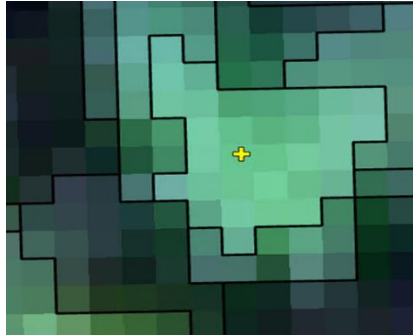

The invasion of forest ecosystems by exotic diseases and insects is one of the most detrimental threats to their stability and productivity (Vitousek, *et al.*, 1996; Morin, *et al.*, 2015). Forest health and forest degradation, known to guide losses in species diversity and timber resources, are increasingly coming to the attention of forest managers (Thompson, *et al.*, 2013; Gunn, *et al.*, 2019; Meng, *et al.*, 2019). These negative effects are subject to a positive feedback loop with climate change for much of the world and are further heightening the concern of forest owners and managers as they require demand more intense monitoring of their forest communities (Lehmann *et al.*, 2015; Wilson *et al.*, 2019). One of the most sought-after types of information pertaining to regional stressors is the distribution and environmental factors that influence forest diseases and pests (Wyka, *et al.*, 2017; Janowiak, *et al.*, 2018; Simoes, *et al.*, 2019). In our study, we showed that UAS imagery correctly classify forest health classes with an overall accuracy that was 14.93% higher than high-resolution airborne imagery. The lowest class specific producers' accuracy was for stressed deciduous trees. Many of these trees were incorrectly labeled as healthy. The redundancy in the green and red image bands when using a composite of the SODA and Sequoia sensors did not have a negative influence on the classification accuracy. Instead, using all the image bands from both sensors resulted in a 1.52% increase in overall accuracy. Additionally, the MDI test conducted during the classification of the UAS imagery showed that the spectral indices (e.g., NDVI and NGRDI) were some of the most important image features along with the red edge band, which is unique to the Sequoia sensor. Our results are in agreement with several other studies (Zhang, *et al.*, 2015; Mulatu, *et al.*, 2019; Otsu, *et al.*, 2019). Lastly, when the forest health classes were generalized to 'healthy', 'stressed', and 'degraded', to avoid species misclassification, the UAS still outperformed the airborne imagery. During independent analysis of coniferous and deciduous species, the UAS

imagery reached an overall classification accuracy for forest health of 71.19%. In similar studies, UAS imagery was used to assess specific tree species and disturbance types. In a study by Nasi et al., (2018), a hyperspectral sensor was used to survey Norway spruce (*Picea abies L. Karst.*) that had been infested by European spruce bark beetles (*Ips typographus L.*). Their evaluation resulted in an overall accuracies of 79% for airborne imagery and 81% for UAS imagery for similar forest health classes to our study (Nasi et al., 2019). In Cardil et al., (2017) researchers studied two pine dominated areas experiencing defoliation due to pine processionary moth (*Thaumetopoea pityocampa*). Using only a natural color camera onboard a UAS, tree level defoliation was correctly identified with an overall accuracy of 79% (Cardil, et al., 2017). Time relevant, field-based surveys of forest health at actionable scales incurs too high of a cost, emphasizing the need for remote sensing tools (Kampen, et al., 2019). Many contemporary investigations focus on one or two specific tree species or stressors. New England forests, however, feature a multitude of natural and anthropogenic disturbances as well as an exceptionally high species diversity at local scales (Janowiak, et al., 2018; Pasquarella, et al., 2018; Simoes, et al., 2019). A competent management tool for land managers in this region should be able to identify stressed or degraded individual trees from among the species rich population that is naturally present.

Despite the successes that this research and similar studies have found in the application of UAS for fine scale forest health monitoring, there are several sources of uncertainty that should be further explored. Due to the variability in response that individual trees exhibit to stress, disease, or pests, other researchers have regarded UAS as serving only as a predictor of areas requiring priority management (Barbedo, 2019). Even using a binary classification of ‘healthy’ or ‘degraded’ trees, many environmental factors in natural ecosystems may have

adversely affected our ‘healthy’ reference trees. While methods do exist to collect field-based spectral reflectance data, which could provide a more direct comparison to UAS remotely sensed image features, these methods elicit considerable time and resources for large study areas especially in complex, mixed-species forests (Tree and Slusser, 2005; Adam, *et al.*, 2017; Jha, *et al.*, 2019; Zhu, *et al.*, 2019). Another source of uncertainty in this study was the reliance on the Parrot Sequoia+ multispectral sensor. Despite the sunshine sensor and calibration plate coupled with the Parrot Sequoia+, this sensor is subject to influences of the camera temperature, atmospheric conditions, and variability in the sunshine sensor orientation during flight (Olsson, *et al.*, 2021). Prior to use for normalizing the irradiance of the multispectral images, the sunshine sensor data should be smoothed. This pre-processing would create a more radiometrically consistent estimate of reflectance across flights and especially across study areas (Berni, *et al.*, 2009; Jensen, 2016; Olsson, *et al.*, 2021). In our original investigations we also proposed a comparison to satellite sensors with a higher spectral resolution (e.g., Sentinel-2), as a way to more fully understand the spectral properties of these forest health classes. Early on in the classification however, it became clear that such satellite sensors lacked the spatial resolution to sufficiently address our reference trees. **Table 21** provides representation of these data sources and the scale of the individual tree observations.

Table 21. Characterization of individual trees using three sources of remotely sensed imagery. (1) UAS natural color imagery, segmented to provide an analysis of a singular Eastern hemlock (*Tsuga canadensis*). (2) NAIP imagery, segmented to analyze this same tree. (3) Sentinel-2 imagery, depicting a singular 10 m pixel (in yellow) overlaid on the UAS segmented individual tree crowns.

Spatial Resolution and the Scale of Individual Tree Analysis		
UAS (11.6 cm pixel)	NAIP (60 cm pixel)	Sentinel-1 (10 m pixel)
		

Instead of a comparison between UAS and other remote sensing platforms, data fusion remains a promising expectation for future research with these complex forests. The constraints of frequent monitoring make piloted aircraft techniques logistically challenging (Berra, *et al.*, 2019). Image fusion allows users to overcome the shortcomings of single data source limitations. For example, with the fusion of satellite and UAS imagery, users could overcome the low spatial resolution of most satellite sensors and the limited coverage that can be accomplished by UAS (Jenerowicz, *et al.*, 2017; Alvarez-Vanhard, *et al.*, 2020). Lastly, using UAS as an intermediate step for ground-level observations could also increase the efficiencies found in data scaling (Kampen, *et al.*, 2019; Reville, *et al.*, 2020). UAS, as opposed to field measurements, allow for a far greater abundance of reference measurements to be made for scaling models (Kattenborn, *et al.*, 2019).

These imagery combinations may help monitor fine scale change patterns over diverse ecosystems (Xia, *et al.*, 2017). To accurately engage methods of data fusion between UAS and other sensors, several challenges should be examined. The first being spectral intercalibration. Despite independent radiometric calibration of the UAS data, there can remain differences between the spectral values measured by the UAS and satellite data (Alvarez-Vanhard, *et al.*, 2020). Another fundamental challenge is the co-registration of such high-resolution imagery. Even with real-time kinematic (RTK) receivers on the misalignment of either data source by mere pixels could have a dramatic impact on the accuracy of their resulting data product (Jensen, 2016; Xia, *et al.*, 2017; Kattenborn, *et al.*, 2019). Lastly, there is a consequential challenge in collecting imagery from both data source on the same date. Even with only a few days of separation between collecting such UAS and satellite images, differences in spectral reflectance, solar/viewing angles, or environmental conditions could cause inconsistencies in the data fusion process (Jenerowicz, *et al.*, 2017; Xia, *et al.*, 2017).

CONCLUSIONS

The distribution and severity of forest health stressors present too great of an impact on natural ecosystems for field-based monitoring to capture and monitor alone. These events are causing billions of dollars in diminished ecosystem services and management costs across a variety of keystone tree species. Unmanned Aerial Systems (UAS) provide forest and natural resource managers with the ability to evaluate and monitor individual trees across scales that are consistent with their silvicultural practices. In our study, we examined the viability of UAS for classifying various levels of forest health within complex, mixed-species, forests in New England. These results serve as a basis for prioritizing field investigations of stands identified to consist of stressed or degraded trees. Using a composite of natural color and multispectral UAS

imagery we achieved overall classification accuracies ranging between 65.43% and 71.19%. Some limitations in our approach include the imprecise calibration of our multispectral imagery and the variation on characteristics found among ‘healthy’ trees in natural environments. A necessary next step for this research is the fusion, rather than comparison, of these UAS with more widely available remotely sensed imagery. Such a step would expand the operational feasibility of UAS and address many of the challenges in precision forest health monitoring and management.

CONCLUSIONS

To engage the challenges facing forests in the 21st requires both a better understanding of their patterns and drivers, as well as a greater amount of information on the intricacies of forest ecosystems in general (Ge, *et al.*, 2007; Young, 2010; Ackerly, *et al.*, 2015; Asbeck, *et al.*, 2021). There are numerous natural resources and data science disciplines working collaboratively in these efforts. In our research, we examine one promising remote sensing tool, Unmanned Aerial Systems, which embrace compelling developments in many of these fields.

In the first chapter, we compared the ability of UAS to classify forest compositions to other sources of high-resolution remotely sensed imagery. The results detailed that UAS provided the highest overall classification accuracy for local scale forest composition. Machine learning digital classifications outperformed photo interpretation methods, achieving accuracies as high as 70.48%, at the individual tree level for four forest classes. The individual tree detection accuracy, for complex mixed-species forests, was promising at 93.9% for the tree detection rate. Further refinement of image segmentation techniques to properly delineate

distinct species in overlapping canopies would benefit the mapping of local scale forest composition in such environments (Yan, *et al.*, 2018; Lobo Torres, *et al.*, 2020; Gu and Congalton, 2021).

In the second chapter, we estimated individual tree and stand level attributes using UAS digital photogrammetry. Individual tree diameter at breast height, based on estimations using crown geometry produced an average estimation error of 13.15 cm ($r = 0.3792$). Again, the difficulties in accurately delineating individual trees proved one of the most prominent challenges. For stand level estimations, such as basal area per hectare, photogrammetric estimates performed well for stands larger than nine ha. For such stands, BA/ha was overestimated by just 14.629%. Other stand level attributes such as trees per hectare, quadratic mean diameter, and stand density index showed similarly promising results, given the efficiency of these surveying techniques. While analyzing these spatial data, one of the primary limitations of this procedure was the tendency for the MCWS workflow to over segment the largest trees and under segment the smallest trees. This is seen by comparing the field-measured dbh measurements, and those estimated using the UAS digital photogrammetry (**Figure 11**).

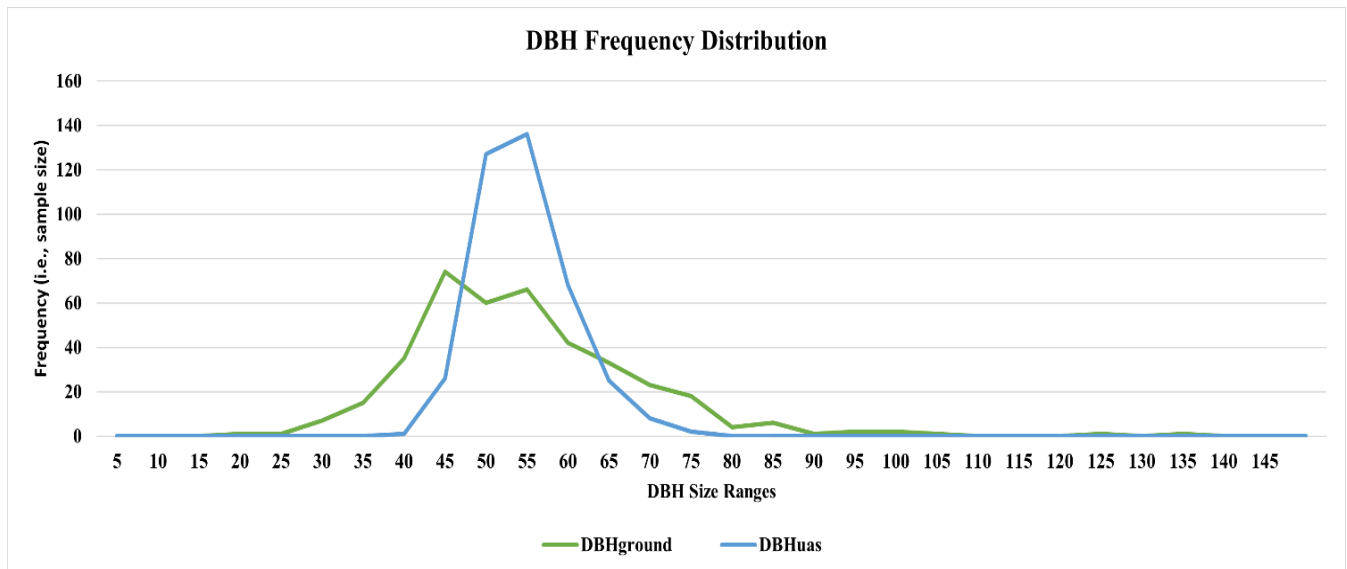


Figure 11. Frequency distributions (i.e., sample sizes) plotted by diameter at breast height (dbh) size ranges for both field-measured reference trees and these same tree diameters estimated using digital photogrammetry.

As a secondary objective for this study, we included an investigation of the ability for UAS to survey rare community characteristics. In our analysis of mapping large trees in complex forests, this research provided an efficient and novel solution to the challenges previously experienced during field-based sampling methods (Lutz, *et al.*, 2012; Harris, *et al.*, 2021). As with the limitations experienced while measuring other individual tree characteristics during this study, further refinement of each analysis step (e.g., segmentation, feature extraction, and supervised classification) will inevitably promote these efforts as a suitable technique for conservationists.

The third chapter recognized the need for data on forest composition and health at scales that are similar to silvicultural practices (Kampen, *et al.*, 2019). With this study, we enriched our assessment of individual tree and stand level characteristics from chapters 1 and 2 by incorporating an evaluation of individual tree health. Using a composite of UAS natural color and multispectral imagery, we successfully detected, delineated, and classified the health of individual trees. The overall classification accuracy for forest health ranged from 65.43% to

71.19% using digitally classified UAS imagery. While other studies have demonstrated higher accuracies for species- and disturbance- specific assessments (such as (Cardil, *et al.*, 2017; Näsi, *et al.*, 2018)) our objective remained to provide an approach relevant to forest managers confronting complex, mixed-species forests with multifaceted disturbance regimes (Janowiak, *et al.*, 2018; Kirchhoefer, *et al.*, 2019).

While carrying out these studies we identified several factors prompting further research and discussion. A notable extension of our work would infer data fusion. While multi-sensor UAS configurations are becoming more common, a true expansion for each of our studies would include the scaling of these methods to airborne or moderate resolution satellite imagery (Sankey, *et al.*, 2017; Kampen, *et al.*, 2019; Kattenborn, *et al.*, 2019; Revill, *et al.*, 2020). The fusion of UAS and other remotely sensed data sources would provide a pathway for more deeply exploring the spectral characteristics of our UAS data and increase the transferability of these methods to regional level assessments (Hernandez-Santin, *et al.*, 2019; Alvarez-Vanhard, *et al.*, 2020). For example, with sufficient evaluation these techniques could come to match or surpass the geographic coverage of leading forest health assessment methods (Coleman, *et al.*, 2018; Berra, *et al.*, 2019; Schepaschenko, *et al.*, 2019). Another necessary augmentation of this research would be the expansion of our methods for the analysis of urban environments. Urban forests provide global communities with countless ecosystem services (McPherson, *et al.*, 1997; Wolf, 2008; Dearborn and Kark, 2010). Some studies have already explored case-specific urban forestry applications, more research is needed to emphasis both the benefits that these trees offer and the degradation that they are experiencing (Wu, 2014; Hassaan, *et al.*, 2016; Liu, *et al.*, 2017). Lastly, no discussion of UAS applications can ignore the influence of current regulatory frameworks. While decades of use have proven the benefits of UAS for countless disciplines,

these applications, at least in the U.S. still exist in an atmosphere of uncertainty (Dalamagkidis, *et al.*, 2008; Colomina and Molina, 2014; Cummings, *et al.*, 2017; Fraser and Congalton, 2018). Both the general use of these systems, and the funding of their use in scientific research are not without routine turbulence. As hardware and software technologies continue to progress, the true future of these methods will be decided by their associated policy, regulation, and public advocacy.

LITERATURE CITED

- Abdullah, S., Tahar, K.N., Rashid, M.F.A., Osoman, M.A., 2019. Capabilities of UAV-Based Watershed Segmentation Method for Estimating Tree Crown: A Case Study of Oil Palm Tree. *IOP Conf. Ser. Earth Environ. Sci.* 385, 1–8. <https://doi.org/10.1088/1755-1315/385/1/012015>
- Ackerly, D.D., Cornwell, W.K., Weiss, S.B., Flint, L.E., Flint, A.L., 2015. A geographic mosaic of climate change impacts on terrestrial vegetation: Which areas are most at risk? *PLoS One* 10, 1–30. <https://doi.org/10.1371/journal.pone.0130629>
- Adam, E., Deng, H., Odindi, J., Abdel-Rahman, E.M., Mutanga, O., 2017. Detecting the early stage of phaeosphaeria leaf spot infestations in maize crop using in situ hyperspectral data and guided regularized random forest algorithm. *J. Spectrosc.* 2017. <https://doi.org/10.1155/2017/6961387>
- Aguilar, F.J., Nemmaoui, A., Aguilar, M.A., Peñalver, A., 2019. Fusion of terrestrial laser scanning and RPAS image-based point clouds in Mediterranean forest inventories. *Dyna* 94, 131–136. <https://doi.org/10.6036/8882>
- Ali, A., Lin, S.L., He, J.K., Kong, F.M., Yu, J.H., Jiang, H.S., 2019. Big-sized trees overrule remaining trees' attributes and species richness as determinants of aboveground biomass in tropical forests. *Glob. Chang. Biol.* 25, 2810–2824. <https://doi.org/10.1111/gcb.14707>
- Alonzo, M., Bookhagen, B., Roberts, D.A., 2014. Urban tree species mapping using hyperspectral and lidar data fusion. *Remote Sens. Environ.* 148, 70–83. <https://doi.org/10.1016/j.rse.2014.03.018>
- Alvarez-Vanhard, E., Houet, T., Mony, C., Lecoq, L., Corpetti, T., 2020. Can UAVs fill the gap between in situ surveys and satellites for habitat mapping? *Remote Sens. Environ.* 243. <https://doi.org/10.1016/j.rse.2020.111780>
- Anderson, J.R., Hardy, E.E., Roach, J.T., Witmer, R.E., 1976. A land use and land cover classification system for use with remote sensor data. *Geol. Surv. Prof. Pap.* 964, 41 pp.
- Asbeck, T., Großmann, J., Paillet, Y., Winiger, N., Bauhus, J., 2021. The Use of Tree-Related Microhabitats as Forest Biodiversity Indicators and to Guide Integrated Forest Management. *Curr. For. Reports* 7, 59–68. <https://doi.org/10.1007/s40725-020-00132-5>
- Aukema, J.E., Leung, B., Kovacs, K., Chivers, C., Britton, K.O., Englin, J., Frankel, S.J., Haight, R.G., Holmes, T.P., Liebhold, A.M., McCullough, D.G., von Holle, B., 2011. Economic impacts of Non-Native forest insects in the continental United States. *PLoS One* 6, 1–8. <https://doi.org/10.1371/journal.pone.0024587>
- Avery, T.E., 1969. *Forester's Guide To Aerial Photo Interpretation*. U.S. Department of Agriculture. Forest Service. Agriculture handbook No 308.
- Baena, S., Moat, J., Whaley, O., Boyd, D.S., 2017. Identifying species from the air: UAVs and the very high resolution challenge for plant conservation. *PLoS One* 12, 1–22. <https://doi.org/10.1371/journal.pone.0188714>

- Barbedo, J.G.A., 2019. A review on the use of unmanned aerial vehicles and imaging sensors for monitoring and assessing plant stresses. *Drones* 3, 1–27. <https://doi.org/10.3390/drones3020040>
- Barnhart, R.K., Hottman, S.B., Marshall, D.M., Shappee, E., 2012. *Introduction to Unmanned Aerial Systems*, 1st Editio. ed. CRC Press, Boca, Raton, FL.
- Baylis, S.M., Herrod, A., Hodgson, J.C., Clarke, R.H., Mott, R., 2016. Precision wildlife monitoring using unmanned aerial vehicles. *Sci. Rep.* 6, 1–7. <https://doi.org/10.1038/srep22574>
- Belgiu, M., Drăgu, L., 2016. Random forest in remote sensing: A review of applications and future directions. *ISPRS J. Photogramm. Remote Sens.* 114, 24–31. <https://doi.org/10.1016/j.isprsjprs.2016.01.011>
- Berhane, T.M., Lane, C.R., Wu, Q., Autrey, B.C., Anenkhonov, O.A., Chepinoga, V. V., Liu, H., 2018. Decision-tree, rule-based, and random forest classification of high-resolution multispectral imagery for wetland mapping and inventory. *Remote Sens.* 10. <https://doi.org/10.3390/rs10040580>
- Berni, J., Zarco-Tejada, P.J., Suarez, L., Fereres, E., 2009. Thermal and Narrowband Multispectral Remote Sensing for Vegetation Monitoring From an Unmanned Aerial Vehicle. *IEEE Trans. Geosci. Remote Sens.* 47, 722–738. <https://doi.org/10.1109/TGRS.2008.2010457>
- Berra, E.F., Gaulton, R., Barr, S., 2019. Assessing spring phenology of a temperate woodland: A multiscale comparison of ground, unmanned aerial vehicle and Landsat satellite observations. *Remote Sens. Environ.* 223, 229–242. <https://doi.org/10.1016/j.rse.2019.01.010>
- Betchold, W.A., Patterson, P.L., 2005. *The Enhanced Forest Inventory and Analysis Program - National Sampling Design and Estimation Procedures*. United States Dep. Agric. South. Res. Stn. SRS-80.
- Bigler, C., Vitasse, Y., 2021. Premature leaf discoloration of European deciduous trees is caused by drought and heat in late spring and cold spells in early fall. *Agric. For. Meteorol.* 307, 108492. <https://doi.org/10.1016/j.agrformet.2021.108492>
- Blaschke, T., 2010. Object based image analysis for remote sensing. *ISPRS J. Photogramm. Remote Sens.* 65, 2–16. <https://doi.org/10.1016/j.isprsjprs.2009.06.004>
- Bohlin, J., Bohlin, I., Jonzén, J., Nilsson, M., 2017. Mapping forest attributes using data from stereophotogrammetry of aerial images and field data from the national forest inventory. *Silva Fenn.* 51, 1–18. <https://doi.org/10.14214/sf.2021>
- Bohlin, J., Bohlin, I., Jonzén, J., Nilsson, M., de Oliveira, L.F.R., Lassiter, H.A., Wilkinson, B., Whitley, T., Ifju, P., Logan, S.R., Peter, G.F., Vogel, J.G., Martin, T.A., Gillis, M.D., Omule, A.Y., Brierley, T., Goldbergs, G., Maier, S.W., Levick, S.R., Edwards, A., Gu, J., Grybas, H., Congalton, R.G., Hyypä, H.J., Hyypä, J.M., Iizuka, K., Yonehara, T., Itoh, M., Kosugi, Y., Shang, C., Coops, N.C., Wulder, M.A., White, J.C., Hermosilla, T., Wieser, M., Mandlbürger, G., Hollaus, M., Otepka, J., Glira, P., Pfeifer, N., 2020. Estimating Tree

- Height and Diameter at Breast Height (DBH) from Digital surface models and orthophotos obtained with an unmanned aerial system for a Japanese Cypress (*Chamaecyparis obtusa*) Forest. *Remote Sens.* 10, 1–11. <https://doi.org/10.5558/tfc81214-2>
- Bohlin, J., Wallerman, J., Fransson, J.E.S., 2012. Forest variable estimation using photogrammetric matching of digital aerial images in combination with a high-resolution DEM. *Scand. J. For. Res.* 27, 692–699. <https://doi.org/10.1080/02827581.2012.686625>
- Boisvenue, C., White, J.C., 2019. Information needs of next-generation forest carbon models: Opportunities for remote sensing science. *Remote Sens.* 11. <https://doi.org/10.3390/rs11040463>
- Bonnor, G.M., 1964. A tree volume table for red pine by crown width and height. *For. Chronicles* 40, 339–346.
- Breiman, L., 2001. Random Forests. *Mach. Learn.* 45, 5–32.
- Broders, K., Munck, I., Wyka, S., Iriarte, G., Beaudoin, E., 2015. Characterization of fungal pathogens associated with white pine needle damage (WPND) in Northeastern North America. *Forests* 6, 4088–4104. <https://doi.org/10.3390/f6114088>
- Brown de Colstoun, E.C., Story, M.H., Thompson, C., Commisso, K., Smith, T.G., Irons, J.R., 2003. National Park vegetation mapping using multitemporal Landsat 7 data and a decision tree classifier. *Remote Sens. Environ.* 85, 316–327.
- Bullock, J.L., Hainje, R., Habib, A., Horton, D., Bullock, D.M., 2019. Public Safety Implementation of Unmanned Aerial Systems for Photogrammetric Mapping of Crash Scenes. *Transp. Res. Rec.* 2673, 567–574. <https://doi.org/10.1177/0361198119850804>
- Burns, J., Delparte, D., Gates, R., Takabayashi, M., 2015. Integrating structure-from-motion photogrammetry with geospatial software as a novel technique for quantifying 3D ecological characteristics of coral reefs. *PeerJ* 3, e1077. <https://doi.org/10.7717/peerj.1077>
- Burns, R.M., Honkala, B.H., 1990. *Silvics of North America*. Agric. 654 2, 877.
- Burrough, P.A., 2001. GIS and geostatistics: Essential partners for spatial analysis. *Environ. Ecol. Stat.* 8, 361–377.
- Cade, B.S., 1997. Comparisons of Tree Basal Area and Canopy Cover in Habitat Models: Subalpine Forest. *J. Wildl. Manage.* 61, 326. <https://doi.org/10.2307/3802588>
- Cale, J.A., Garrison-Johnston, M.T., Teale, S.A., Castello, J.D., 2017. Beech bark disease in North America: Over a century of research revisited. *For. Ecol. Manage.* 394, 86–103. <https://doi.org/10.1016/j.foreco.2017.03.031>
- Candiago, S., Remondino, F., De Giglio, M., Dubbini, M., Gattelli, M., 2015. Evaluating multispectral images and vegetation indices for precision farming applications from UAV images. *Remote Sens.* 7, 4026–4047. <https://doi.org/10.3390/rs70404026>
- Cao, L., Liu, H., Fu, X., Zhang, Z., Shen, X., Ruan, H., 2019. Comparison of UAV LiDAR and digital aerial photogrammetry point clouds for estimating forest structural attributes in subtropical planted forests. *Forests* 10, 1–26. <https://doi.org/10.3390/f10020145>

- Cardil, A., Vepakomma, U., Brotons, L., 2017. Assessing pine processionary moth defoliation using unmanned aerial systems. *Forests* 8. <https://doi.org/10.3390/f8100402>
- Carey, J.H., 1993. *Quercus velutina*. Fire Eff. Inf. Syst. U.S. Dep. Agric. For. Serv. Rocky Mt. Res. Station. Fire Sci. Lab. URL <https://www.fs.fed.us/database/feis/plants/tree/quevel/all.html>
- Carey, J.H., 1992. *Tsuga canadensis*. Fire Eff. Inf. Syst. U.S. Dep. Agric. For. Serv. Rocky Mt. Res. Station. Fire Sci. Lab. URL <https://www.fs.fed.us/database/feis/plants/tree/tsucan/all.html>
- Chaerle, L., Van Der Straeten, D., 2000. Imaging Techniques and the early detection of plant stress. *Trends Plant Sci.* 5, 495–501. <https://doi.org/> [https://doi.org/10.1016/S1360-1385\(00\)01781-7](https://doi.org/10.1016/S1360-1385(00)01781-7)
- Chandel, A.K., Molaei, B., Khot, L.R., Peters, R.T., Stöckle, C.O., 2020. High resolution geospatial evapotranspiration mapping of irrigated field crops using multispectral and thermal infrared imagery with metric energy balance model. *Drones* 4, 1–19. <https://doi.org/10.3390/drones4030052>
- Chapelle, O., Haffner, P., Vapnik, V.N., 1999. Support vector machines for histogram-based image classification. *IEEE Trans. Neural Networks* 10, 1055–1064. <https://doi.org/10.1109/72.788646>
- Chen, Jun, Chen, Jin, Liao, A., Cao, X., Chen, L., Chen, X., He, C., Han, G., Peng, S., Lu, M., Zhang, W., Tong, X., Mills, J., 2015. Global land cover mapping at 30 m resolution: A POK-based operational approach. *ISPRS J. Photogramm. Remote Sens.* 103, 7–27. <https://doi.org/10.1016/j.isprsjprs.2014.09.002>
- Chen, Y., Hakala, T., Karjalainen, M., Feng, Z., Tang, J., Litkey, P., Kukko, A., Jaakkola, A., Hyypä, J., 2017. UAV -Borne Profiling radar for Forest Research. *Remote Sens.* 9, 58. <https://doi.org/10.3390/rs9010058>
- Chen, Y., Ming, D., Zhao, L., Lv, B., Zhou, K., Qing, Y., 2018. Review on high spatial resolution remote sensing image segmentation evaluation. *Photogramm. Eng. Remote Sensing* 84, 629–646. <https://doi.org/10.14358/PERS.84.10.629>
- Choi, S., Kim, Y., Lee, J.H., You, H., Jang, B.J., Jung, K.H., 2019. Minimizing Device-to-Device Variation in the Spectral Response of Portable Spectrometers. *J. Sensors* 2019. <https://doi.org/10.1155/2019/8392583>
- Clinton, N., Holt, A., Scarborough, J., Yan, L., Gong, P., 2010. Accuracy Assessment measures for object-based image segmentation goodness. *Photogrammetric Eng. Remote Sens.* 76, 289–299.
- Coleman, T.W., Graves, A.D., Heath, Z., Flowers, R.W., Hanavan, R.P., Cluck, D.R., Ryerson, D., 2018. Accuracy of aerial detection surveys for mapping insect and disease disturbances in the United States. *For. Ecol. Manage.* 430, 321–336. <https://doi.org/10.1016/j.foreco.2018.08.020>
- Colomina, I., Molina, P., 2014. Unmanned aerial systems for photogrammetry and remote sensing: A review. *ISPRS J. Photogramm. Remote Sens.* 92, 79–97.

<https://doi.org/10.1016/j.isprsjprs.2014.02.013>

- Colwell, R.N., 1955. Some uses of Three-Dimensional Models for Illustrating Photogrammetric Principles. *Photogramm. Eng.* 20.
- Congalton, R.G., Green, K., 2019. *Assessing the Accuracy of Remotely Sensed Data: Principles and Practices*, Third Edit. ed. CRC Press, Boca, Raton, FL.
- Congalton, R.G., Green, K., Teply, J., 1993. Mapping old growth forests on national forest and park lands in the Pacific Northwest from remotely sensed data. *Photogramm. Eng. Remote Sens.* 59, 529–535.
- Congalton, R.G., Gu, J., Yadav, K., Thenkabail, P., Ozdogan, M., 2014. Global land cover mapping: A review and uncertainty analysis. *Remote Sens.* 6, 12070–12093. <https://doi.org/10.3390/rs61212070>
- Coppin, P.R., Bauer, M.E., 1996. Digital Change Detection in Forest Ecosystems with Remote Sensing Imagery. *Remote Sens. Rev.* 13, 207–234.
- Corte, A.P.D., Rex, F.E., de Almeida, D.R.A., Sanquetta, C.R., Silva, C.A., Moura, M.M., Wilkinson, B., Zambrano, A.M.A., da Cunha Neto, E.M., Veras, H.F.P., de Moraes, A., Klauberg, C., Mohan, M., Cardil, A., Broadbent, E.N., 2020. Measuring individual tree diameter and height using gatereye high-density UAV-lidar in an integrated crop-livestock-forest system. *Remote Sens.* 12. <https://doi.org/10.3390/rs12050863>
- Costanza, R.R., de Groot, R., Farber, S., Grasso, M., Hannon, B., Limburg, K., Naeem, S., O'Neill, R. V., Paruelo, J., Raskin, R.G., Sutton, P., van den Belt, M., 1997. The Value of the world's ecosystem services and natural capital. *Nature* 253–256.
- Cummings, A., McKee, A., Kulkarni, K., Markandey, N., 2017. The Rise of UAVs. *Photogramm. Eng. Remote Sens.* 83, 317–325. <https://doi.org/10.14358/pers.83.4.317>
- Curtis, R.O., Marshall, D.D., 2000. Why quadratic mean diameter? *West. J. Appl. For.* 15, 137–139.
- Dalamagkidis, K., Valavanis, K.P., Piegler, L.A., 2008. On unmanned aircraft systems issues, challenges and operational restrictions preventing integration into the National Airspace System. *Prog. Aerosp. Sci.* 44, 503–519. <https://doi.org/10.1016/j.paerosci.2008.08.001>
- Dandois, J.P., Olano, M., Ellis, E.C., 2015. Optimal altitude, overlap, and weather conditions for computer vision uav estimates of forest structure. *Remote Sens.* 7, 13895–13920. <https://doi.org/10.3390/rs71013895>
- Day, D., Weaver, W., Wilsing, L., 2016. Accuracy of UAS Photogrammetry: A Comparative Evaluation. *Photogramm. Eng. Remote Sens.* 82, 909–914. <https://doi.org/10.14358/pers.82.12.909>
- de Oliveira, L.F., Lassiter, H.A., Wilkinson, B., Whitley, T., Ifju, P., Logan, S.R., Peter, G.F., Vogel, J.G., Martin, T.A., 2021. Moving to Automated Tree Inventory: Comparison of UAS_Derived Lidar and Photogrammetric Data with Manual Ground Estimates. *Remote Sens.* 13, 72. <https://doi.org/10.3390/rs13010072>

- Dearborn, D.C., Kark, S., 2010. Motivations for Conserving Urban Biodiversity. *Conserv. Biol.* 24, 432–440. <https://doi.org/10.1111/j.1523-1739.2009.01328.x>
- Desclée, B., Bogaert, P., Defourny, P., 2006. Forest change detection by statistical object-based method. *Remote Sens. Environ.* 102, 1–11. <https://doi.org/10.1016/j.rse.2006.01.013>
- Ducey, M.J., 2001. Workshop Proceedings: Forest Measurements for Natural Resource Professionals., in: *Natural Resource Network: Connecting Research, Teaching, and Outreach*. University of New Hampshire Cooperative Extension, University of New Hampshire, p. 71 pp.
- Ducey, M.J., Gunn, J.S., Whitman, A.A., 2013. Late-successional and old-growth forests in the northeastern United States: Structure, dynamics, and prospects for restoration. *Forests* 4, 1055–1086. <https://doi.org/10.3390/f4041055>
- Ducey, M.J., Knapp, R.A., 2010. A stand density index for complex mixed species forests in the northeastern United States. *For. Ecol. Manage.* 260, 1613–1622. <https://doi.org/10.1016/j.foreco.2010.08.014>
- Effiom, A.E., van Leeuwen, L.M., Nyktas, P., Okojie, J.A., Erdbrügger, J., 2019. Combining unmanned aerial vehicle and multispectral Pleiades data for tree species identification, a prerequisite for accurate carbon estimation. *J. Appl. Remote Sens.* 13, 1–20. <https://doi.org/10.1117/1.JRS.13.034530>
- Eisenhaure, S., 2018. Kingman Farm Management and Operations Plan 2018.
- EMotion, S., 2021. senseFly Drone Flight Management software versions 3.15 (eBee Plus) and 3.19) eBee X. URL <https://www.sensefly.com/software/emotion/>
- EOS, 2021. Arrow 200 RTK GNSS. EOS Position. Syst. URL https://eos-gnss.com/product/arrow-series/arrow-200/?gclid=Cj0KCQjw2tCGBhCLARIsABJGmZ47-nIPNrAu7Xobgf3POHGIV4mMLHHWZz25lyHM6UuI_pPCu7b2gMaAukeEALw_wcB
- Eyre, F.H., 1980. *Forest Cover Types of the United States and Canada*: Society of American Foresters 148 pp.
- FAA, 2021. *Certificated Remote Pilots Including Commercial Operators*: Federal Aviation Administration. URL https://www.faa.gov/uas/commercial_operators/
- Falkowski, M.J., Evans, J.S., Martinuzzi, S., Gessler, P.E., Hudak, A.T., 2009. Characterizing forest succession with lidar data: An evaluation for the Inland Northwest, USA. *Remote Sens. Environ.* 113, 946–956. <https://doi.org/10.1016/j.rse.2009.01.003>
- FAO, 2016. *Forests and Agriculture: Land-Use Challenges and Opportunities*, State of the world's forests. FAO, Rome.
- FAO, 2000. *Global Forest Resource Assessment 2000 (FRA 2000)*.
- Fassnacht, F.E., Latifi, H., Stereńczak, K., Modzelewska, A., Lefsky, M., Waser, L.T., Straub, C., Ghosh, A., 2016. Review of studies on tree species classification from remotely sensed data. *Remote Sens. Environ.* 186, 64–87. <https://doi.org/10.1016/j.rse.2016.08.013>
- Fernández-álvarez, M., Armesto, J., Picos, J., 2019. LiDAR-based wildfire prevention in WUI:

- The automatic detection, measurement and evaluation of forest fuels. *Forests* 10. <https://doi.org/10.3390/f10020148>
- Fonstad, M.A., Dietrich, J.T., Courville, B.C., Jensen, J.L., Carbonneau, P.E., 2013. Topographic structure from motion: a new development in photogrammetric measurement. *Earth Surf. Process. Landforms* 38, 421–430. <https://doi.org/10.1002/esp.3366>
- Foody, G.M., 2015. Valuing map validation: The need for rigorous land cover map accuracy assessment in economic valuations of ecosystem services. *Ecol. Econ.* 111, 23–28. <https://doi.org/10.1016/j.ecolecon.2015.01.003>
- Foody, G.M., 2002. Status of land cover classification accuracy assessment. *Remote Sens. Environ.* 80, 185–201. [https://doi.org/10.1016/S0034-4257\(01\)00295-4](https://doi.org/10.1016/S0034-4257(01)00295-4)
- Foody, G.M., 1999. The continuum of classification fuzziness in thematic mapping. *Photogramm. Eng. Remote Sensing* 65, 443–451.
- Forrester, D.I., 2014. The spatial and temporal dynamics of species interactions in mixed-species forests: From pattern to process. *For. Ecol. Manage.* 312, 282–292. <https://doi.org/10.1016/j.foreco.2013.10.003>
- Franklin, S.E., Ahmed, O.S., 2018. Deciduous tree species classification using object-based analysis and machine learning with unmanned aerial vehicle multispectral data. *Int. J. Remote Sens.* 39, 5236–5245. <https://doi.org/10.1080/01431161.2017.1363442>
- Fraser, B.T., Congalton, R.G., 2021b. A Comparison of Methods for Determining Forest Composition from High-Spatial Resolution Remotely Sensed Imagery. *Forests In Review*.
- Fraser, B.T., Congalton, R.G., 2021a. Estimating Primary Forest Attributes and Rare Community Characteristics using Unmanned Aerial Systems (UAS): An Enrichment of Conventional Forest Inventories. *Remote Sens.* 13, 2971. <https://doi.org/10.3390/rs13152971>
- Fraser, B.T., Congalton, R.G., 2019. Evaluating the Effectiveness of Unmanned Aerial Systems (UAS) for Collecting Thematic Map Accuracy Assessment Reference Data in New England Forests. *Forests* 10, 24. <https://doi.org/10.3390/f10010024>
- Fraser, B.T., Congalton, R.G., 2018. Issues in Unmanned Aerial Systems (UAS) data collection of complex forest environments. *Remote Sens.* 10. <https://doi.org/10.3390/rs10060908>
- Frauman, E., Wolff, E., 2005. Segmentation of Very High Spatial Resolution Satellite Images in Urban Areas for Segments-Based Classification. *Proc. ISPRS 5th Int. Symp. Remote Sens. Urban Areas*.
- Fritz, A., Kattenborn, T., Koch, B., 2013. UAV-BASED PHOTOGRAMMETRIC POINT CLOUDS & TREE STEM MAPPING IN OPEN STANDS IN COMPARISON TO TERRESTRIAL LASER SCANNER POINT CLOUDS. *ISPRS - Int. Arch. Photogramm. Remote Sens. Spat. Inf. Sci.* XL-1/W2, 141–146. <https://doi.org/10.5194/isprsarchives-xl-1-w2-141-2013>
- Frolking, S., Palace, M.W., Clark, D.B., Chambers, J.Q., Shugart, H.H., Hurtt, G.C., 2009. Forest disturbance and recovery: A general review in the context of spaceborne remote sensing of impacts on aboveground biomass and canopy structure: *J. Geophys. Res.*

Biogeosciences 114, n/a--n/a. <https://doi.org/10.1029/2008JG000911>

- Fuchs, H.J., 2003. Methodisch Anasatze zur Erfassung von Waldbaumen mittels digitaler Luftbildauswertung. Gottingen University.
- Gago, J., Douthe, C., Coopman, R.E., Gallego, P.P., Ribas-Carbo, M., Flexas, J., Escalona, J., Medrano, H., 2015. UAVs challenge to assess water stress for sustainable agriculture. *Agric. Water Manag.* 153, 9–19. <https://doi.org/10.1016/j.agwat.2015.01.020>
- Ganz, S., Käber, Y., Adler, P., 2019. Measuring Tree Height with Remote Sensing — A Comparison of Photogrammetric and LiDAR Data with Di ff erent Field Measurements.
- García, M., Saatchi, S., Ustin, S., Balzter, H., 2018. Modelling forest canopy height by integrating airborne LiDAR samples with satellite Radar and multispectral imagery. *Int. J. Appl. Earth Obs. Geoinf.* 66, 159–173. <https://doi.org/10.1016/j.jag.2017.11.017>
- Gatica-Saavedra, P., Echeverría, C., Nelson, C.R., 2017. Ecological indicators for assessing ecological success of forest restoration: a world review. *Restor. Ecol.* 25, 850–857. <https://doi.org/10.1111/rec.12586>
- Ge, J., Qi, J., Lofgren, B.M., Moore, N., Torbick, N., Olson, J.M., 2007. Impacts of land use/cover classification accuracy on regional climate simulations. *J. Geophys. Res. Atmos.* 112, 1–12. <https://doi.org/10.1029/2006JD007404>
- Gerhards, M., Schlerf, M., Mallick, K., Udelhoven, T., 2019. Challenges and future perspectives of multi-/Hyperspectral thermal infrared remote sensing for crop water-stress detection: A review. *Remote Sens.* 11. <https://doi.org/10.3390/rs11101240>
- Gillan, J.K., Karl, J.W., van Leeuwen, W.J.D., 2020. Integrating drone imagery with existing rangeland monitoring programs. *Environ. Monit. Assess.* 192, 10661. <https://doi.org/10.1007/s10661-020-8216-3>
- Gillis, M.D., Omule, A.Y., Brierley, T., 2005. Monitoring Canada’s forests: The national forest inventory. *For. Chron.* 81, 214–221. <https://doi.org/10.5558/tfc81214-2>
- Gini, R., Passoni, D., Pinto, L., Sona, G., 2014. Use of unmanned aerial systems for multispectral survey and tree classification: A test in a park area of northern Italy. *Eur. J. Remote Sens.* 47, 251–269. <https://doi.org/10.5721/EuJRS20144716>
- Gini, R., Sona, G., Ronchetti, G., Passoni, D., Pinto, L., 2018. Improving Tree Species Classification Using UAS Multispectral Images and texture Measures. *Int. J. Geo-Information* 7.
- Goetz, S., Dubayah, R., 2011. Advances in remote sensing technology and implications for measuring and monitoring forest carbon stocks and change. *Carbon Manag.* 2, 231–244. <https://doi.org/10.4155/cmt.11.18>
- Goldbergs, G., Maier, S.W., Levick, S.R., Edwards, A., 2018. Efficiency of individual tree detection approaches based on light-weight and low-cost UAS imagery in Australian Savannas. *Remote Sens.* 10. <https://doi.org/10.3390/rs10020161>
- Goodbody, T.R.H., Coops, N.C., Hermosilla, T., Tompalski, P., Crawford, P., 2018. Assessing

- the status of forest regeneration using digital aerial photogrammetry and unmanned aerial systems. *Int. J. Remote Sens.* 39, 5246–5264.
<https://doi.org/10.1080/01431161.2017.1402387>
- Goodbody, T.R.H., Coops, N.C., Marshall, P.L., Tompalski, P., Crawford, P., 2017. Unmanned aerial systems for precision forest inventory purposes: A review and case study. *For. Chron.* 93, 71–81. <https://doi.org/10.5558/tfc2017-012>
- Goodbody, T.R.H., Tompalski, P., Coops, N.C., Hopkinson, C., Treitz, P., van Ewijk, K., 2020. Forest inventory and diversity attribute modelling using structural and intensity metrics from multi-spectral airborne laser scanning data. *Remote Sens.* 12.
<https://doi.org/10.3390/rs12132109>
- Goodchild, M.F., 1992. Geographical Data Modeling *Computers and Geosciences* 18,4, 401-408.
- Google Earth, 2021. Google Earth Satellite Imagery. URL
<https://earth.google.com/web/@10.757402,34.78251121,620.99875321a,19577839.73696211d,35y,0h,0t,0r/data=Ci4SLBIgOGQ2YmFjYjU2ZDZlMTFIOThiNTM2YjMzNGRiYmRhYTAlCGxheWVyc18w>
- GRANIT, 2021. GRANIT LiDAR Distribution Site. URL <https://lidar.unh.edu/map/>
- Green, R., 1979. *Sampling Design and Statistical Methods for Environmental Biologists*. John Wiley and Sons Inc., NY, NY. U.S.
- Grulke, N., Bienz, C., Hrinkevich, K., Maxfield, J., Uyeda, K., 2020. Quantitative and qualitative approaches to assess tree vigor and stand health in dry pine forests. *For. Ecol. Manage.* 465, 118085. <https://doi.org/10.1016/j.foreco.2020.118085>
- Gu, J., Congalton, R.G., 2021. Individual Tree Crown Delineation From UAS Imagery Based on Region Growing by Over-Segments With a Competitive Mechanism. *IEEE Trans. Geosci. Remote Sens.* 1–11. <https://doi.org/10.1109/TGRS.2021.3074289>
- Gu, Jianyu, Grybas, H., Congalton, R.G., 2020. A comparison of forest tree crown delineation from unmanned aerial imagery using canopy height models vs. spectral lightness. *Forests* 11. <https://doi.org/10.3390/F11060605>
- Gu, J., Grybas, H., Congalton, R.G., 2020. Individual Tree Crown Delineation from UAS Imagery Based on Region Growing and Growth Space Considerations. *Remote Sens.* 12, 2363.
- Guidi, L., Lo Piccolo, E., Landi, M., 2019. Chlorophyll fluorescence, photoinhibition and abiotic stress: Does it make any difference the fact to be a C3 or C4 species? *Front. Plant Sci.* 10, 1–11. <https://doi.org/10.3389/fpls.2019.00174>
- Guimarães, N., Pádua, L., Marques, P., Silva, N., Peres, E., Sousa, J.J., 2020. Forestry remote sensing from unmanned aerial vehicles: A review focusing on the data, processing and potentialities. *Remote Sens.* 12. <https://doi.org/10.3390/rs12061046>
- Gunn, J.S., Ducey, M.J., Belair, E., 2019. Evaluating degradation in a North American temperate forest. *For. Ecol. Manage.* 432, 415–426. <https://doi.org/10.1016/j.foreco.2018.09.046>

- Gunn, J.S., Ducey, M.J., Buchholz, T., Belair, E.P., 2020. Forest Carbon Resilience of Eastern Spruce Budworm (*Choristoneura fumiferana*) Salvage Harvesting in the Northeastern United States. *Front. For. Glob. Chang.* 3, 1–13. <https://doi.org/10.3389/ffgc.2020.00014>
- Hadas, E., Jozkow, G., Walicka, A., Borkowski, A., 2019. Apple orchard inventory with a LiDAR equipped unmanned aerial system. *Int. J. Appl. Earth Obs. Geoinf.* 82, 101911. <https://doi.org/10.1016/j.jag.2019.101911>
- Hallett, R., Hallett, T., 2018. Citizen Science and Tree Health Assessment: How useful are the data? *Arboric. urban For.* 44, 236–247.
- Hallett, R., Johnson, M.L., Sonti, N.F., 2018. Assessing the tree health impacts of salt water flooding in coastal cities : A case study in New York City. *Landsc. Urban Plan.* 177, 171–177. <https://doi.org/10.1016/j.landurbplan.2018.05.004>
- Hallett, R.A., Bailey, S.W., Horsley, S.B., Long, R.P., 2006. Influence of nutrition and stress on sugar maple at a regional scale. *Can. J. For. Res.* 36, 2235–2246. <https://doi.org/10.1139/x06-120>
- Hansen, A.J., Neilson, R.P., Dale, V.H., Flather, C.H., Iverson, L.R., Currie, D.J., Shafer, S., Cook, R., Bartlein, P.J., 2001. Global Change in Forests: Responses of Species, Communities, and Biomes. *Bioscience* 51, 765. [https://doi.org/10.1641/0006-3568\(2001\)051\[0765:GCIFRO\]2.0.CO;2](https://doi.org/10.1641/0006-3568(2001)051[0765:GCIFRO]2.0.CO;2)
- Hardin, P.J., Jackson, M.W., 2005. An Unmanned Aerial Vehicle for Rangeland Photography 6.
- Harris, D.J., Ndolo Ebika, S.T., Sanz, C.M., Madingou, M.P.N., Morgan, D.B., 2021. Large trees in tropical rain forests require big plots. *Plants People Planet* 3, 282–294. <https://doi.org/10.1002/ppp3.10194>
- Harris, P.M., Ventura, S.J., 1995. The integration of geographic data with remotely sensed imagery to improve classification in an urban area. *Photogrammetric Eng. Remote Sens.* 61, 993–998.
- Hartel, T., Hanspach, J., Moga, C.I., Holban, L., Szapanyos, Á., Tamás, R., Hováth, C., Réti, K.O., 2018. Abundance of large old trees in wood-pastures of Transylvania (Romania). *Sci. Total Environ.* 613–614, 263–270. <https://doi.org/10.1016/j.scitotenv.2017.09.048>
- Harwin, S., Lucieer, A., 2012. Assessing the accuracy of georeferenced point clouds produced via multi-view stereopsis from Unmanned Aerial Vehicle (UAV) imagery. *Remote Sens.* 4, 1573–1599. <https://doi.org/10.3390/rs4061573>
- Hassaan, O., Nasir, A.K., Roth, H., Khan, M.F., 2016. Precision Forestry: Trees Counting in Urban Areas Using Visible Imagery based on an Unmanned Aerial Vehicle. *IFAC-PapersOnLine* 49, 16–21. <https://doi.org/10.1016/j.ifacol.2016.10.004>
- He, H.S., Mladenoff, D.J., Radeloff, V.C., Crow, T.R., 1998. Integration of GIS Data and Classified Satellite Imagery for Regional Forest Assessment. *Ecol. Appl.* 8, 12.
- He, Y., Lee, E., Warner, T.A., 2017. A time series of annual land use and land cover maps of China from 1982 to 2013 generated using AVHRR GIMMS NDVI3g data. *Remote Sens. Environ.* 199, 201–217. <https://doi.org/10.1016/j.rse.2017.07.010>

- Hernandez-Santin, L., Rudge, M.L., Bartolo, R.E., Erskine, P.D., 2019. Identifying species and monitoring understorey from uas-derived data: A literature review and future directions. *Drones* 3, 1–18. <https://doi.org/10.3390/drones3010009>
- Hinkley, E.A., Zajkowski, T., 2011. USDA forest service-NASA: Unmanned aerial systems demonstrations - pushing the leading edge in fire mapping. *Geocarto Int.* 26, 103–111. <https://doi.org/10.1080/10106049.2011.555823>
- Hirschmugl, M., Ofner, M., Raggam, J., Schardt, M., 2007. Single tree detection in very high resolution remote sensing data. *Remote Sens. Environ.* 110, 533–544. <https://doi.org/10.1016/j.rse.2007.02.029>
- Hoffbeck, J.P., Landgrebe, D.A., 1996. Classification of Remote Sensing Images Having High Spectral Resolution. *Remote Sensing Environ.* 57, 119–126.
- Hogland, J., Anderson, N., St. Peter, J., Drake, J., Medley, P., 2018. Mapping Forest Characteristics at Fine Resolution across Large Landscapes of the Southeastern United States Using NAIP Imagery and FIA Field Plot Data. *ISPRS Int. J. Geo-Information* 7, 140. <https://doi.org/10.3390/ijgi7040140>
- Hölbling, D., Eisank, C., Albrecht, F., Vecchiotti, F., Friedl, B., Weinke, E., Kociu, A., 2017. Comparing manual and semi-automated landslide mapping based on optical satellite images from different sensors. *Geosci.* 7. <https://doi.org/10.3390/geosciences7020037>
- Holloway, J., Mengersen, K., 2018. Statistical Machine Learning Methods and Remote Sensing for Sustainable Development Goals: A review. *Remote Sens. Environ.* 10. <https://doi.org/10.1126/science.1103618>
- Horcher, A., Visser, R.J.M., 2004. Unmanned Aerial Vehicles: Applications for Natural Resource Management and Monitoring.- COFE (Council on. For. Eng. Annu. 1212.
- Horsley, S.B., Long, R.P., Bailey, S.W., Hallett, R.A., Wargo, P.M., 2002. Health of Eastern North American sugar maple forests and factors affecting decline. *North. J. Appl. For.* 19, 34–44. <https://doi.org/10.1093/njaf/19.1.34>
- HTHC, 2021. Healthy Trees Healthy Cities. URL <https://healthytreeshealthycitiesapp.org/>
- Hugenholtz, C.H., Whitehead, K., Brown, O.W., Barchyn, T.E., Moorman, B.J., LeClair, A., Riddell, K., Hamilton, T., 2013. Geomorphological mapping with a small unmanned aircraft system (sUAS): Feature detection and accuracy assessment of a photogrammetrically-derived digital terrain model. *Geomorphology* 194, 16–24. <https://doi.org/10.1016/j.geomorph.2013.03.023>
- Husch, B., Miller, C.I., Beers, T.W., 1972. *Forest Mensuration*, 2nd Editio. ed. Ronald Press Company, NY.
- Hwang, S., Lee, I., 2011. Current Status of Tree Height Estimation from Airborne LiDAR Data. *Korean J. Remote Sens.* 27, 389–401.
- Hyypä, H.J., Hyypä, J.M., 2001. Effects of stand size on the accuracy of remote sensing-based forest inventory. *IEEE Trans. Geosci. Remote Sens.* 39, 2613–2621. <https://doi.org/10.1109/36.974996>

- Hyypä, J., Hyypä, H., Inkinen, M., Engdahl, M., Linko, S., Zhu, Y.-H., 2000. Accuracy comparison of various remote sensing data sources in the retrieval of forest stand attributes. *For. Ecol. Manage.* 128, 109–120. [https://doi.org/10.1016/S0378-1127\(99\)00278-9](https://doi.org/10.1016/S0378-1127(99)00278-9)
- Iizuka, K., Yonehara, T., Itoh, M., Kosugi, Y., 2017. Estimating Tree Height and Diameter at Breast Height (DBH) from Digital Surface Models and Orthophotos Obtained with an Unmanned Aerial System for Japanese Cypress (*Chamaecyparis obtusa*) Forest. *Remote Sens.* 10, 13. <https://doi.org/10.3390/rs10010013>
- Innes, J.L., 1998. An assessment of the use of crown structure for the determination of the health of beech (*Fagus sylvatica*). *Forestry* 71, 113–130. <https://doi.org/10.1093/forestry/71.2.113>
- IPCC, 2000. Land Use, Land-Use Change, and Forestry: Summary for Policymakers.
- James, M.R., Robson, S., d'Oleire-Oltmanns, S., Niethammer, U., 2017. Optimising UAV topographic surveys processed with structure-from-motion: Ground control quality, quantity and bundle adjustment. *Geomorphology* 280, 51–66. <https://doi.org/10.1016/j.geomorph.2016.11.021>
- Janowiak, M.K., D'Amato, A.W., Swanston, C.W., Iverson, L., Thompson, F.R., Diak, W.D., Matthews, S., Peters, M.P., Prasad, A., Fraser, J.S., Brandt, L.A., Butler-Leopold, P., Handler, S.D., Shannon, P.D., Burbank, D., Campbell, J., Cogbill, C., Duveneck, M.J., Emery, M.R., Fisichelli, N., Foster, J., Hushaw, J., Kenefic, L., Mahaffey, A., Morelli, T.L., Reo, N.J., Schaberg, P.G., Simmons, K.R., Weiskittel, A., Wilmot, S., Hollinger, D., Lane, E., Rustad, L., Templer, P.H., 2018. New England and Northern New York Forest Ecosystem Vulnerability Assessment and Synthesis : A Report from the New England Climate Change Response Framework Project 234. <https://doi.org/10.2737/NRS-GTR-173>
- Jenerowicz, A., Siok, K., Woroszkiewicz, M., Orych, A., 2017. The fusion of satellite and UAV data: simulation of high spatial resolution band 76. <https://doi.org/10.1117/12.2278669>
- Jensen, J., 2016. *Introductory Digital Image Processing: A remote sensing perspective*, 4th editio. ed. Pearson Education Inc., Glenview, IL.
- Jha, C.S., Rakesh, Singhal, J., Reddy, C.S., Rajashekar, G., Maity, S., Patnaik, C., Das, A., Misra, A., Singh, C.P., Mohapatra, J., Krishnayya, N.S.R., Kiran, S., Townsend, P., Martinez, M.H., 2019. Characterization of species diversity and forest health using AVIRIS-NG hyperspectral remote sensing data. *Curr. Sci.* 116, 1124–1135. <https://doi.org/10.18520/cs/v116/i7/1124-1135>
- Jones, G.M., Keane, J.J., Gutiérrez, R.J., Peery, M.Z., 2018. Declining old-forest species as a legacy of large trees lost. *Divers. Distrib.* 24, 341–351. <https://doi.org/10.1111/ddi.12682>
- Jones, G.P., Pearlstine, L.G., Percival, H.F., 2006. An Assessment of Small Unmanned Aerial Vehicles for Wildlife Research. *Wildl. Soc. Bull.* 34, 750–758. [https://doi.org/10.2193/0091-7648\(2006\)34\[750:aaosua\]2.0.co;2](https://doi.org/10.2193/0091-7648(2006)34[750:aaosua]2.0.co;2)
- Justice, D., Deely, A., Rubin, F., 2002. *Final Report: New Hampshire Land Cover Assessment*.
- Juutinen, A., Mönkkönen, M., 2004. Testing alternative indicators for biodiversity conservation in old-growth boreal forests: Ecology and economics. *Ecol. Econ.* 50, 35–48.

<https://doi.org/10.1016/j.ecolecon.2004.02.006>

- Kakaes, K., Greenwood, F., Lippincott, M., Dosemagen, S., Meier, P., Wich, S., 2015. Drones and Aerial Observation: New Technologies for property rights, human rights, and global development a primer.
- Kampen, M., Vienna, L.S., Immitzer, M., Vienna, L.S., 2019. UAV-Based Multispectral Data for Tree Species Classification and Tree Vitality Analysis. Dreilandertagung der DGPF, der OVG und der SGPF Wien, Osterr. – Publ. der DGPF, Band 28 623–639.
- Kattenborn, T., Lopatin, J., Förster, M., Braun, A.C., Fassnacht, F.E., 2019. UAV data as alternative to field sampling to map woody invasive species based on combined Sentinel-1 and Sentinel-2 data. *Remote Sens. Environ.* 227, 61–73.
<https://doi.org/10.1016/j.rse.2019.03.025>
- Kebrle, D., Zasadil, P., Hošek, J., Barták, V., Šťastný, K., 2021. Large trees as a key factor for bird diversity in spruce-dominated production forests: Implications for conservation management. *For. Ecol. Manage.* 496. <https://doi.org/10.1016/j.foreco.2021.119460>
- Kerr, J.T., Ostrovsky, M., 2003. From space to species: Ecological applications for remote sensing. *Trends Ecol. Evol.* 18, 299–305. [https://doi.org/10.1016/S0169-5347\(03\)00071-5](https://doi.org/10.1016/S0169-5347(03)00071-5)
- Kershaw, J.A., Ducey, M.J., Beers, T.W., Husch, B., 2016. *Forest Mensuration*, 5th Editio. ed. John Wiley and Sons Ltd, Hoboken, NJ.
- King, D.I., Schlossberg, S., 2014. Synthesis of the conservation value of the early-successional stage in forests of eastern North America. *For. Ecol. Manage.* 324, 186–195.
<https://doi.org/10.1016/j.foreco.2013.12.001>
- Kirchhoefer, M., Schumacher, J., Adler, P., 2019. Potential of remote sensing-based forest attribute models for harmonising large-scale forest inventories on regional level: a case study in Southwest Germany. *Ann. For. Sci.* 76. <https://doi.org/10.1007/s13595-019-0804-4>
- Kirui, K.B., Kairo, J., Bosire, K.M., Viergever, S., Rudra, S., Huxham, M., Briers, R.A., 2013. Mapping of mangrove forest land cover change along the Kenya coastline using Landsat imagery. *Ocean Coast. Manag.* 83.
- Ko, Y., Lee, J.H., McPherson, E.G., Roman, L.A., 2015. Long-term monitoring of Sacramento Shade program trees: Tree survival, growth and energy-saving performance. *Landsc. Urban Plan.* 143, 183–191. <https://doi.org/10.1016/j.landurbplan.2015.07.017>
- Koch, B., Hernández, J., Hartig, F., Berger, C., Corvalán, P., Fassnacht, F.E., Latifi, H., 2015. Stratified aboveground forest biomass estimation by remote sensing data. *Int. J. Appl. Earth Obs. Geoinf.* 38, 229–241. <https://doi.org/10.1016/j.jag.2015.01.016>
- Kopinga, J., Burg, J. Van Den, 1995. Using Soil and Foliar Analysis To Diagnose the Nutritional Status of Urban Trees 21, 17–24.
- Krzywinski, M., Altman, N., 2017. Corrigendum: Classification and regression trees. *Nat. Methods* 14, 757–758.
- Kuchler, A.W., 1976. *Vegetation Mapping*. The Ronald Press Company, New York, NY.

- Kuželka, K., Surový, P., 2018. Mapping forest structure using uas inside flight capabilities. *Sensors (Switzerland)* 18. <https://doi.org/10.3390/s18072245>
- Lambin, E.F., Turner, B.L., Geist, H.J., Agbola, S.B., Angelsen, A., Folke, C., Bruce, J.W., Coomes, O.T., Dirzo, R., George, P.S., Homewood, K., Imbernon, J., Leemans, R., Li, X., Moran, E.F., Mortimore, M., Ramakrishnan, P.S., Richards, J.F., Steffen, W., Stone, G.D., Svedin, U., Veldkamp, T.A., 2001. The causes of land-use and land-cover change : moving beyond the myths 11, 261–269.
- Lamson, N.I., 1987. D.b.h./Crown Diameter Relationships in Mixed Appalachian Hardwood stands, US Department of Agriculture. Forest Service Research Paper.
- Lausch, A., Erasmi, S., King, D.J., Magdon, P., Heurich, M., 2017. Understanding forest health with Remote sensing-Part II-A review of approaches and data models. *Remote Sens.* 9, 1–33. <https://doi.org/10.3390/rs9020129>
- Lausch, A., Erasmi, S., King, D.J., Magdon, P., Heurich, M., 2016. Understanding forest health with remote sensing-Part I-A review of spectral traits, processes and remote-sensing characteristics. *Remote Sens.* 8, 1–44. <https://doi.org/10.3390/rs8121029>
- Leckie, D.G., Gougeon, F.A., Walsworth, N., Paradine, D., 2003. Stand delineation and composition estimation using semi-automated individual tree crown analysis. *Remote Sens. Environ.* 85, 355–369. [https://doi.org/10.1016/S0034-4257\(03\)00013-0](https://doi.org/10.1016/S0034-4257(03)00013-0)
- Lehmann, J.R.K., Nieberding, F., Prinz, T., Knoth, C., 2015. Analysis of unmanned aerial system-based CIR images in forestry-a new perspective to monitor pest infestation levels. *Forests* 6, 594–612. <https://doi.org/10.3390/f6030594>
- Lelong, C.C.D., Burger, P., Jubelin, G., Roux, B., Labbé, S., Baret, F., 2008. Assessment of unmanned aerial vehicles imagery for quantitative monitoring of wheat crop in small plots. *Sensors* 8, 3557–3585. <https://doi.org/10.3390/s8053557>
- Leukert, K., Darwish, A., Reinhardt, W., 2004. Transferability of Knowledge-based Classification Rules, in: *ISPRS - International Archives of the Photogrammetry, Remote Sensing and Spatial Information Sciences Theme Session 11: Automatic Image Interpretation in the GIS Environment*. p. 6 pp.
- Liang, X., Hyypä, J., Kaartinen, H., Lehtomäki, M., Pyörälä, J., Pfeifer, N., Holopainen, M., Brolly, G., Francesco, P., Hackenberg, J., Huang, H., Jo, H.W., Katoh, M., Liu, L., Mokoš, M., Morel, J., Olofsson, K., Poveda-Lopez, J., Trochta, J., Wang, D., Wang, J., Xi, Z., Yang, B., Zheng, G., Kankare, V., Luoma, V., Yu, X., Chen, L., Vastaranta, M., Saarinen, N., Wang, Y., 2018. International benchmarking of terrestrial laser scanning approaches for forest inventories. *ISPRS J. Photogramm. Remote Sens.* 144, 137–179. <https://doi.org/10.1016/j.isprsjprs.2018.06.021>
- Liang, X., Wang, Y., Pyörälä, J., Lehtomäki, M., Yu, X., Kaartinen, H., Kukko, A., Honkavaara, E., Issaoui, A.E.I., Nevalainen, O., Vaaja, M., Virtanen, J.P., Katoh, M., Deng, S., 2019. Forest in situ observations using unmanned aerial vehicle as an alternative of terrestrial measurements. *For. Ecosyst.* 6. <https://doi.org/10.1186/s40663-019-0173-3>
- Lillesand, T., Kiefer, R.W., Chipman, J., 2015. *Remote Sensing and Image Interpretation*, 7th ed.

John Wiley and Sons Ltd, USA.

- Lindenmayer, D.B., Laurance, W.F., Franklin, J.F., 2012. Global Decline in Large Old Trees. *Science* (80-.). 338, 1305–1306. <https://doi.org/10.1126/science.1231070>
- Lindenmayer, D.B., Margules, C.R., Botkin, D.B., 2000. Indicators of Biodiversity for Ecologically Sustainable Forest Management. *Conserv. Biol.* 14, 941–950. <https://doi.org/10.1046/j.1523-1739.2000.98533.x>
- Liu, L., Coops, N.C., Aven, N.W., Pang, Y., 2017. Mapping urban tree species using integrated airborne hyperspectral and LiDAR remote sensing data. *Remote Sens. Environ.* 200, 170–182. <https://doi.org/10.1016/j.rse.2017.08.010>
- Liu, L., Lim, S., Shen, X., Yebra, M., 2019. A hybrid method for segmenting individual trees from airborne lidar data. *Comput. Electron. Agric.* 163, 104871. <https://doi.org/10.1016/j.compag.2019.104871>
- Liu, T., Yang, X., 2015. Monitoring land changes in an urban area using satellite imagery, GIS and landscape metrics. *Appl. Geogr.* 56, 42–54. <https://doi.org/10.1016/j.apgeog.2014.10.002>
- Lobo Torres, D., Queiroz Feitosa, R., Nigri Happ, P., Elena Cué La Rosa, L., Marcato Junior, J., Martins, J., Olã Bressan, P., Gonçalves, W.N., Liesenberg, V., 2020. Applying Fully Convolutional Architectures for Semantic Segmentation of a Single Tree Species in Urban Environment on High Resolution UAV Optical Imagery. *Sensors* 20, 563. <https://doi.org/10.3390/s20020563>
- Lockhart, B.R., Weih jr., R.C., Smith, K.M., Weih, R.C., Smith, K.M., 2005. Crown Radius and Diameter at Breast Height Relationships for Six Bottomland Hardwood Species. *J. Ark. Acad. Sci.* 59, 110–115.
- Loh, W.-Y., 2011. Classification and regression trees. *WIREs Data Min. Knowl. Discov.* 1, 14–23.
- Longley, P.A., Goodchild, M.F., Maguire, D.J., Rhind, D.W., 2015. *Geographic Information Science and Systems*, 4th Editio. ed. John Wiley and Sons Inc., Hoboken, NJ.
- Louhaichi, M., M. Borman, and D. Johnson. 2001. Spatially Located Platform and Aerial Photography for Documentation of Grazing Impacts on Wheat. *Geocarto International* 16,1, 65-70.
- Lu, B., He, Y., Liu, H.H.T., Bartholomé, E., Belward, A.S., Blaschke, T., Cook, B.D., Bolstad, P. V., Martin, J.G., Heinsch, F.A., Davis, K.J., Wang, W., Desai, A.R., Teclaw, R.M., Fassnacht, F.E., Latifi, H., Stereńczak, K., Modzelewska, A., Lefsky, M., Waser, L.T., Straub, C., Ghosh, A., Goetz, S.J., Prince, S.D., Hall, R.J., Skakun, R.S., Arsenault, E.J., Case, B.S., Hansen, M.C., Stehman, S. V., Potapov, P. V., Loveland, T.R., Townshend, J.R.G., DeFries, R.S., Pittman, K.W., Arunarwati, B., Stolle, F., Steinger, M.K., Carroll, M., DiMiceli, C., Hay, G.J., Castilla, G., Wulder, M.A., Ruiz, J.R., Hogland, J.S., Anderson, N.M., Kartikeyan, B., Sarkar, A., Majumder, K.L., Kelcey, J.M., Lausch, A., Erasmi, S., King, D.J., Magdon, P., Heurich, M., Lennartz, S.P., Congalton, R.G., Lu, B., He, Y., Liu, H.H.T., Masek, J.G., Goward, S.N., Kennedy, R.E., Cohen, W.B., Moisen,

- G.G., Schleeweis, K., Huang, C., McCullough, D.G., Siegert, N.W., McRoberts, R.E., Tomppo, E.O., Meng, Y., Cao, B., Dong, C., Dong, X., Mukhopadhyay, S., Peeters, F.M., Ontiveros, J.S.C., Smith, S., Snape, S., Poley, L.G., McDermid, G.J., Pourrahmati, M.R., Ranson, K.J., Sun, G., Lang, R.H., Chauhan, N.S., Cacciola, R.J., Kilic, O., Turner, N.R., Perroy, R.L., Hon, K., Whitehead, K., Hugenholtz, C.H., Wilson, D.C., Morin, R.S., Frelich, L.E., Ek, A.R., 2018. Mapping vegetation biophysical and biochemical properties using unmanned aerial vehicles-acquired imagery. *Int. J. Remote Sens.* 39, 5265–5287. <https://doi.org/10.1080/01431161.2017.1363441>
- Lu, D., Weng, Q., 2007. A survey of image classification methods and techniques for improving classification performance. *Int. J. Remote Sens.* 28, 823–870. <https://doi.org/10.1080/01431160600746456>
- Lutz, J.A., Furniss, T.J., Johnson, D.J., Davies, S.J., Allen, D., Alonso, A., Anderson-Teixeira, K.J., Andrade, A., Baltzer, J., Becker, K.M.L., Blomdahl, E.M., Bourg, N.A., Bunyavejchewin, S., Burslem, D.F.R.P., Cansler, C.A., Cao, K., Cao, M., Cárdenas, D., Chang, L.W., Chao, K.J., Chao, W.C., Chiang, J.M., Chu, C., Chuyong, G.B., Clay, K., Condit, R., Cordell, S., Dattaraja, H.S., Duque, A., Ewango, C.E.N., Fischer, G.A., Fletcher, C., Freund, J.A., Giardina, C., Germain, S.J., Gilbert, G.S., Hao, Z., Hart, T., Hau, B.C.H., He, F., Hector, A., Howe, R.W., Hsieh, C.F., Hu, Y.H., Hubbell, S.P., Inman-Narahari, F.M., Itoh, A., Janík, D., Kassim, A.R., Kenfack, D., Korte, L., Král, K., Larson, A.J., Li, Y., De, Lin, Y., Liu, S., Lum, S., Ma, K., Makana, J.R., Malhi, Y., McMahon, S.M., McShea, W.J., Memiaghe, H.R., Mi, X., Morecroft, M., Musili, P.M., Myers, J.A., Novotny, V., de Oliveira, A., Ong, P., Orwig, D.A., Ostertag, R., Parker, G.G., Patankar, R., Phillips, R.P., Reynolds, G., Sack, L., Song, G.Z.M., Su, S.H., Sukumar, R., Sun, I.F., Suresh, H.S., Swanson, M.E., Tan, S., Thomas, D.W., Thompson, J., Uriarte, M., Valencia, R., Vicentini, A., Vrška, T., Wang, X., Weiblen, G.D., Wolf, A., Wu, S.H., Xu, H., Yamakura, T., Yap, S., Zimmerman, J.K., 2018. Global importance of large-diameter trees. *Glob. Ecol. Biogeogr.* 27, 849–864. <https://doi.org/10.1111/geb.12747>
- Lutz, J.A., Larson, A.J., Freund, J.A., Swanson, M.E., Bible, K.J., 2013. The importance of large-diameter trees to forest structural heterogeneity. *PLoS One* 8. <https://doi.org/10.1371/journal.pone.0082784>
- Lutz, J.A., Larson, A.J., Swanson, M.E., Freund, J.A., 2012. Ecological importance of large-diameter trees in a temperate mixed-conifer forest. *PLoS One* 7. <https://doi.org/10.1371/journal.pone.0036131>
- MacLean, M.G., Campbell, M.J., Maynard, D.S., Ducey, M.J., Congalton, R.G., 2012. Requirements for labelling forest polygons in an object-based image analysis classification. University of New Hampshire.
- MacLean, M.G., Congalton, D.R.G., 2012. Map Accuracy Assessment Issues when using an Object-oriented Approach, in: *ASPRS Annual Conference Proceedings 2012*. Sacramento, CA, p. 5.
- Marshall, D.M., Barnhart, R.K., Shappee, E., Most, M., 2016. *Introduction to Unmanned Aerial Systems*, Second Ed. ed. CRC Press, Boca Raton, FL.
- Martin, M.E., Newman, S.D., Aber, J.D., Congalton, R.G., 1998. *Determining Forest Species*

- Composition Using High Spectral Resolution Remote Sensing Data. *Remote Sens. Environ.* 65, 249–254. [https://doi.org/10.1016/S0034-4257\(98\)00035-2](https://doi.org/10.1016/S0034-4257(98)00035-2)
- Maturbong, B., Wing, M.G., Strimbu, B., Burnett, J., 2019. Forest inventory sensitivity to {UAS}-based image processing algorithms. *Ann. For. Res.* 0. <https://doi.org/10.15287/afr.2018.1282>
- Maxwell, A.E., Warner, T.A., Fang, F., 2018a. Implementation of machine-learning classification in remote sensing: An applied review. *Int. J. Remote Sens.* 39, 2784–2817. <https://doi.org/10.1080/01431161.2018.1433343>
- Maxwell, A.E., Warner, T.A., Vanderbilt, B.C., Ramezan, C.A., 2017. Land cover classification and feature extraction from National Agriculture Imagery Program (NAIP) Orthoimagery: A review. *Photogramm. Eng. Remote Sensing* 83, 737–747. <https://doi.org/10.14358/PERS.83.10.737>
- McCune, B., 2000. Lichen Communities as Indicators of Forest Health. *Bryologist* 103, 353–356. [https://doi.org/10.1639/0007-2745\(2000\)103\[0353:LCAIOF\]2.0.CO;2](https://doi.org/10.1639/0007-2745(2000)103[0353:LCAIOF]2.0.CO;2)
- McKinney, M.L., 2006. Urbanization as a major cause of biotic homogenization. *Biol. Conserv.* 127, 247–260. <https://doi.org/10.1016/j.biocon.2005.09.005>
- McLaughlin, S., Percy, K., 1999. Forest health in North America: some perspectives on actual and potential roles of climate and air pollution. *Water, Air Soil Pollut.* 116, 151–197.
- McPHERSON, E.G., Nowak, D., Heisler, G., Grimmond, S., Souch, C., 1997. Quantifying urban forest structure, function, and value: the Chicago Urban Forest Climate Project 1, 49–61.
- Meng, J., Li, S., Wang, W., Liu, Q., Xie, S., Ma, W., 2016. Mapping forest health using spectral and textural information extracted from SPOT-5 satellite images. *Remote Sens.* 8. <https://doi.org/10.3390/rs8090719>
- Meng, Y., Cao, B., Dong, C., Dong, X., 2019. Mount Taishan Forest ecosystem health assessment based on forest inventory data. *Forests* 10, 1–14. <https://doi.org/10.3390/f10080657>
- Merino, L., Caballero, F., Martínez-De-Dios, J.R., Maza, I., Ollero, A., 2012. An unmanned aircraft system for automatic forest fire monitoring and measurement. *J. Intell. Robot. Syst. Theory Appl.* 65, 533–548. <https://doi.org/10.1007/s10846-011-9560-x>
- Michener, W.K., Jones, M.B., 2012. Ecoinformatics: Supporting ecology as a data-intensive science. *Trends Ecol. Evol.* 27, 85–93. <https://doi.org/10.1016/j.tree.2011.11.016>
- Michez, A., Piégay, H., Lisein, J., Claessens, H., Lejeune, P., 2016. Classification of riparian forest species and health condition using multi-temporal and hyperspatial imagery from unmanned aerial system. *Environ. Monit. Assess.* 188, 1–19. <https://doi.org/10.1007/s10661-015-4996-2>
- Minor, C.O., 1951. Stem-crown diameter relations in Southern Pine. *J. For.* 59, 490–493.
- Mishra, N.B., Mainali, K.P., Shrestha, B.B., Radenz, J., Karki, D., 2018. Species-level vegetation mapping in a Himalayan treeline ecotone using unmanned aerial system (UAS)

- imagery. *ISPRS Int. J. Geo-Information* 7. <https://doi.org/10.3390/ijgi7110445>
- Moessner, K.E., 1953. Photo interpretation in forest inventories. *Photogr. Engin.* 496–507.
- Mohan, M., Silva, C.A., Klauberg, C., Jat, P., Catts, G., Cardil, A., Hudak, A.T., Dia, M., 2017. Individual tree detection from unmanned aerial vehicle (UAV) derived canopy height model in an open canopy mixed conifer forest. *Forests* 8, 1–17. <https://doi.org/10.3390/f8090340>
- Morin, R.S., Barnett, C.J., Butler, B.J., Crocker, S.J., Domke, G.M., Hansen, M.H., Hatfield, M.A., Horton, J., Kurtz, C.M., Lister, T.W., Miles, P.D., Nelson, M.D., Piva, R.J., Wilmot, S., Widmann, R.H., Woodall, C.W., Zaino, R., 2015. *Forests of Vermont and New Hampshire 2012. Resour. Bull. NRS-95* 80.
- Muhamad-Afizzul, M., Siti-Yasmin, Y., Hamdan, O., Tan, S.A., 2019. Estimating stand-level structural and biophysical variables of lowland dipterocarp forest using airborne LiDAR data. *J. Trop. For. Sci.* 31, 312–323. <https://doi.org/10.26525/jtfs2019.31.3.312>
- Mulatu, K.A., Decuyper, M., Brede, B., Kooistra, L., Reiche, J., Mora, B., Herold, M., 2019. Linking terrestrial LiDAR scanner and conventional forest structure measurements with multi-modal satellite data. *Forests* 10, 1–19. <https://doi.org/10.3390/f10030291>
- Næsset, E., Gobakken, T., McRoberts, R.E., 2019. A model-dependent method for monitoring subtle changes in vegetation height in the boreal-alpine ecotone using bi-temporal, three dimensional point data from airborne laser scanning. *Remote Sens.* 11. <https://doi.org/10.3390/rs11151804>
- Naidoo, R., Balmford, A., Costanza, R., Fisher, B., Green, R.E., Lehner, B., Malcolm, T.R., Ricketts, T.H., 2008. Global mapping of ecosystem services and conservation priorities. *Proc. Natl. Acad. Sci.* 105, 9495–9500. <https://doi.org/10.1073/pnas.0707823105>
- Narumalani, S., Zhou, Y., Jensen, J.R., 1997. Application of remote sensing and geographic information systems to the delineation and analysis of riparian buffer zones. *Aquat. Bot.* 58, 393–409. [https://doi.org/10.1016/S0304-3770\(97\)00048-X](https://doi.org/10.1016/S0304-3770(97)00048-X)
- Näsi, R., Honkavaara, E., Blomqvist, M., Lyytikäinen-Saarenmaa, P., Hakala, T., Viljanen, N., Kantola, T., Holopainen, M., 2018. Remote sensing of bark beetle damage in urban forests at individual tree level using a novel hyperspectral camera from UAV and aircraft. *Urban For. Urban Green.* 30, 72–83. <https://doi.org/10.1016/j.ufug.2018.01.010>
- Näsi, R., Honkavaara, E., Tuominen, S., Saari, H., Pölönen, I., Hakala, T., Viljanen, N., Soukkamäki, J., Näkki, I., Ojanen, H., Reinikainen, J., 2016. Uas based tree species identification using the novel fpi based hyperspectral cameras in visible, nir and swir spectral ranges. *Int. Arch. Photogramm. Remote Sens. Spat. Inf. Sci. - ISPRS Arch.* 2016-Janua, 1143–1148. <https://doi.org/10.5194/isprsarchives-XLI-B1-1143-2016>
- Nex, F., Remondino, F., 2014. UAV for 3D mapping applications: A review. *Appl. Geomatics* 6, 1–15. <https://doi.org/10.1007/s12518-013-0120-x>
- NOAA, 2019. *Continuously Operating Reference Stations (CORS) National Oceanic and Atmospheric Administration.*
- Noordermeer, L., Bollandsås, O.M., Ørka, H.O., Næsset, E., Gobakken, T., 2019. Comparing the

- accuracies of forest attributes predicted from airborne laser scanning and digital aerial photogrammetry in operational forest inventories. *Remote Sens. Environ.* 226, 26–37. <https://doi.org/10.1016/j.rse.2019.03.027>
- Noss, R.F., 1999. Assessing and monitoring forest biodiversity: A suggested framework and indicators. *For. Ecol. Manage.* 115, 135–146. [https://doi.org/10.1016/S0378-1127\(98\)00394-6](https://doi.org/10.1016/S0378-1127(98)00394-6)
- Nowacki, G.J., Abrams, M.D., 2015. Is climate an important driver of post-European vegetation change in the Eastern United States? *Glob. Chang. Biol.* 21, 314–334. <https://doi.org/10.1111/gcb.12663>
- Nowak, D.J., Crane, D.E., Stevens, J.C., Hoehn, R.E., Walton, J.T., 2008. A Ground-Based Method of Assessing Urban Forest Structure and Ecosystem Services 34, 347–358.
- Oldoni, L. V, Cattani, C.E. V, Mercante, E., Johann, J.A., Antunes, J.F.G., Almeida, L., 2019. Annual cropland mapping using data mining and {OLI} {Landsat}-8. *Rev. Bras. Eng. Agrícola e Ambient.* 23, 952–958. <https://doi.org/10.1590/1807-1929/agriambi.v23n12p952-958>
- Oliver, C.D., Larson, B.A., 1996. *Forest Stand Dynamics*, Updated Ed. ed. John Wiley & Sons, New York.
- Olsson, P.O., Vivekar, A., Adler, K., Garcia Millan, V.E., Koc, A., Alamrani, M., Eklundh, L., 2021. Radiometric correction of multispectral uas images: Evaluating the accuracy of the parrot sequoia camera and sunshine sensor. *Remote Sens.* 13, 1–26. <https://doi.org/10.3390/rs13040577>
- Orwig, D.A., Foster, D.R., 1998. Forest Response to the Introduced Hemlock Woolly Adelgid in Southern New England, USA. *Journal of Torrey Botanical Society* 125, 60–73.
- Otsu, K., Pla, M., Duane, A., Cardil, A., Brotons, L., 2019. Estimating the threshold of detection on tree crown defoliation using vegetation indices from uas multispectral imagery. *Drones* 3, 1–23. <https://doi.org/10.3390/drones3040080>
- Otukei, J.R., Blaschke, T., 2010. Land cover change assessment using decision trees, support vector machines and maximum likelihood classification algorithms. *Int. J. Appl. Earth Obs. Geoinf.* 12, 27–31. <https://doi.org/10.1016/j.jag.2009.11.002>
- Pal, M., Mather, P.M., 2005. Support vector machines for classification in remote sensing. *Int. J. Remote Sens.* 26, 1007–1011. <https://doi.org/10.1080/01431160512331314083>
- Pal, N.R., Pal, S.K., 1993. A review on image segmentation techniques. *Pattern Recognit.* 26, 1277–1294. [https://doi.org/10.1016/0031-3203\(93\)90135-J](https://doi.org/10.1016/0031-3203(93)90135-J)
- Pan, Y., McCullough, K., Hollinger, D.Y., 2018. Forest biodiversity, relationships to structural and functional attributes, and stability in New England forests. *For. Ecosyst.* 5, 1–12. <https://doi.org/10.1186/s40663-018-0132-4>
- Panagiotidis, D., Abdollahnejad, A., Surovy, P., Chiteculo, V., 2017. Determining tree height and crown diameter from high-resolution UAV imagery. *Int. J. Remote Sens.* 38, 2392–2410. <https://doi.org/10.1080/01431161.2016.1264028>

- Pasquarella, V.J., Elkinton, J.S., Bradley, B.A., 2018. Extensive gypsy moth defoliation in Southern New England characterized using Landsat satellite observations. *Biol. Invasions* 20, 3047–3053. <https://doi.org/10.1007/s10530-018-1778-0>
- Pause, M., Schweitzer, C., Rosenthal, M., Keuck, V., Bumberger, J., Dietrich, P., Heurich, M., Jung, A., Lausch, A., 2016. In situ/remote sensing integration to assess forest health-a review. *Remote Sens.* 8, 1–21. <https://doi.org/10.3390/rs8060471>
- Pax-Lenney, M., Woodcock, C.E., Macomber, S.A., Gopal, S., Song, C., 2001. Forest mapping with a generalized classifier and Landsat TM data. *Remote Sens. Environ.* 77, 241–250.
- Pedregosa, F., Varoquaux, G., Gramfort, A., Michel, V., Thirion, B., Grisel, O., Blondel, M., Prettenhofer, P., Weiss, R., Dubourg, V., Vanderplas, J., Passos, A., Cournapeau, D., Brucher, M., Perrot, M., Duchesnay, E., 2011. Scikit-learn: Machine Learning in Python. *JMLR* 12, 2825–2830.
- Persad, R.A., Armenakis, C., 2017. Automatic 3D Surface Co-Registration Using Keypoint Matching. *Photogramm. Eng. Remote Sens.* 83, 137–151. <https://doi.org/10.14358/pers.83.2.137>
- Poland, T.M., McCullough, D.G., 2006. Emerald ash borer: invasion of the urban forest and the threat to North America's ash resource. *J. For.* 104, 118–124.
- Pontius, J., Hallett, R., 2014. Comprehensive Methods for Earlier Detection and Monitoring of Forest Decline. *For. Sci.* 60, 1156–1163. <https://doi.org/10.5849/forsci.13-121>
- Pontius, J., Hanavan, R.P., Hallett, R.A., Cook, B.D., Corp, L.A., 2017. High spatial resolution spectral unmixing for mapping ash species across a complex urban environment. *Remote Sens. Environ.* 199, 360–369. <https://doi.org/10.1016/j.rse.2017.07.027>
- Pretzsch, H., 2019. The effect of tree crown allometry on community dynamics in mixed-species stands versus monocultures. A review and perspectives for modeling and silvicultural regulation. *Forests* 10. <https://doi.org/10.3390/f10090810>
- Pretzsch, H., Biber, P., Uhl, E., Dahlhausen, J., Rötzer, T., Caldentey, J., Koike, T., van Con, T., Chavanne, A., Seifert, T., Toit, B. du, Farnden, C., Pauleit, S., 2015. Crown size and growing space requirement of common tree species in urban centres, parks, and forests. *Urban For. Urban Green.* 14, 466–479. <https://doi.org/10.1016/j.ufug.2015.04.006>
- Pugh, S.A., 1997. Applying Spatial Autocorrelation Analysis to Evaluate Error in New England Forest Cover-type maps derived from Landsat Thematic Mapper Data. Masters Sci. Thesis, Univ. New Hampsh.
- Puliti, S., Ørka, H.O., Gobakken, T., Næsset, E., 2015. Inventory of small forest areas using an unmanned aerial system. *Remote Sens.* 7, 9632–9654. <https://doi.org/10.3390/rs70809632>
- Puliti, S., Talbot, B., Astrup, R., 2018. Tree-stump detection, segmentation, classification, and measurement using Unmanned aerial vehicle (UAV) imagery. *Forests* 9. <https://doi.org/10.3390/f9030102>
- Püschel, H., Sauerbier, M., Eisenbeiss, H., 2008. A 3D MODEL OF CASTLE LANDENBERG (CH) FROM COMBINED PHOTOGRAMMETRIC PROCESSING OF TERRESTRIAL

AND UAV-BASED IMAGES 6.

- Radoux, J., Bogaert, P., Fasbender, D., Defourny, P., 2011. Thematic accuracy assessment of geographic object-based image classification. *Int. J. Geogr. Inf. Sci.* 25, 895–911. <https://doi.org/10.1080/13658816.2010.498378>
- Rautiainen, M., Mõttus, M., Stenberg, P., Ervasti, S., 2008. Crown envelope shape measurements and models. *Silva Fenn.* 42, 19–33. <https://doi.org/10.14214/sf.261>
- Redford, K.H., 1992. The Empty Forest. *Bioscience* 42, 412–422. <https://doi.org/10.2307/1311860>
- Revill, A., Florence, A., Macarthur, A., Hoad, S., Rees, R., Williams, M., 2020. Quantifying uncertainty and bridging the scaling gap in the retrieval of leaf area index by coupling sentinel-2 and UAV observations. *Remote Sens.* 12. <https://doi.org/10.3390/rs12111843>
- Royle, D.D., Lathrop, R.G., 1997. Monitoring Hemlock Forest Health in New Jersey Using Landsat TM Data and Change Detection Techniques. *For. Sc* 49, 9.
- Rudge, M.L.M., Levick, S.R., Bartolo, R.E., Erskine, P.D., 2021. Modelling the diameter distribution of savanna trees with drone-based LiDAR. *Remote Sens.* 13, 1–18. <https://doi.org/10.3390/rs13071266>
- Saeed, S., Yujun, S., Beckline, M., Chen, L., Zhang, B., Ahmad, A., Mannan, A., Khan, A., Iqbal, A., 2019. Forest edge effect on biomass carbon along altitudinal gradients in {Chinese} {Fir} (\textit{{Cunninghamia} lanceolata}): {A} study from {Southeastern} {China}. *Carbon Manag.* 10, 11–22. <https://doi.org/10.1080/17583004.2018.1537517>
- Sankey, T., Donager, J., McVay, J., Sankey, J.B., 2017. UAV lidar and hyperspectral fusion for forest monitoring in the southwestern USA. *Remote Sens. Environ.* 195, 30–43. <https://doi.org/10.1016/j.rse.2017.04.007>
- Schepaschenko, D., See, L., Lesiv, M., Bastin, J.F., Mollicone, D., Tsendbazar, N.E., Bastin, L., McCallum, I., Laso Bayas, J.C., Baklanov, A., Perger, C., Dürauer, M., Fritz, S., 2019. Recent Advances in Forest Observation with Visual Interpretation of Very High-Resolution Imagery. *Surv. Geophys.* 40, 839–862. <https://doi.org/10.1007/s10712-019-09533-z>
- Schrader-Patton, C., Grulke, N., Bienz, C., 2021. Assessment of ponderosa pine vigor using four-band aerial imagery in south central oregon: Crown objects to landscapes. *Forests* 12. <https://doi.org/10.3390/f12050612>
- senseFly, 2021. Parrot Sequoia+ Multispectral Camera. URL <https://www.sensefly.com/camera/parrot-sequoia/>
- senseFly, 2019a. eBee X Fixed-wing Mapping Drone. URL <https://www.sensefly.com/drone/abee-x-fixed-wing-drone/>
- senseFly, 2019b. senseFly Aeria X Photogrammetry Camera. URL <https://www.sensefly.com/camera/sensefly-aeria-x-photogrammetry-camera/>
- senseFly, 2019c. senseFly S.O.D.A. Photogrammetry Camera. URL <https://www.sensefly.com/camera/sensefly-soda-photogrammetry-camera/>

- senseFly, 2018. eBee Plus Drone User Manual v1.8. senseFly Parrot Gr. 1.8, 107.
- Shang, C., Coops, N.C., Wulder, M.A., White, J.C., Hermosilla, T., 2020. Update and spatial extension of strategic forest inventories using time series remote sensing and modeling. *Int. J. Appl. Earth Obs. Geoinf.* 84, 101956. <https://doi.org/10.1016/j.jag.2019.101956>
- Shen, X., Cao, L., 2017. Tree-species classification in subtropical forests using airborne hyperspectral and LiDAR data. *Remote Sens.* 9. <https://doi.org/10.3390/rs9111180>
- Simoës, J., Markowski-Lindsay, M., Butler, B.J., Kittredge, D.B., Thompson, J., Orwig, D., 2019. Assessing New England family forest owners' invasive insect awareness. *J. Ext.* 57.
- Smigaj, M., Gaulton, R., Suárez, J.C., Barr, S.L., 2019. Canopy temperature from an Unmanned Aerial Vehicle as an indicator of tree stress associated with red band needle blight severity. *For. Ecol. Manage.* 433, 699–708. <https://doi.org/10.1016/j.foreco.2018.11.032>
- Smith, M.W., Carrivick, J.L., Quincey, D.J., 2016. Structure from motion photogrammetry in physical geography. *Prog. Phys. Geogr. Earth Environ.* 40, 247–275. <https://doi.org/10.1177/0309133315615805>
- Smith, W.B., 2002. Forest inventory and analysis: A national inventory and monitoring program. *Environ. Pollut.* 116. [https://doi.org/10.1016/S0269-7491\(01\)00255-X](https://doi.org/10.1016/S0269-7491(01)00255-X)
- Snedcor, G.W., Cochran, W.G., 1980. *Statistical Methods*, Seventh Ed. ed. John Wiley and Sons.
- Sokal, R.R., 1974. Classification: Purposes, Principles, Progress, Prospects. *Sci. New Ser.* 185, 1115–1123.
- Sonti, S.H., 2015. Application of Geographic Information System (GIS) in Forest Management. *J. Geogr. Nat. Disasters* 05. <https://doi.org/10.4172/2167-0587.1000145>
- Spurr, S.H., 1948. *Aerial Photographs in Forestry*.
- Stage, A.R., Rennie, J.C., 1994. Fixed radius or variable plots? *J. For.* 92, 20–24.
- Steinman, J., 2004. *Forest health monitoring in the North-eastern United States: disturbances and conditions during 1993–2002*. Newtown Square, PA.
- Šumarstvo, P., Pripadajuće, D.I., 2010. PRECISION FORESTRY – DEFINITION AND TECHNOLOGIES 2 . SCOPE OF RESEARCH – Problematika istraživanja. *Forestry* 603–611.
- Tang, L., Shao, G., 2015. Drone remote sensing for forestry research and practices. *J. For. Res.* 26, 791–797. <https://doi.org/10.1007/s11676-015-0088-y>
- Taylor, S.E., McDonald, T.P., Veal, M.W., Corley, F.W., Grift, T.E., 2002. Precision Forestry: Operational tactics for today and tomorrow. 25th Annu. Meet. Counc. For. Eng. 6.
- Taylor, S.E., Veal, M.W., Grift, T.E., 2016. Forest stand inventory based on combined aerial and terrestrial close-range photogrammetry. *Forests* 7, 1–14. <https://doi.org/10.3390/f7080165>
- Thompson, I.D., Guariguata, M.R., Okabe, K., Bahamondez, C., Nasi, R., Heynell, V., Sabogal, C., 2013. An operational framework for defining and monitoring forest degradation. *Ecol. Soc.* <https://doi.org/https://doi.org/10.5751/ES-05443-180220>.

- Tirmenstein, D.A., 1991. *Quercus alba*. Fire Eff. Inf. Syst. U.S. Dep. Agric. For. Serv. Rocky Mt. Res. Stn. URL <https://www.fs.fed.us/database/feis/plants/tree/quealb/all.html>
- Tomppo, E., Katila, M., 1991. Satellite image-based national forest inventory of Finland for publication in the Igarss'91 digest. IEEE 1x2971-0/9, 1141–1144. <https://doi.org/10.1109/igarss.1991.579272>
- Townshend, J., Li, W., Gurney, C., McManus, J., Justice, C., 1991. Global land cover classification by remote sensing: present capabilities and future possibilities. *Remote Sens. Environ.* 35, 243–255. [https://doi.org/10.1016/0034-4257\(91\)90016-y](https://doi.org/10.1016/0034-4257(91)90016-y)
- Tree, R.M., Slusser, J., 2005. Measurement of spectral signatures of invasive plant species with a low cost spectrometer, in: Bernhard, G., Slusser, J.R., Herman, J.R., Gao, W. (Eds.), *Ultraviolet Ground- and Space-Based Measurements, Models, and Effects V*. SPIE, pp. 264–272.
- Tucker, C.J., Townshend, J.R.G., Goff, T.E., 1985. African land-cover classification using satellite data. *Science* (80-.). 227, 369–375. <https://doi.org/10.1126/science.227.4685.369>
- Turner, N., Perroy, R., Hon, K., 2017. Lava flow hazard prediction and monitoring with UAS: A case study from the 2014-2017 Pahoehoe lava crisis Hawai'i. *J. Appl. Volcanol.* 6.
- Ullman, S., 1979. The {Interpretation} of {Structure} from {Motion}. *Proc. R. Soc. London. Ser. B, Biol. Sci.* 203, 405–426.
- USDA, 2021. NAIP Imagery. URL <https://www.fsa.usda.gov/programs-and-services/aerial-photography/imagery-programs/naip-imagery/>
- USGCRP, 2017. Accomplishments of the U.S. Global Change Research Program. Washington, D.C. <https://doi.org/10.17226/24670>
- Verhoeven, G., Doneus, M., Briese, C., Vermeulen, F., 2012. Mapping by matching: A computer vision-based approach to fast and accurate georeferencing of archaeological aerial photographs. *J. Archaeol. Sci.* 39, 2060–2070. <https://doi.org/10.1016/j.jas.2012.02.022>
- Verhulp, J., Niekerk, A. V., 2017. Transferability of decision trees for land cover classification in heterogeneous area. *South African J. Geomatics* 6, 30–46.
- Vierling, K.T., Vierling, L.A., Gould, W.A., Martinuzzi, S., Clawges, R.M., 2008. Lidar: Shedding new light on habitat characterization and modeling. *Front. Ecol. Environ.* 6, 90–98. <https://doi.org/10.1890/070001>
- Vitousek, P.M., 2016. Beyond Global Warming : Ecology and Global Change Stable URL : <http://www.jstor.org/stable/1941591> REFERENCES Linked references are available on JSTOR for this article : You may need to log in to JSTOR to access the linked references . Your use of the JST 75, 1861–1876.
- Vitousek, P.M., D'Antonio, C.M., Loope, L.L., Westbrooks, R., 1996. Biological invasions as global environmental change. *Am. Sci.* 84, 468–478.
- Ward, K.T., Johnson, G.R., 2007. Geospatial methods provide timely and comprehensive urban forest information. *Urban For. Urban Green.* 6, 15–22.

<https://doi.org/10.1016/j.ufug.2006.11.002>

- Weidner, U., 2008. Contribution to the assessment of segmentation quality for remote sensing applications. *Int. Arch. Photogramm. Remote Sens. Spat. Inf. Sci.* 37, 479–484.
- Wessel, M., Brandmeier, M., Tiede, D., 2018. Evaluation of different machine learning algorithms for scalable classification of tree types and tree species based on Sentinel-2 data. *Remote Sens.* 10. <https://doi.org/10.3390/rs10091419>
- Westoby, M.J., Brasington, J., Glasser, N.F., Hambrey, M.J., Reynolds, J.M., 2012. “Structure-from-Motion” photogrammetry: A low-cost, effective tool for geoscience applications. *Geomorphology* 179, 300–314. <https://doi.org/10.1016/j.geomorph.2012.08.021>
- Whitman, A.A., Hagan, J.M., 2007. An index to identify late-successional forest in temperate and boreal zones. *For. Ecol. Manage.* 246, 144–154. <https://doi.org/10.1016/j.foreco.2007.03.004>
- Wieser, M., Mandlbürger, G., Hollaus, M., Otepka, J., Glira, P., Pfeifer, N., 2017. A case study of UAS borne laser scanning for measurement of tree stem diameter. *Remote Sens.* 9, 1–11. <https://doi.org/10.3390/rs9111154>
- Wilson, D.C., Morin, R.S., Frelich, L.E., Ek, A.R., 2019. Monitoring disturbance intervals in forests: a case study of increasing forest disturbance in Minnesota. *Ann. For. Sci.* 76. <https://doi.org/10.1007/s13595-019-0858-3>
- Wolf, K., 2008. City {Trees} and {Property} {Values} 5.
- Woodall, C.W., Miles, P.D., Vissage, J.S., 2005. Determining maximum stand density index in mixed species stands for strategic-scale stocking assessments. *For. Ecol. Manage.* 216, 367–377.
- Woodlands, U., 2021. University of New Hampshire Office of Woodlands and Natural Areas. URL <https://colsa.unh.edu/woodlands>
- Wu, J., 2014. Urban ecology and sustainability: The state-of-the-science and future directions. *Landsc. Urban Plan.* 125, 209–221. <https://doi.org/10.1016/j.landurbplan.2014.01.018>
- Wyka, S.A., Smith, C., Munck, I.A., Rock, B.N., Ziniti, B.L., Broders, K., 2017. Emergence of white pine needle damage in the northeastern United States is associated with changes in pathogen pressure in response to climate change. *Glob. Chang. Biol.* 23, 394–405. <https://doi.org/10.1111/gcb.13359>
- Xia, H., Zhao, W., Li, A., Bian, J., Zhang, Z., 2017. Subpixel inundation mapping using landsat-8 OLI and UAV data for a wetland region on the zoige plateau, China. *Remote Sens.* 9, 1–22. <https://doi.org/10.3390/rs9010031>
- Xie, Y., Sha, Z., Yu, M., 2008. Remote sensing imagery in vegetation mapping: a review. *J. Plant Ecol.* 1, 9–23. <https://doi.org/10.1093/jpe/rtm005>
- Xu, Z., Shen, X., Cao, L., Coops, N.C., Goodbody, T.R.H., Zhong, T., Zhao, W., Sun, Q., Ba, S., Zhang, Z., Wu, X., 2020. Tree species classification using UAS-based digital aerial photogrammetry point clouds and multispectral imageries in subtropical natural forests. *Int.*

- J. Appl. Earth Obs. Geoinf. 92, 102173. <https://doi.org/10.1016/j.jag.2020.102173>
- Yadav, K., Congalton, R.G., 2017. Issues with large area thematic accuracy assessment for mapping cropland extent: A tale of three continents. *Remote Sens.* 10. <https://doi.org/10.3390/rs10010053>
- Yan, W., Guan, H., Cao, L., Yu, Y., Gao, S., Lu, J.Y., 2018. An automated hierarchical approach for three-dimensional segmentation of single trees using UAV LiDAR data. *Remote Sens.* 10. <https://doi.org/10.3390/rs10121999>
- Yang, J., He, Y., Caspersen, J., 2017. Region merging using local spectral angle thresholds: A more accurate method for hybrid segmentation of remote sensing images. *Remote Sens. Environ.* 190, 137–148.
- Young, R.F., 2010. Managing municipal green space for ecosystem services. *Urban For. Urban Green.* 9, 313–321. <https://doi.org/10.1016/j.ufug.2010.06.007>
- Yu, Q., Gong, P., Clinton, N., Biging, G., Kelly, M., Schirokauer, D., 2014. Meta-discoveries from a Synthesis of Satellite-based Land-Cover Mapping Research. *Photogrammetric Eng. Remote Sens.* 35, 4573–4588.
- Yuan, Z., Ali, A., Sanaei, A., Ruiz-Benito, P., Jucker, T., Fang, L., Bai, E., Ye, J., Lin, F., Fang, S., Hao, Z., Wang, X., 2021. Few large trees, rather than plant diversity and acomposition, drive the above-ground biomass stock and dynamics of temperate forests in northeast China. *For. Ecol. Manage.* 481. <https://doi.org/10.1016/j.foreco.2020.118698>
- Yurtseven, H., Çoban, S., Akgül, M., Akay, A.O., 2019. Individual tree measurements in a planted woodland with terrestrial laser scanner. *Turkish J. Agric. For.* 43, 192–208. <https://doi.org/10.3906/tar-1805-5>
- Zaman, B., Jensen, A.M., McKee, M., 2011. Use of high-resolution multispectral imagery acquired with an autonomous unmanned aerial vehicle to quantify the spread of an invasive wetlands species, in: 2011 IEEE International Geoscience and Remote Sensing Symposium. IEEE, Vancouver, BC, Canada, pp. 803–806. <https://doi.org/10.1109/IGARSS.2011.6049252>
- Zhang, C., Kovacs, J.M., 2012. The application of small unmanned aerial systems for precision agriculture: A review. *Precis. Agric.* 13, 693–712. <https://doi.org/10.1007/s11119-012-9274-5>
- Zhang, L., Sun, X., Wu, T., Zhang, H., 2015. An Analysis of Shadow Effects on Spectral Vegetation Indexes Using a Ground-Based Imaging Spectrometer. *IEEE Geosci. Remote Sens. Lett.* 12, 2188–2192. <https://doi.org/10.1109/LGRS.2015.2450218>
- Zhang, X., Qiu, F., Zhan, C., Zhang, Q., Li, Z., Wu, Y., Huang, Y., Chen, X., 2020. Acquisitions and applications of forest canopy hyperspectral imageries at hotspot and multiview angle using unmanned aerial vehicle platform. *J. Appl. Remote Sens.* 14, 1. <https://doi.org/10.1117/1.jrs.14.022212>
- Zhao, D., Pang, Y., Liu, L., Li, Z., 2020. Individual tree classification using airborne lidar and hyperspectral data in a natural mixed forest of northeast China. *Forests* 11, 1–19. <https://doi.org/10.3390/f11030303>

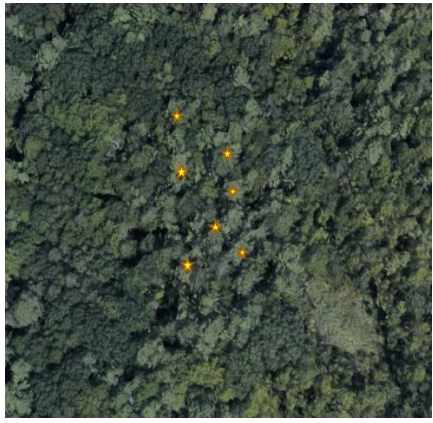
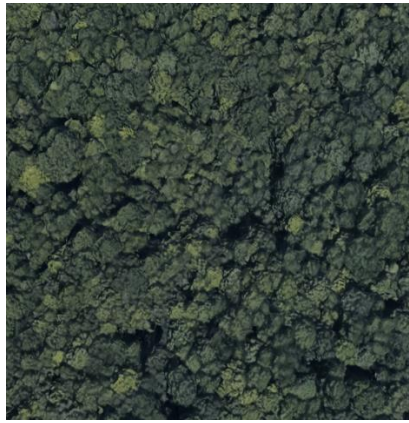

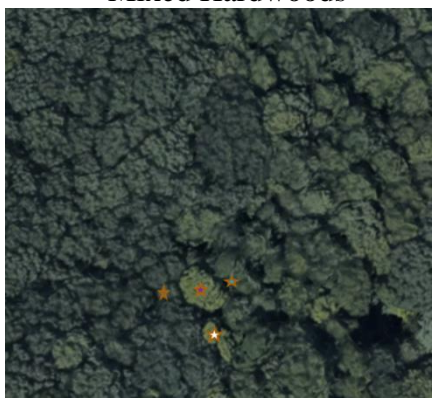

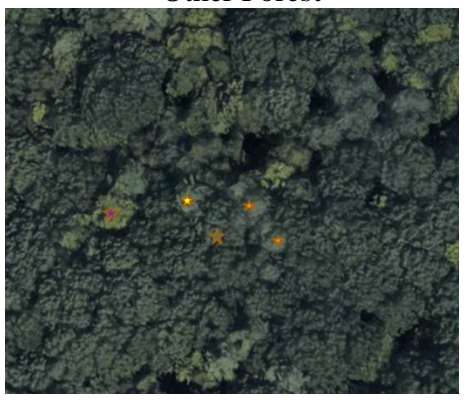
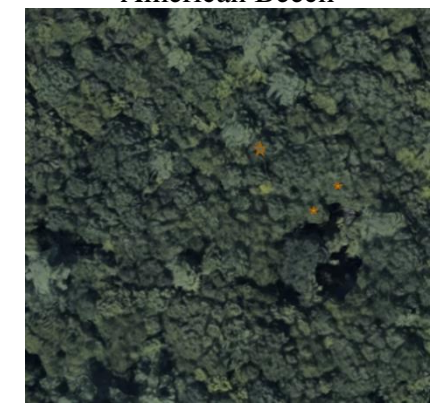
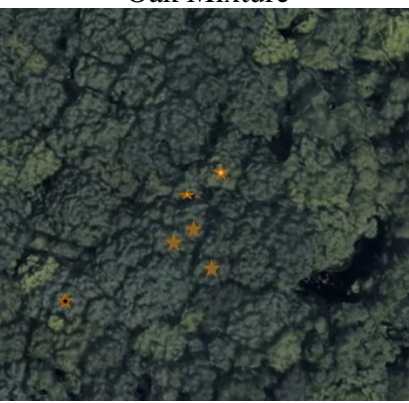

- Zhou, J., Zhou, G., Wei, H., Zhang, X., 2018. ESTIMATION OF THE PLOT-LEVEL FOREST PARAMETERS FROM TERRESTRIAL LASER SCANNING DATA, in: IGARSS 2018 - 2018 IEEE International Geoscience and Remote Sensing Symposium. IEEE, pp. 9014–9017.
- Zhou, X., Zhang, X., 2020. Individual tree parameters estimation for plantation forests based on UAV oblique photography. *IEEE Access* 8, 96184–96198. <https://doi.org/10.1109/ACCESS.2020.2994911>
- Zhu, X., Skidmore, A.K., Darvishzadeh, R., Wang, T., 2019. Estimation of forest leaf water content through inversion of a radiative transfer model from LiDAR and hyperspectral data. *Int. J. Appl. Earth Obs. Geoinf.* 74, 120–129. <https://doi.org/10.1016/j.jag.2018.09.008>

APPENDICIES

APPENDIX 1. CHAPTER 1




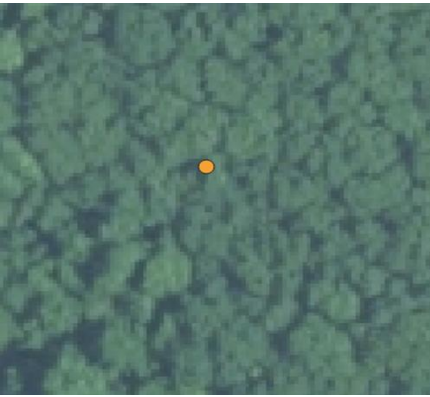



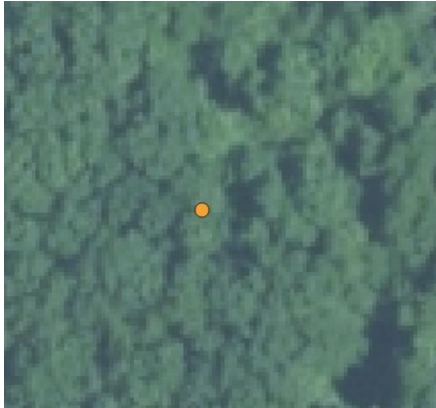
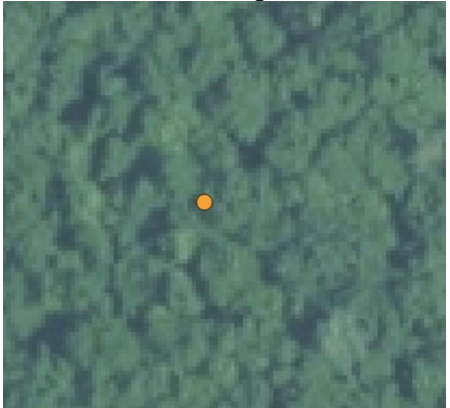
Google Earth Photo Interpretation Key

Table 22. Google Earth Photo Interpretation Key for the nine forest classes defined in Chapter 1. Symbols (stars) represent inventory plot measured trees of the listed species composition.

<p>White Pine</p> 	<p>Eastern Hemlock</p> 	<p>Mixed Conifer</p> 
<p>Mixed Hardwoods</p> 	<p>Mixed Forest</p> 	<p>Other Forest</p> 
<p>American Beech</p> 	<p>Oak Mixture</p> 	<p>Red Maple</p> 


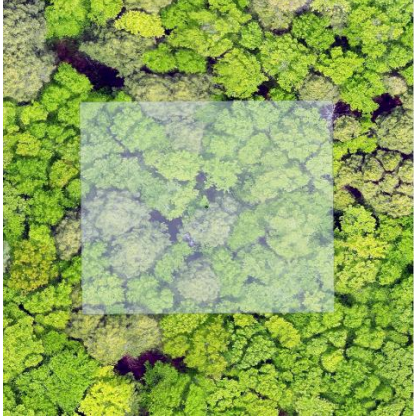






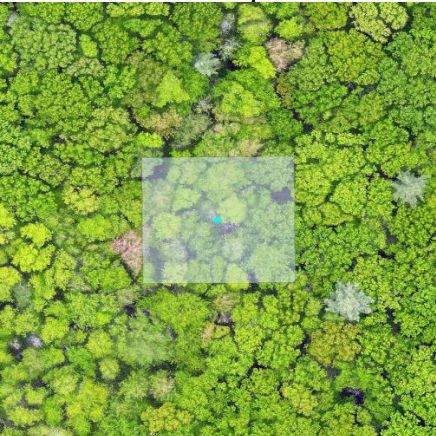
NAIP Photo Interpretation Key

Table 23. NAIP Imagery Photo Interpretation Key for the nine forest classes defined in Chapter 1. Symbols (circles) represent the inventory plot locations (center GPS point).

<p>White Pine</p> 	<p>Eastern Hemlock</p> 	<p>Mixed Conifer</p> 
<p>Mixed Hardwoods</p> 	<p>Mixed Forest</p> 	<p>Other Forest</p> 
<p>American Beech</p> 	<p>Oak Mixture</p> 	<p>Red Maple</p> 

UAS Photo Interpretation Key

Table 24. UAS Imagery Photo Interpretation Key for the nine forest classes defined in Chapter 1. Opaque squares represent the 30 x 30 m fixed area placed around each forest inventory plot center, used as the reference area for plot level composition photo interpretations. Only the trees within this area were included in the classification of forest composition.

<p>White Pine</p> 	<p>Eastern Hemlock</p> 	<p>Mixed Conifer</p> 
<p>Mixed Hardwoods</p> 	<p>Mixed Forest</p> 	<p>Other Forest</p> 
<p>American Beech</p> 	<p>Oak Mixture</p> 	<p>Red Maple</p> 

Classification Features

Table 25. Classification features (i.e., attributes or variables) used for the supervised classification of the NAIP (29 total) and UAS (26 total) imagery.

Classification Features		
Spectral		
Greenness		Std. Dev. red Band
Mean of red Band		Std. Dev. green Band
Mean of green Band		Std. Dev. blue Band
Mean of blue Band		Std. Dev. NIR Band
Mean of NIR		
HIS Transformation		
HIS = Hue, Intensity, Saturation		Greenness = $\frac{(\text{Mean Green} - \text{Mean Red}) + (\text{Mean Green} - \text{Mean Blue})}{(2 * \text{Mean Green}) + (\text{Mean Red}) + (\text{Mean Blue})}$
Texture		
GLCM	Homogeneity	GLCM Mean
GLCM Contrast		GLCM Correlation
GLCM Dissimilarity		GLDV Mean
GLCM Entropy		GLDV Contrast
GLCM = Gray Level Co-Occurrence Matrix		GLDV = Gray Level Difference Vector
Geometric		
Area (m2)		Compactness
Border Index		Asymmetry
Border Length		Density
Length/Width		Radius of Longest Ellipsoid
Roundness		Radius of Shortest Ellipsoid
		Shape Index
NAIP Imagery Only		

Photo Interpretation Uncertainty

Table 26. Thematic (overall) accuracy for plot level photo interpretations using each of the three high-spatial resolution remotely sensed data sources.

Plot Level Photo Interpretation Accuracy for High-Resolution Remotely Sensed Data Sources			
	Google Earth	NAIP	UAS
9 Composition Classes	29.90%	31.86%	39.46%
4 Composition Classes	44.85%	46.57%	54.44%

Automated Classification

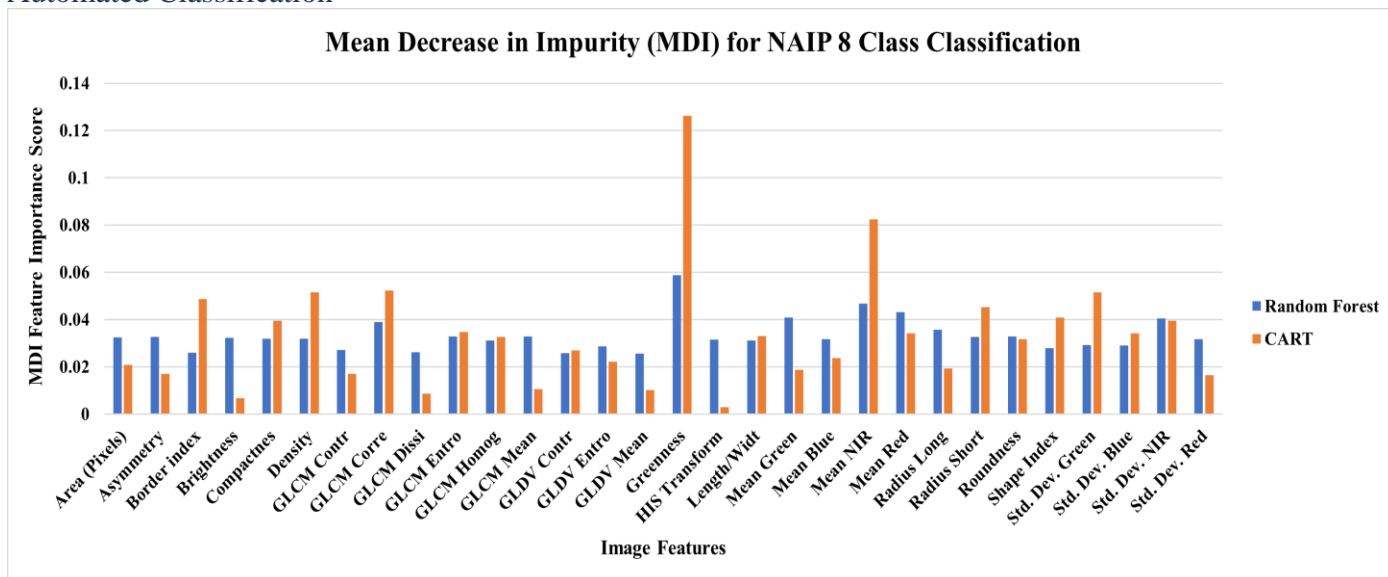


Figure 12. Feature importance for NAIP imagery classification of eight composition classes calculated using the Mean Decrease in Impurity (MDI) test.

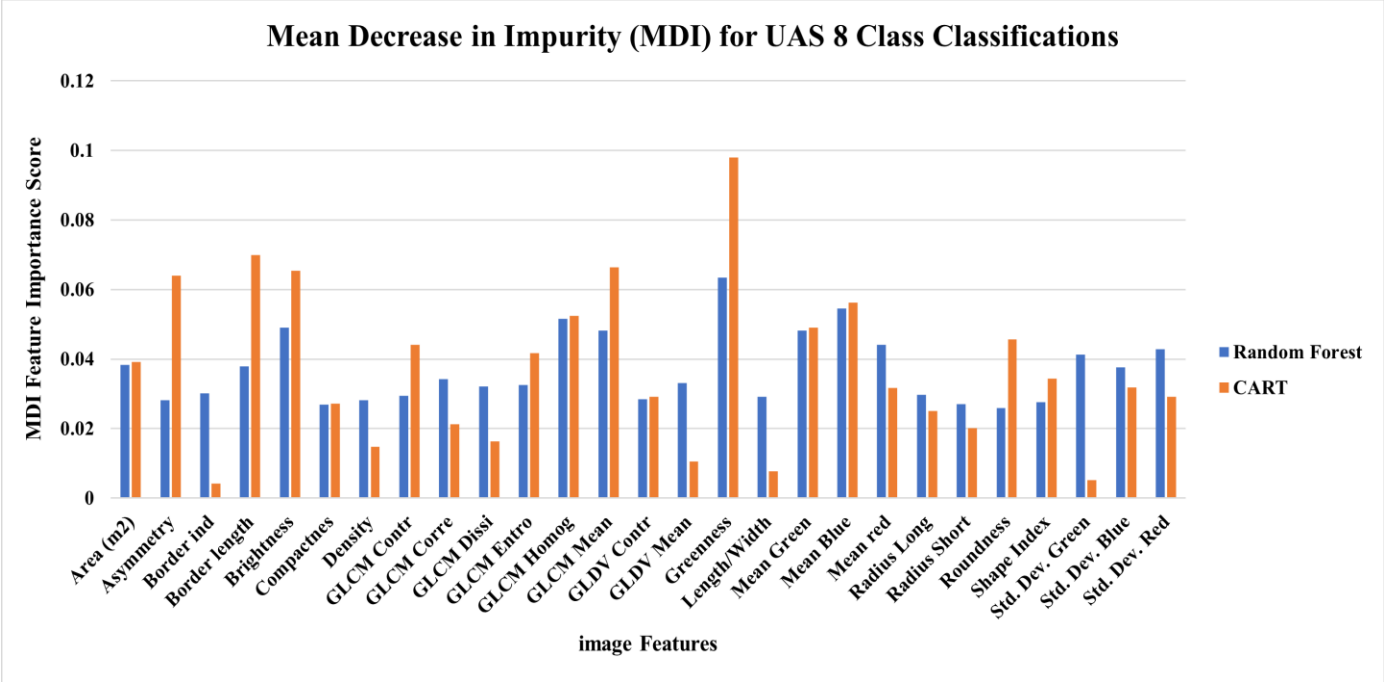


Figure 13. Feature importance for UAS imagery classification of eight composition classes calculated using the Mean Decrease in Impurity (MDI) test.

Table 27. Thematic map accuracy assessment error matrix for individual trees using the UAS imagery and the CART algorithm for eight classes.

		Field (Reference) Data								TOTAL	USERS ACCURACY
		WP	EH	OC	AB	RM	OAK	OH	ES		
UAS Imagery Using the RF Classifier	WP	25	4	7	4	2	1	5	0	48	52.08%
	EH	2	7	2	6	1	6	2	6	32	21.88%
	OC	9	2	12	2	2	5	6	3	41	29.27%
	AB	2	2	1	11	4	5	7	2	34	32.35%
	RM	1	6	5	2	16	11	2	7	50	32.0%
	OAK	2	5	8	4	7	30	12	4	72	41.67%
	OH	4	5	1	3	6	9	2	4	35	5.7%
	ES	1	4	2	3	6	1	4	7	28	25.0%
TOTAL	46	35	38	35	45	68	40	33	110/340		
PRODUCERS ACCURACY	54.35%	20.0%	31.58%	31.43%	35.56%	44.12%	5.0%	21.21%		OVERALL ACCURACY 32.35%	

Table 28. Thematic map accuracy assessment error matrix for individual trees using the UAS imagery and the RF algorithm for eight classes.

		Field (Reference) Data								TOTAL	USERS ACCURACY
		WP	EH	OC	AB	RM	OAK	OH	ES		
UAS Imagery Using the RF Classifier	WP	36	4	10	3	1	1	4	3	62	58.01%
	EH	0	10	0	6	2	3	2	3	26	38.46%
	OC	2	2	18	2	3	7	1	1	36	50.0%
	AB	1	3	1	13	1	3	4	1	27	48.15%
	RM	0	2	1	3	22	3	2	6	39	56.41%
	OAK	1	9	5	5	10	48	13	8	99	48.48%
	OH	6	4	2	1	3	2	12	2	32	37.5%
	ES	0	1	1	2	3	1	2	9	19	47.37%
TOTAL	46	35	38	35	45	68	40	33	168/340		
PRODUCERS ACCURACY		78.26%	28.57%	47.37%	37.14%	48.89%	70.59%	30.0%	27.27%		OVERALL ACCURACY 49.41%

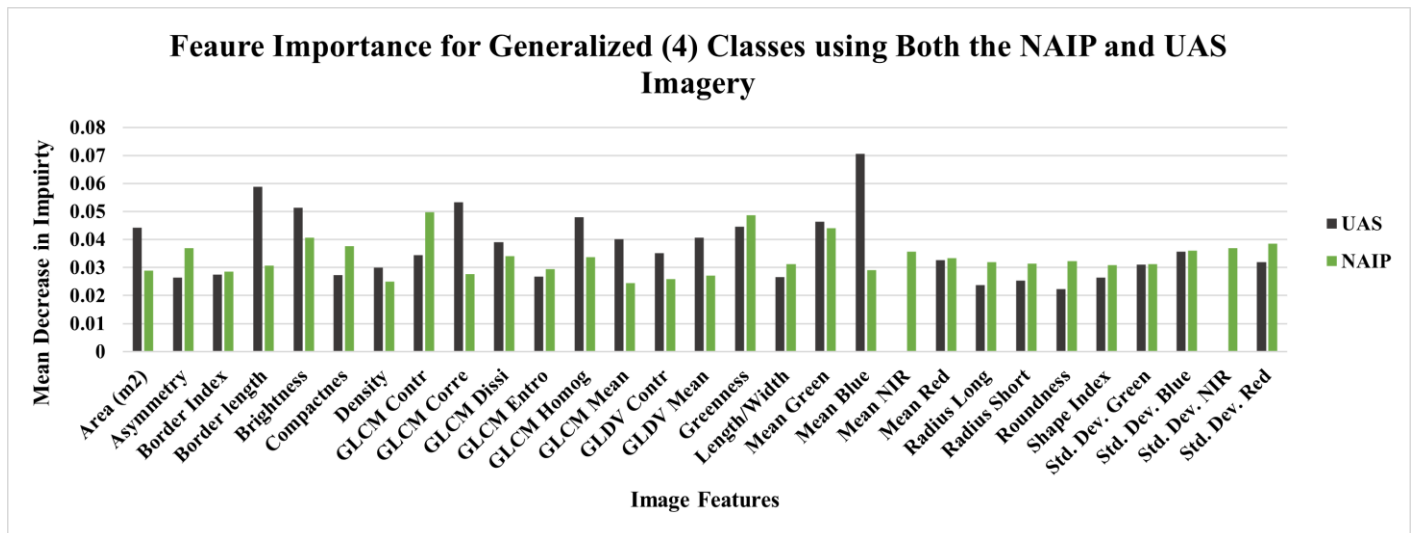


Figure 14. Feature importance for both the UAS and NAIP imagery classification of four composition classes calculated using the MDI test.

APPENDIX 2. CHAPTER 2

Stand Level Classification

- **White Pine** - any forested land surface dominated by tree species, comprising an overstory canopy with greater than 70% basal area per unit area eastern white pine (*Pinus strobus*).
- **Hemlock** - any forested land surface dominated by tree species, comprising an overstory canopy with greater than 70% basal area per unit area eastern hemlock (*Tsuga canadensis*).
- **Mixed Conifer** – any forested land area dominated by trees species comprising an overstory canopy with greater than 66% mixture of coniferous species, but less than 70% of white pine or eastern hemlock independently.
- **Mixed Forests** – any forested land surface dominated by tree species, comprising a heterogeneous mixture of deciduous and coniferous species each comprising greater than 20% basal area per unit area composition. Important species associations include eastern white pine and northern red oak (*Quercus rubra*), red maple (*Acer rubrum*), white ash (*Fraxinus americana*), eastern hemlock, and birches (*Betula spp.*).
- **Red Maple** – any forested land surface dominated by tree species, comprising an overstory canopy with greater than 50% basal area per unit area red maple.
- **Oak** – any forested land surface dominated by tree species, comprising an overstory canopy with greater than 50% basal area per unit area white oak (*Quercus alba*), black oak (*Quercus velutina*), northern red oak (*Quercus rubra*), or mixture of each.
- **American Beech** – any forested land surface dominated by tree species, comprising an overstory canopy with greater than 25% basal area per unit area American beech (*Fagus grandifolia*) composition. This unique class takes precedence over other mentioned hardwood classes if present.
- **Mixed Hardwoods** - any forested land surface dominated by tree species, comprising other deciduous species besides red maple, oak, or American beech that comprises greater than 66% basal area per unit area of the overstory canopy.
- **Other Forest** - any forested land surface dominated by tree species, comprising an overstory composition that is highly distinct, subject to different management or use, and not previously mentioned. This class includes areas dominated by early successional species such as paper birch (*Betula papyrifera*), or aspen (*Populus spp.*).

Tree Level Classification





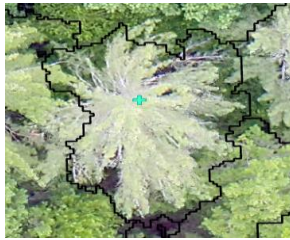







- **White Pine** – Any woody vegetation, taller than 3 meters and larger than 12.7 cm in diameter, representing the species White Pine (*Pinus strobus*).
- **Eastern Hemlock** - Any woody vegetation, taller than 3 meters and larger than 12.7 cm in diameter, representing the species Eastern Hemlock (*Tsuga canadensis*).

- **Other Conifer** - Any woody vegetation, taller than 3 meters and larger than 12.7 cm in diameter, representing coniferous species other than White Pine or Eastern Hemlock. Such species include Red Pine (*Pinus resinosa*), Basal Fir (*Abies balsamea*), and Eastern Red Cedar (*Juniperus virginiana*).
- **Oak** - Any woody vegetation, taller than 3 meters and larger than 12.7 cm in diameter, representing species of the Oak (*Quercus spp.*) family. Such species include Northern Red Oak (*Quercus rubra*), Black Oak (*Quercus velutina*), and White Oak (*Quercus alba*).
- **Red Maple**– Any woody vegetation, taller than 3 meters and larger than 12.7 cm in diameter, representing the species Red Maple (*Acer rubrum*).
- **American Beech**– Any woody vegetation, taller than 3 meters and larger than 12.7 cm in diameter, representing the species American Beech (*Fagus grandifolia*).
- **Other Hardwood** - Any woody vegetation, taller than 3 meters and larger than 12.7 cm in diameter, representing non- early successional deciduous species other than Oaks, Red Maple, or American Beech. Such species include Shagbark Hickory (*Carya ovata*), Sugar Maple (*Acer saccharum*), and Basswood (*Tilia americana*).
- **Other Forest** - Any woody vegetation, taller than 3 meters and larger than 12.7 cm in diameter, representing early successional species such as Birches (*Betula spp.*), Aspen (*Populus spp.*), or Ash (*Fraxinus spp.*).
- **Snags** – Any woody vegetation larger than 12.7 cm in diameter, representing any tree species that is clearly identified as dead but still has a stem taller than 3 meters.

APPENDIX 3. CHAPTER 3

Tree Health Survey Reference Trees

Table 29. Reference Samples collected for forest health survey classes using both field methods and photo interpretation. Both coniferous and deciduous trees of the ‘Healthy’, ‘Stressed’, and ‘Dead/Degraded’ classes collected as reference data using both sampling methods are provided as a guide to their similarity.

	Healthy	Stressed	Dead
Conifer: Field Survey	 <p>SI = 2</p>	 <p>SI = 7</p>	 <p>SI = 10</p>
Conifer: Photo Interpretation			
Deciduous: Field Survey	 <p>SI = 2</p>	 <p>SI = 6</p>	 <p>SI = 10</p>
Deciduous: Photo Interpretation			

Classification Features

Table 30. Image object features created using eCognition for the purpose of forest health classification using (1) UAS and (2) NAIP segmented imagery.

Image Classification Features		
Geometric	Texture	Spectral
Area (Pixels) Asymmetry Border Index Border Length Compactness Density Length\Width Radius of Long Ellipsoid Radius of Short Ellipsoid Shape Index	GLCM Contrast GLCM Correlation GLCM Dissimilarity GLCM Entropy GLCM Mean GLDV Entropy GLDV Mean GLDV Contrast	Brightness Greenness Index Mean red (SODA/NAIP) Mean green (SODA/NAIP) Mean blue (SODA/NAIP) Mean green (Sequoia) Mean red (Sequoia) Mean NIR (Sequoia\NAIP) Mean red edge (Sequoia) NDVI NGRDI Std. Dev. red (SODA/NAIP) Std. Dev. green (SODA/NAIP) Std. Dev. blue (SODA/NAIP) Std. Dev. green (Sequoia) Std. Dev. red (Sequoia) Std. Dev. NIR (Sequoia\NAIP) Std. Dev. red edge (Sequoia)
UAS Only		